Photo-switching of Dabcyl Modified Silicon Microwire Field Effect Transistors

Mkoma Kingu

This dissertation is submitted for the degree of

Masters of Science in Physics

August 2017

I would like to dedicate this thesis to my loving parents and for those who make the impossible a reality . . .

Declaration

I hereby declare that except where specific reference is made to the work of others, the contents of this dissertation are original and have not been submitted in whole or in part for consideration for any other degree or qualification in this, or any other university. This dissertation is my own work and contains nothing which is the outcome of work done in collaboration with others, except as specified in the text and Acknowledgements.

Mkoma Kingu

August 2017

Acknowledgements

I would like to extend my gratitude to Dr M. K. Moodley and Prof C - D. Chen for their supervision and diligent efforts that made this research possible. Helpful discussions with Ying-Ping Wu, Chai-Jung Chu, Ding Huang, Yu-Cheng Chang, Xinkui Huang, Jenny Liu and Pei Hua Chen are truly appreciated. There were several sources of encouragement and motivation. I am expecially grateful to my supervisor Dr. M. K. Moodley, for accepting me into his research group. This research was funded by the National Research Foundation as well as the bilateral Research fund between South Africa and Taiwan. Thanks goes out to the department of Chemistry and Physics for there procurement of the necessary equipment, technical support and resources. The micro wire fabrication was performed at the Core-facility Center, Academia Sinica, Taiwan.

List of Abbreviations

Az - azobenzene

DCC - dicyclohexylcarbodiimide

DMF - N,N-dimethylformamide

TBI - tetra-tert-butyl-azobenzene

Au - Gold

Az11 - 11-(4-(Phenyldiazenyl)phenoxy)undecane-1-thiol

C12 - 1-dodecanethiol

PSS - photostationary state

UV - ultraviolet

vis - visible

fs - femtoseconds

*m*SAM - mixed Self Assembled Monolayer

LEDs - Light Emitting Diodes

OFET - Organic Field Effect Transistor

SiMWFET - Silicon Microwire Field Effect Transistor

LUMO - Lowest Unoccupied Molecular Orbital

HOMO - Highest Occupied Molecular Orbital

2PPE - two-photon photoelectron spectroscopy

AFM atomic force microscopy

NEXAFS - Near Edge X-ray Absorption Fine Structure

CHC - core-hole–clock

SHG - Second Harmonic Generation

STM - Scanning Tunneling Microscopy

TOF - time-of-flight

dH_2O - de-ionized water

DMF - N,N-Dimethylformamide

APTES - (3-amino proplyl)trimethylsaline

dabcyl - 4-Dimethylaminoazobenzene-4'-carboxylic Acid

p-Methyl Red - 4-Dimethylaminoazobenzene-4'-carboxylic Acid

DCC - N, N- dicyclohexylcarbodi-imide

Abstract

Molecules which exist in two different states are known to be metastable. When they switch between states, properties such as electrical conductance change. If the difference in conductance is measurably high and a predictable control of the transition between the two states is found, then these molecules can be used as molecular storage elements. In this contribution we have satisfied these two conditions. Dabcyl/APTES mixed Self Assembled Monolayers (*m*SAMs) on p-type Silicon Microwire Field Effect Transistors (SiMWFETs) have exhibited reversible photoisomerization using low power Light emitting diodes (LEDs). Techniques to obtain more efficient photoswitching in mixed Self Assembled Monolayers (mSAMs) are discussed and implemented. Varying the SiMWFET's gate bias voltage, spacer molecules and large anchor groups were successfully implemented to increase photoisomerization yield. The difference in conductance between these two isomers of dabcyl/APTES *m*SAMs is electrically quantified using the characteristic plots of SiMWFET as well as *I* versus *t* plots. Characterization techniques such as *I* versus V_g comparisons proved that the microwire modification procedures were successful. The difference in current from excited *cis* to *trans* states was 0.05 μA. The efficiency of isomerization is dependent upon the lifetime of the *cis* isomer, cross sectional area, photoisomerization yield and environment conditions. These results infer that adventitious water adsorbed on the surface of the *m*SAM stabilizes the *cis* configuration of dabcyl under ambient conditions.

Table of contents

List of figures

List of tables

Chapter 1

Molecular Switches

1.1 Introduction

The ability to control the conductance of single molecules is expected to have a major impact in nanoscale electronics [1–6]. Azobenzene, a molecule that changes conformation as a result of a *trans/cis* transition when exposed to radiation, could form the basis of a light-driven molecular switch. Isomerization of azobenzene (Fig: 1.1) is a process where the molecule is rotated and inverted simultaneously [7, 8]. The incorporation of molecular switches into mixed Self-Assembled Monolayers allows for changing their properties by light [9]. It is therefore crucial to clarify the electrical transport characteristics of these molecules.

Mixed Self-Assembled monolayers (*m*SAMs) are frequently proposed as robust molecular coatings to tune surface properties [10]. Azo-biphenyl derivatives or alkanethiols ω-functionalized with azobenzene are usually used to achieve this goal [11, 12]. For azobiphenyl SAMs, the photoisomerization has been demonstrated [13]. In azobenzenealkanethiolate SAMs, the chromophore density has to be reduced to enable photoisomerization. We report on the effective photoisomerization of mixed SAMs prepared by step wise modification from APTES to dabcyl.

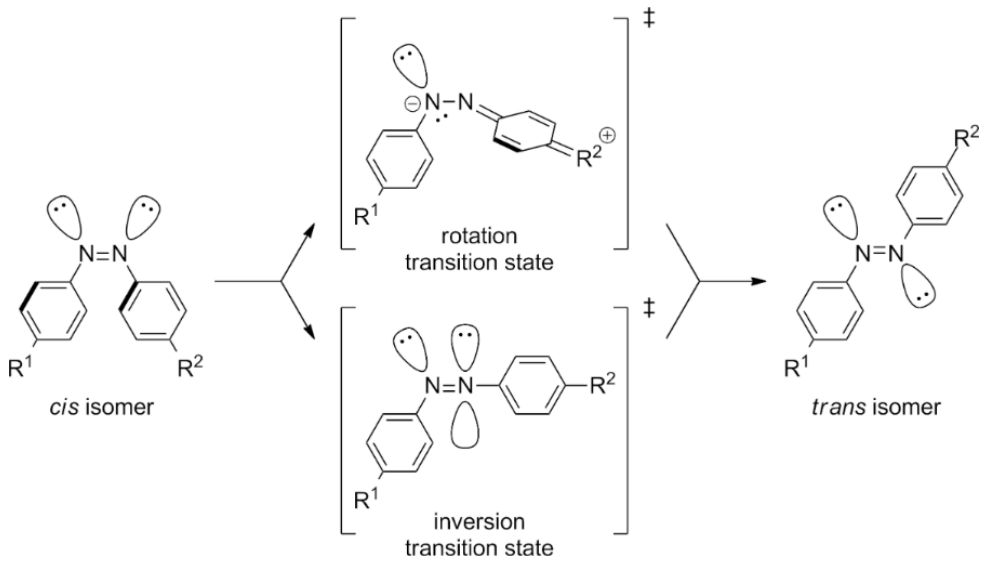

Fig. 1.1 Azobenzene undergoing *cis-trans* isomerism [14].

The molecule 3-Aminopropyl)triethoxysilane (APTES) is a fairly common ink used in micro contact printing [15]. It is an aminosilane commonly used in the process known as silanization, the functionalization of surfaces with alkoxysilane molecules. It can also be used for covalent attaching of organic films to metal oxides such as silica and titania [16–18]. Azobenzene derivatives have various applications such as dyes, inks and rewritable DVDs. Dabcyl, a derivative of azobenzene is a dye mainly used in green florescence [19]. The density of photoswitches in these SAMs can be adjusted by varying the relative concentrations of p-methyl red in DMF solvent. The APTES molecules act as lateral spacers, effectively diluting the photoswitches, which protrude above the APTES SAM layer.

The modification of surface properties requires that a substantial fraction of azobenzene molecules in the SAM isomerizes and that optical switching dominates over thermal isomerization. Therefore, two key requirements are the achievable photoisomerization yield and the thermal stability of the two isomers. In this contribution, we quantify the isomerization yields and rate constants in mixed dabcyl/APTES *m*SAMs by the changes in conductance in vacuum

and air.

Most strikingly, the rate constant of thermal *cis* to *trans* isomerization depends strongly upon the environment. Whereas thermal isomerization takes more than 1 minute in air, it proceeds within a few seconds in vacuum. The influence of the environment on the isomerization of dabcyl functionalized *m*SAMs demands careful consideration. The much slower thermal relaxation in air compared to vacuum is attributed to water adsorbed from ambient air, which stabilizes the more polar *cis* state of dabcyl.

1.1.1 Project Aims and Description

Molecular switches have been one of the most studied nano-technology topics in recent years [20]. Several advances have been implimented to overcome their short comings [10]. These strategies are discussed in this dissertation in more detail.

Photoswitching in densely packed dabcyl self-assembled monolayers (SAMs) is strongly affected by steric constraints [21–23] and excitonic coupling between neighboring chromophores [24]. Hence the control of the chromophore density is essential for enhancing and manipulating the photoisomerization yield [10].

The main objectives are:
To increase the isomerization yield with the use of changes in the substrates conductance, spacer molecules and large anchor groups. To adapt a theoretical model to calculate the photoswitching efficiency of dabcyl/APTES *m*SAM. To record the real-time detection of isomerization with the use of a silicon microwire Field Effect Transistor (SiMWFET) utilising I versus V_g, I versus V_d and I versus t plots. To obtain reversible photoisomerization using low power Light Emitting Diodes (LEDs). To experimentally investigate molecular switch operation in vacuum and

ambient conditions.

1.1.2 Background

Transistors which lie at the heart of integrated electronics have a built in limitations which restrict their size. By harnessing chemistry, researchers are able to reduce the size of switches down to a molecular level [25].

The integration of molecular switches into electronics could lead to new types of electronic devices [26, 27]. The switching of functional molecular properties via conformational changes is a fundamental concept in nature [28]. In many biological systems the specific functions are based on the cooperation of individual molecular units which are enabled and controlled by defined changes in the molecular geometry.

It is always in our best interest to emulate nature [26, 28]. In this contribution the azobenzene molecule (Fig: 1.2 a) forms part of the dabcyl molecule (Fig: 1.2 b). The APTES molecule links the dabcyl molecule to the silicon microwire surface (Fig: 1.2 c). The dabcyl/APTES *m*SAM system functions in a cooperative manner and allows photoisomerization to occur effectively (Fig: 1.2 d).

One prominent example of an optical switch is found in the eye and is responsible for sight. The light-induced *cis to trans* isomerization of retina plays a key role in the vision process. The molecule retinal (Fig: 1.3) is bound to the protein rhodopsin. When it undergoes *trans* isomerism, it detaches from the protein molecule, becomes reactive and starts to catalise the vision process. Retinal is a resilient molecule which can undergo multiple cycles. It does not wear out easily but when it does, the body easily replaces it.

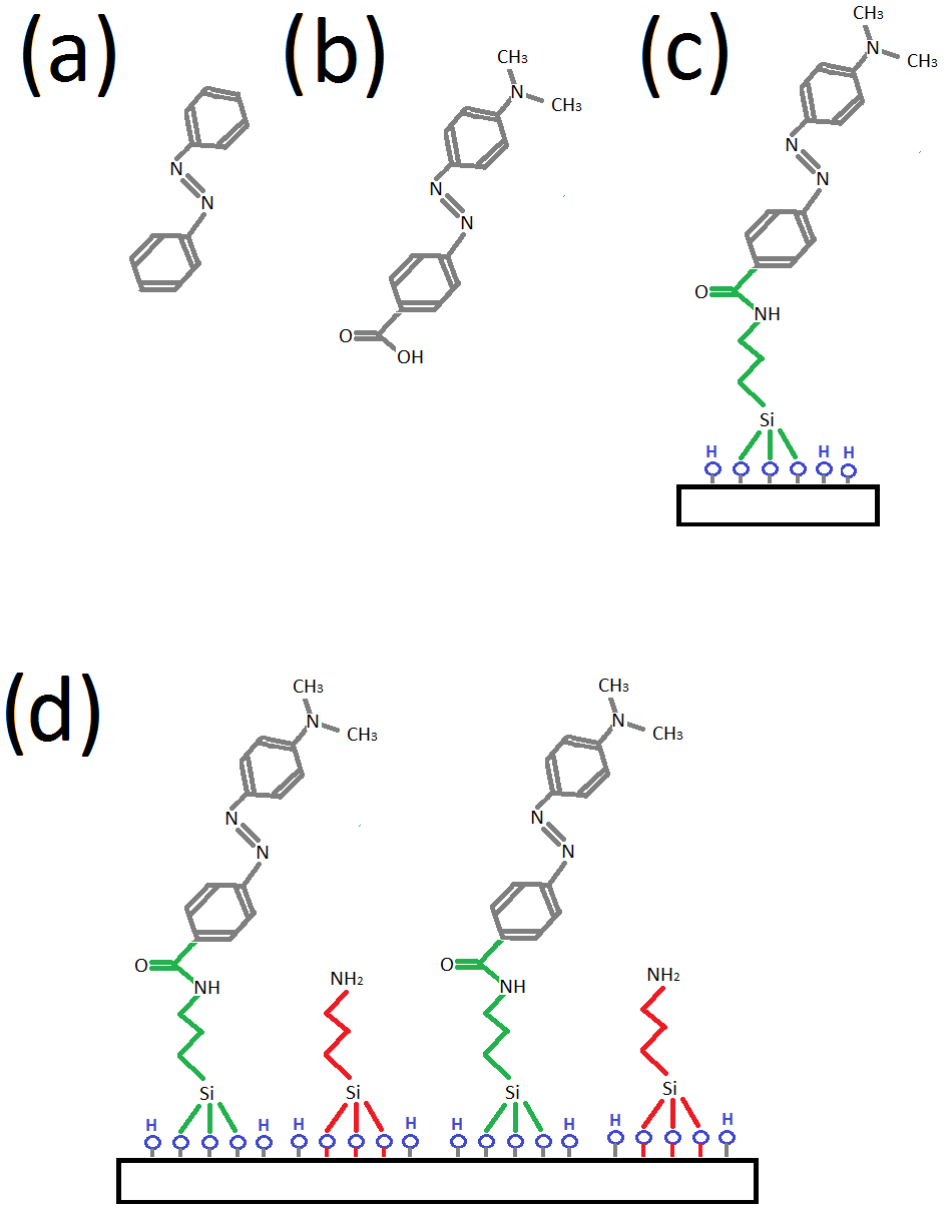

Fig. 1.2 (a) Azobenezene molecule. (b) Dabcyl molecule. (c) APTES functionalised with dabcyl. (c) Dabcyl/APTES *m*SAM system.

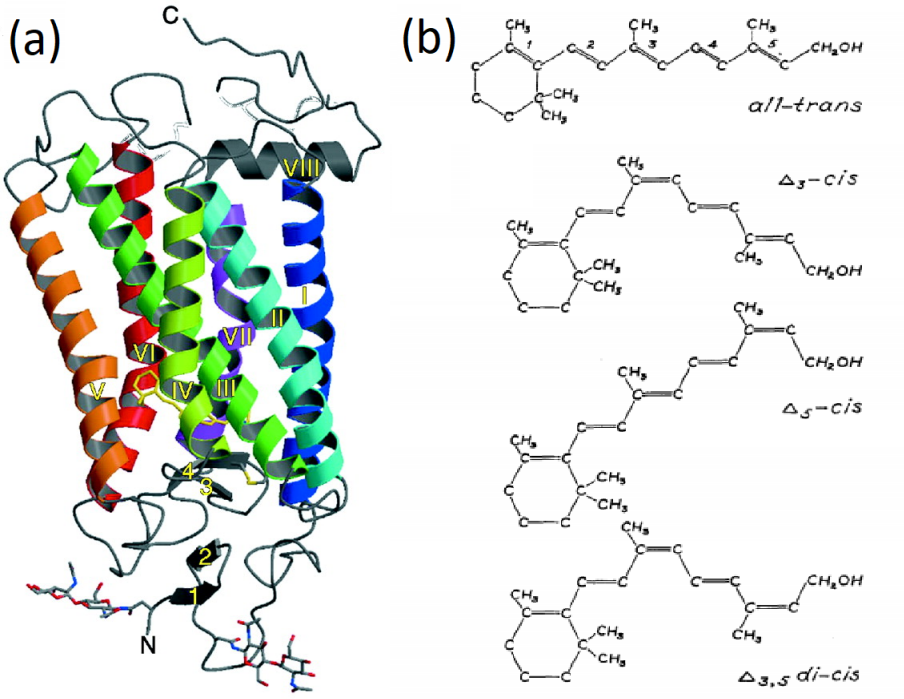

Fig. 1.3 (a) Rhodopsin protien [29]. (b) *Cis-trans* isomerism of retinal molecule [30].

The chip consist of seven microwire channels each with similar electrical characteristics (Fig: 1.4 a). *Cis-trans* photoisomerization and detection using a dabcyl functionalised microwire FET (Fig: 1.4 b). The silicon microwire FET consists of three main parts: The source, drain and gate. The device configuration used in this research is a top contact. The transistor's source and drain are evaporated on top of the organic material (Fig: 1.5).

Further reading on molecular switches is avaliable in the work by Chemistry Nobel laureate Ben Feringa (2016) [32].

There has been successful photoisomerisation detection with Organic Field Effect Transistors (OFETs) [33] but they required UV light for the *cis* state and heat to enter the *trans* state (Fig: 1.6). It is also notable that OFETs operate with higher voltages than conventional electronics. As a result OFETs are relatively less energy efficient.

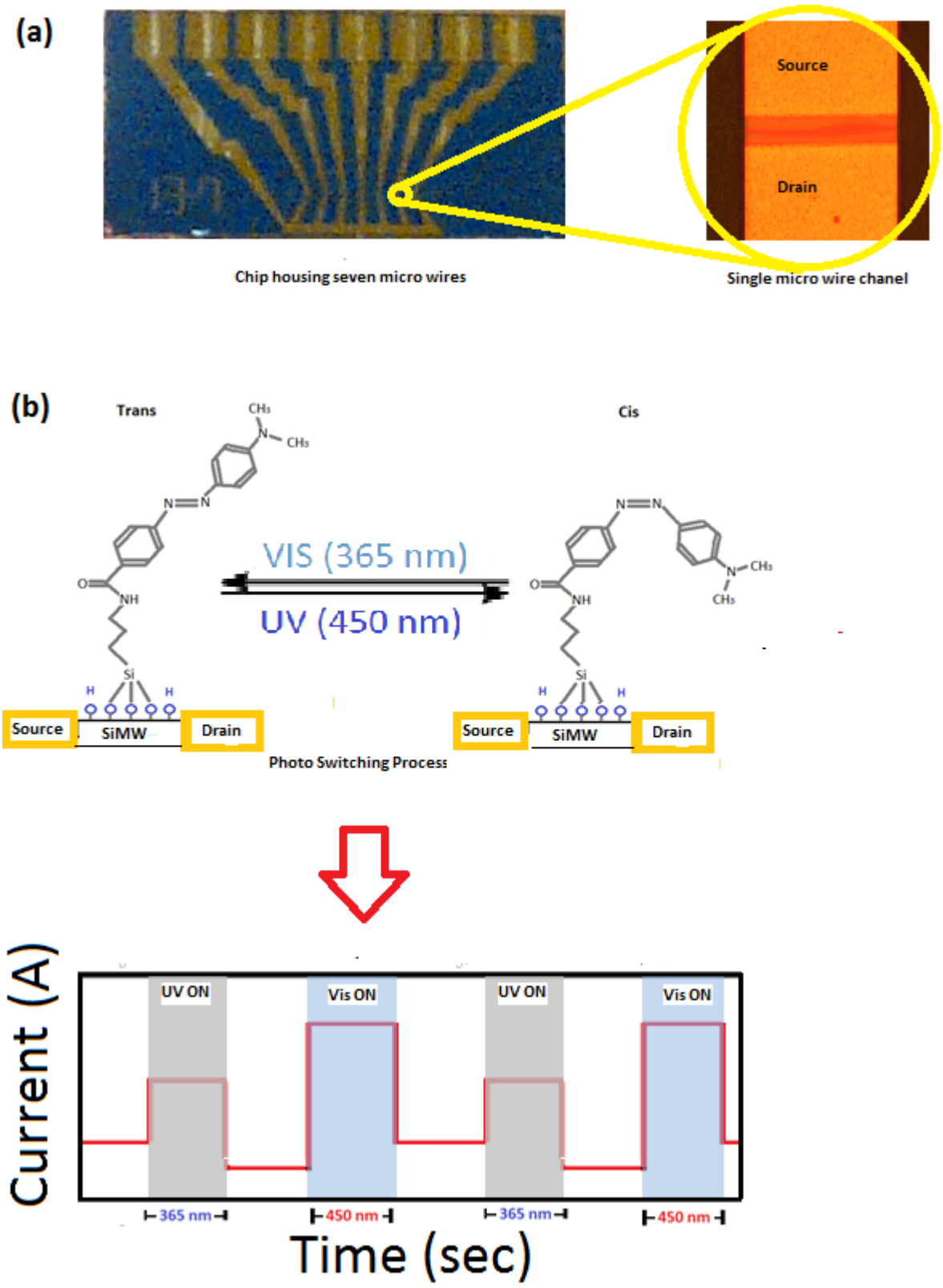

Fig. 1.4 (a) Magnified image of a silicon microwire chip (b) *Cis-trans* isomerism of an azobenzene chromophore functionalized thiol used in this research. Changes in current due to photoisomerization of chromophores [31].

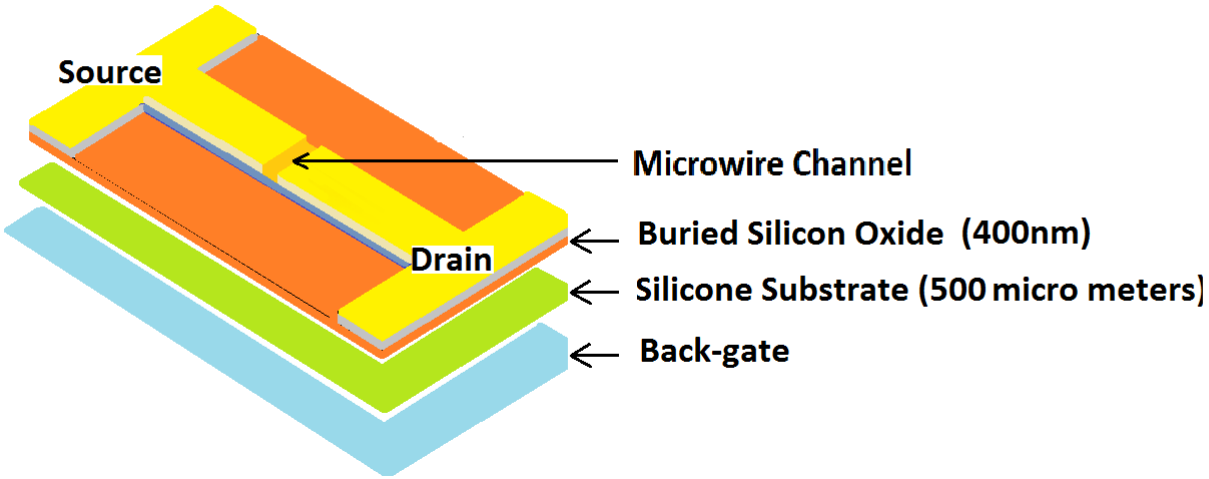

Fig. 1.5 Simple layout of the SiMWFET used in this research.

1.1.3 Interaction between the molecule and the substrate

In this section the interaction between the substrate (silicone microwire) and the receptor molecule is explained (refer to Fig: 1.7). There is a charge and energy transfer towards the surface [34, 35]. A core-hole is created through the absorption of incoming light with a quantity of energy matching the binding energy of the receptor molecule's core electron (a). A $\pi\pi^*$ transition occurs following two possible pathways for energy to be transferred to the substrate [7]. Energy transfer occurs when the excited electron of the molecule decays (b) back exciting an electron hole pair in the substrate (c). If the substrate is a metal, it has an abundance of electron-hole pairs. Then this process is likely to occur. Semiconductors make ideal substrates because their conductive properties can be adjusted by altering the ground voltage at the gate terminal. This makes it possible to vary the number of electron-hole pairs in the substrate. In chemistry the energy transfer between molecules is known as the F*ö*rster transfer.

The other means energy is transferred from the molecule to the substrate is via a charge transfer (d). In this case the excited electron tunnels through the barrier into the substrate [34].

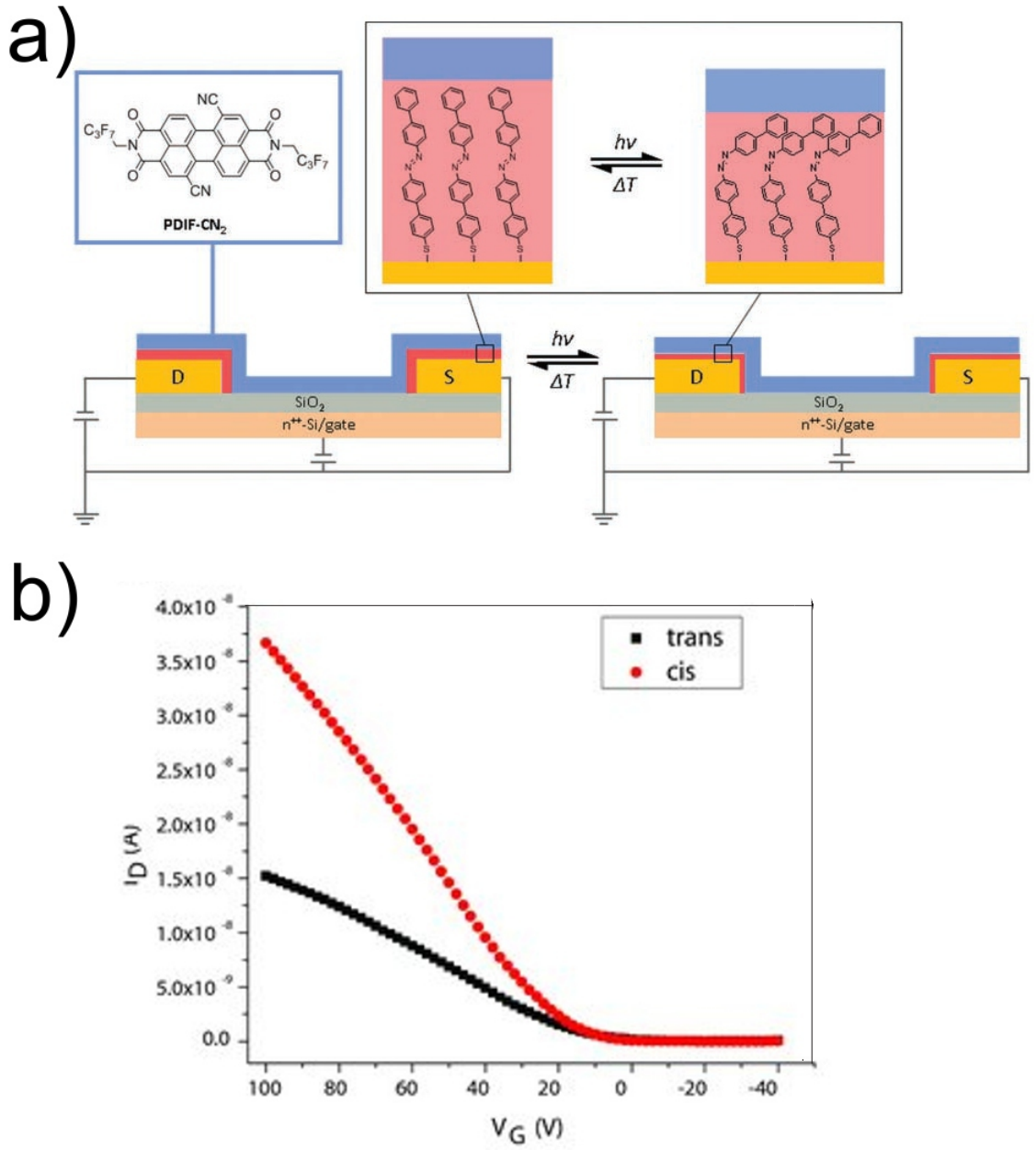

Fig. 1.6 (a) Organic field effect transistor schematic showing the *cis-trans* isomerism on the interface between the Azo-functionalized electrods and the organic semi-conductive material [33]. (b) I versus V_g plots with the *cis* state more conductive relative to the *trans* state. In chapter 4 this measurement would be replicated using dabcyl/APTES mixed SAM.

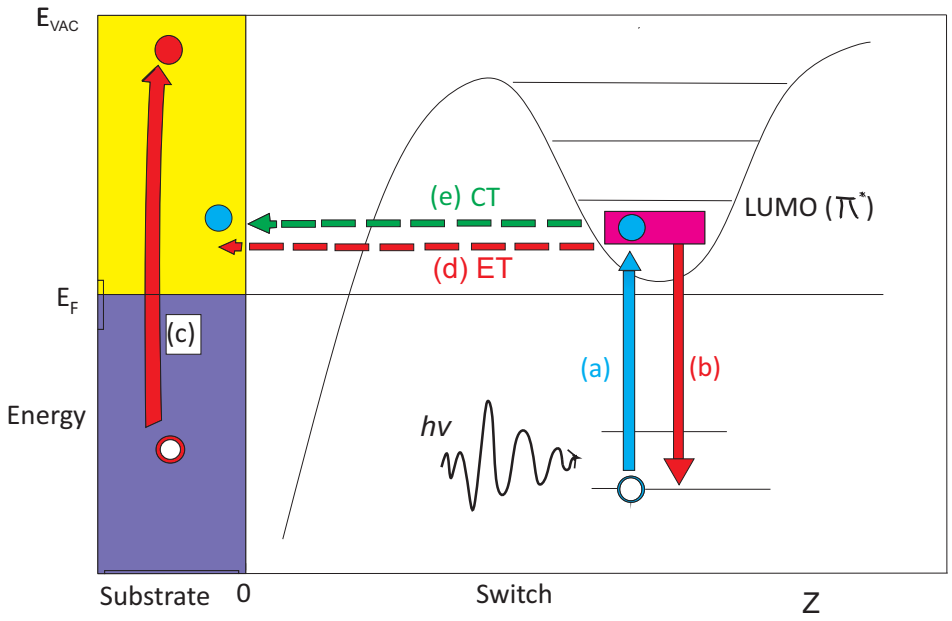

Fig. 1.7 Simplified diagram illustrating energy and charge transfer between the molecular switch and substrate [34, 36].

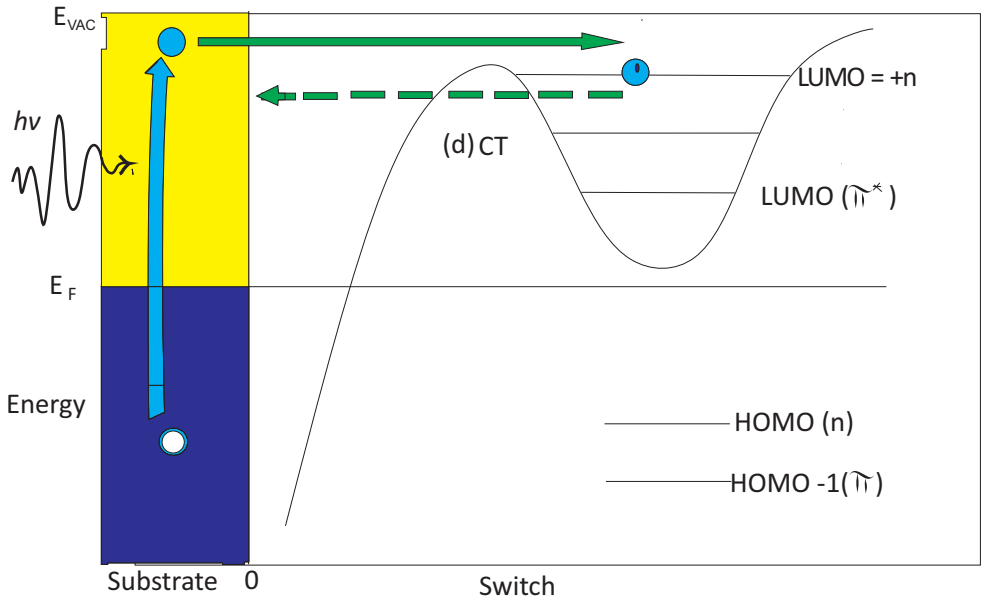

Fig. 1.8 Electron transition from the substrate to the molecule [34, 36].

If these two processes occur ultra-fast [37] the switching will be quenched [38]. It takes 3 pico seconds to switch the molecule and if this process is faster then the molecule will not switch or would do so with difficulty.

Not only is it possible for electrons to transition from the molecule to the surface, it is also possible for electrons to move from the substrate to the molecule Fig: 1.8 and 1.9. When light with energy of 4.2 eV (UV light) interacts with the substrate an electron can be liberated from the substrate into the molecule [36, 39, 40].

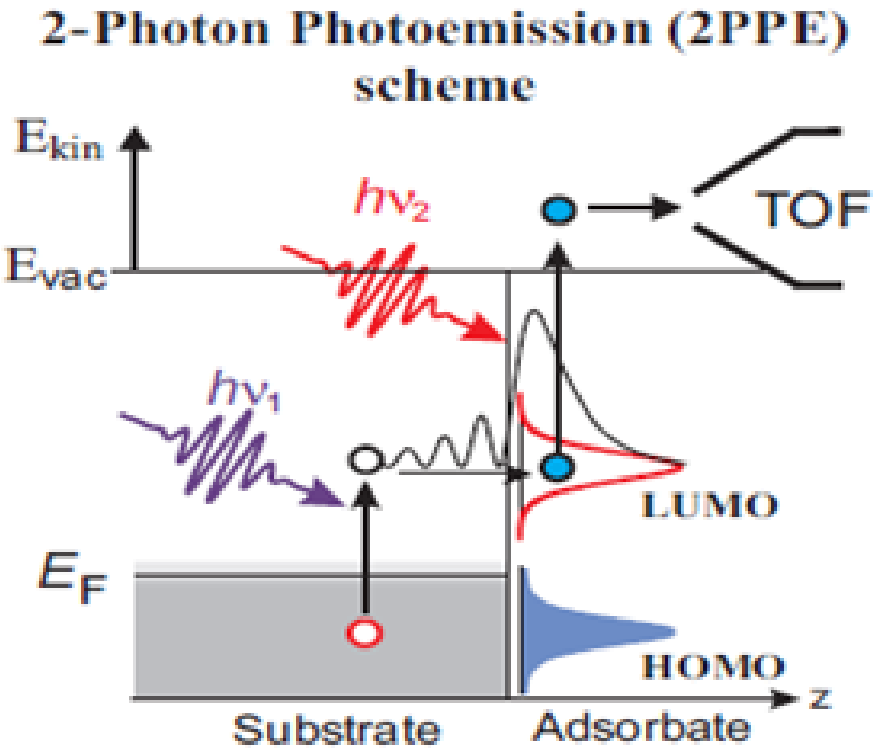

Fig. 1.9 2-Photoemission (2PPE) scheme [39].

1.1.4 Time scale of electron transport using the core - hole clock method

There are multiple ways to measure the time scales of electron transport. One of the simplest methods is known as the core-hole–clock method (CHC) [34, 40, 41]. This method measures the delocalization times of electrons utilizing the lifetime of inner-shell vacancies and the core holes as an internal time standard. The method begins with an electron being excited from a core-hole into an empty orbital (see Fig: 1.10). This process results in an auger decay when one electron fills the core hole while the other electron leaves the system (Fig: 1.11). This results in the energy spectrum being formed (Fig: 1.11 b)

If the molecule is attached to an electrically conductive substrate e.g. metal, electrons from the molecule tunnel into the substrate. This tunnelled electron is no longer shielding the well. When the measured spectrum is recreated it appears similar to the original, except it has a higher energy and has shifted to the right. This occurs because the electron which was at the highest position of the well was screening the transition of the electron which transitioned into the core-hole. This resulted in a lower energy on the spectrum (Fig: 1.12 b, light grey spectrum). The shift of the spectrum between the shielded an unshielded core-hole is known as the spectator shift. In this case for Ar/Pt(111), the spectator shift was 3.8 eV.

The timing is calculated by measuring the life time of the core-hole (Fig: 1.13 a). The spectra of the resonance of the transitions on the upper part of the well are displayed at (Fig: 1.13 b). By integrating the green parts of the spectra it is calculated that it takes approximately 5.5 fs for the electron to decay and fill the core-hole [42]. The green pie chart (Fig: 1.13 a) (right) represents the case when the electron has not tunnelled and the red pie chart represents the case of the electron tunnelling. From the area of these two components the time of electron transport can be determined. In this case the time was 4 fs.

This example is based on an argon atom on a platinum surface. Argon is a noble gas and does not directly bond to the platinum surface. Despite no bond being present, it takes 4 fs for an excited electron in the argon to “jump” into the substrate. The idea of finding a practical

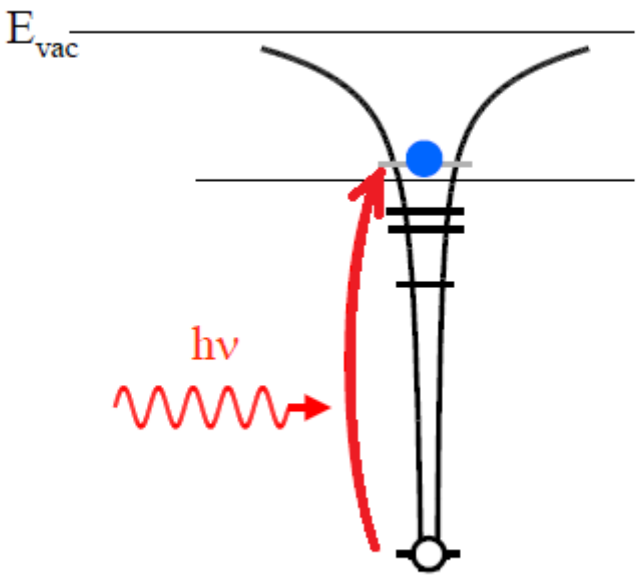

Fig. 1.10 (a) Electron excitation from a core-hole [40, 42].

way of switching a molecule that take only 4 fs seems impossible. Such a transition occurs too rapidly to be measured using the Field Effect Transistors. In the next section a solution to this challenge is addressed.

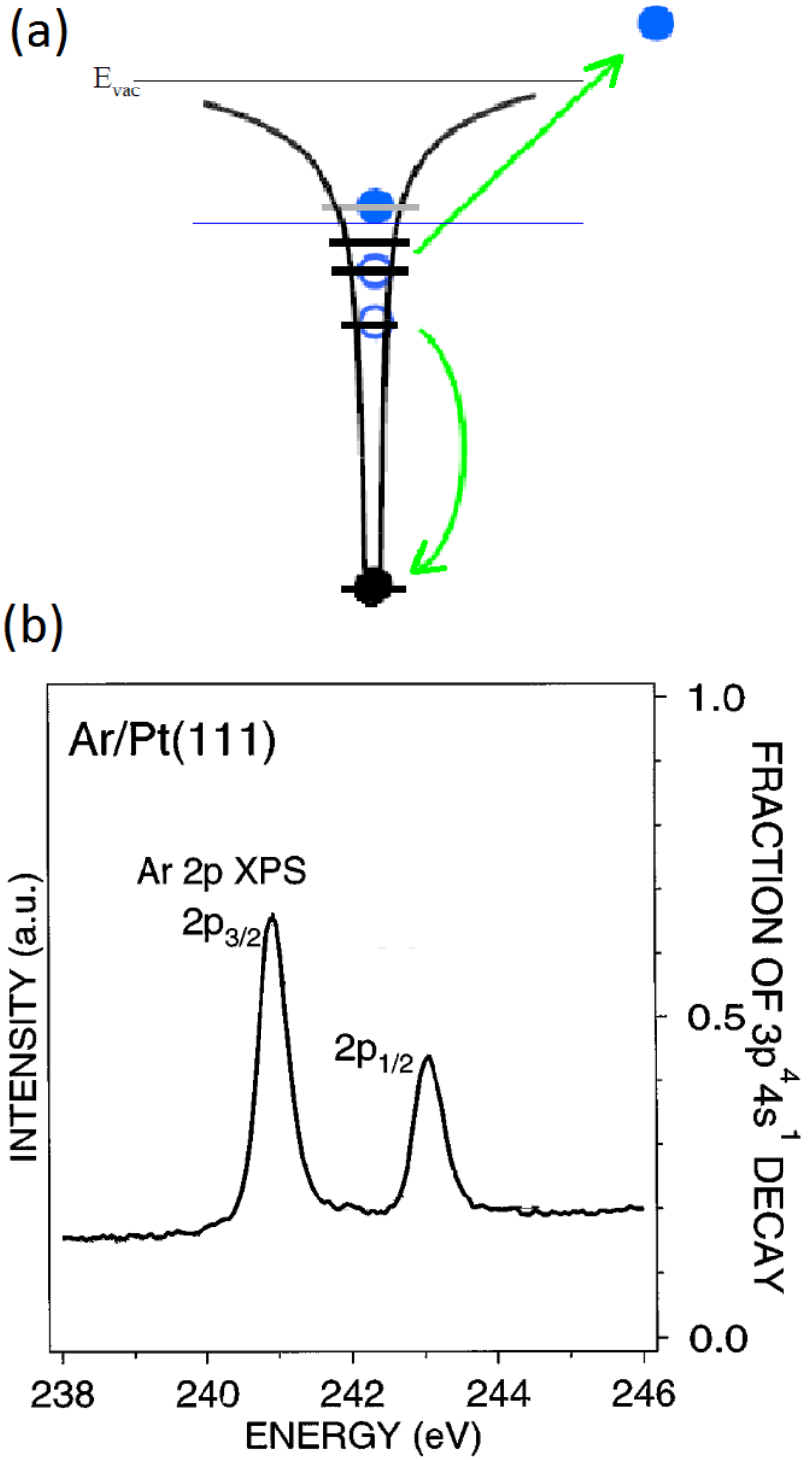

Fig. 1.11 (a) Auger decay of the electron. (b) Energy spectrum of the Auger decay [40, 42].

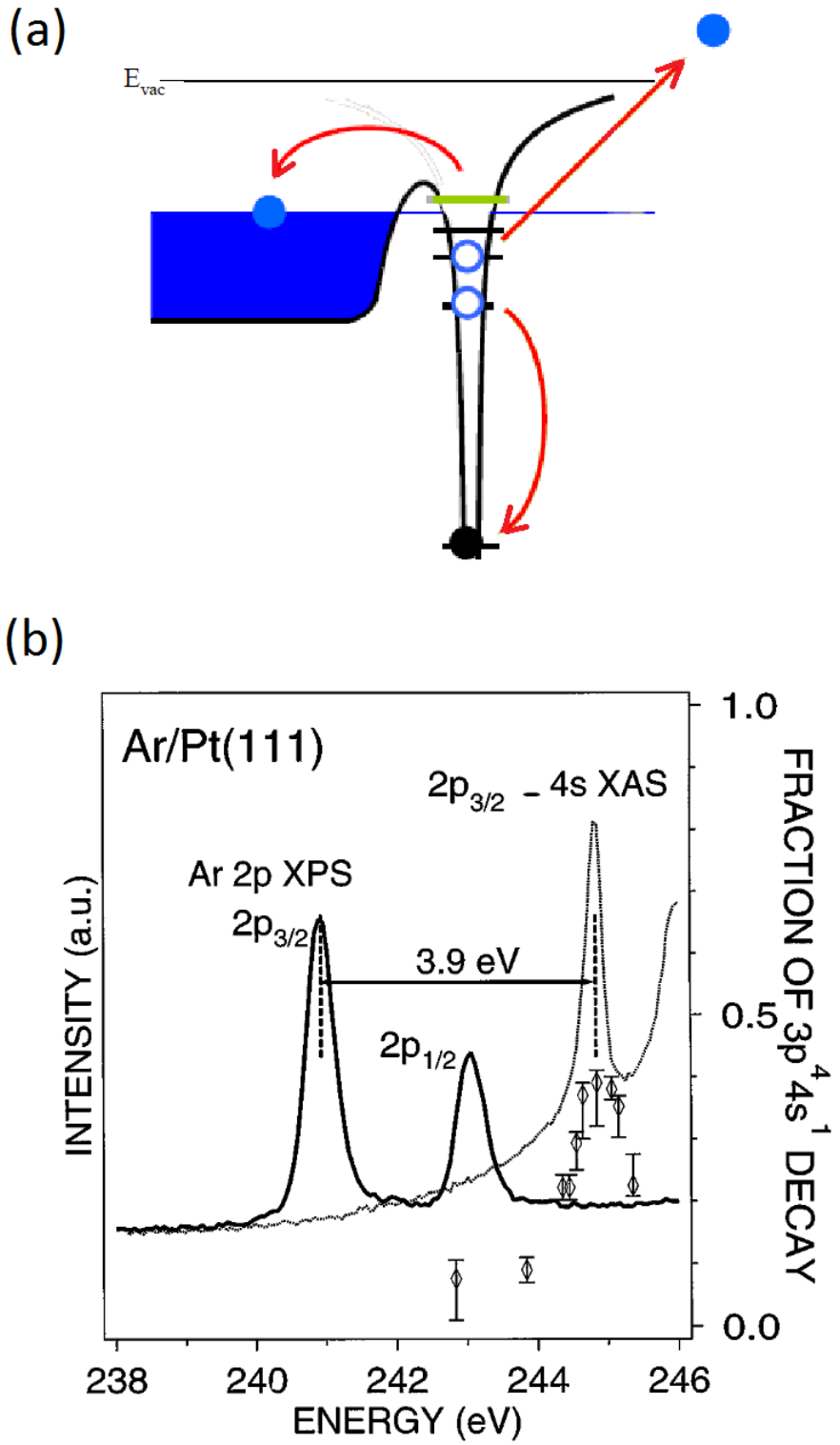

Fig. 1.12 (a) Core-hole clock diagram illustrating electron tunnelling. (b) Ar $2p_{3/2} \rightarrow 4s$ XA and Ar $2p$ XP on a common energy scale. The shift in energy between the two spectra is the spectator shift [40, 42].

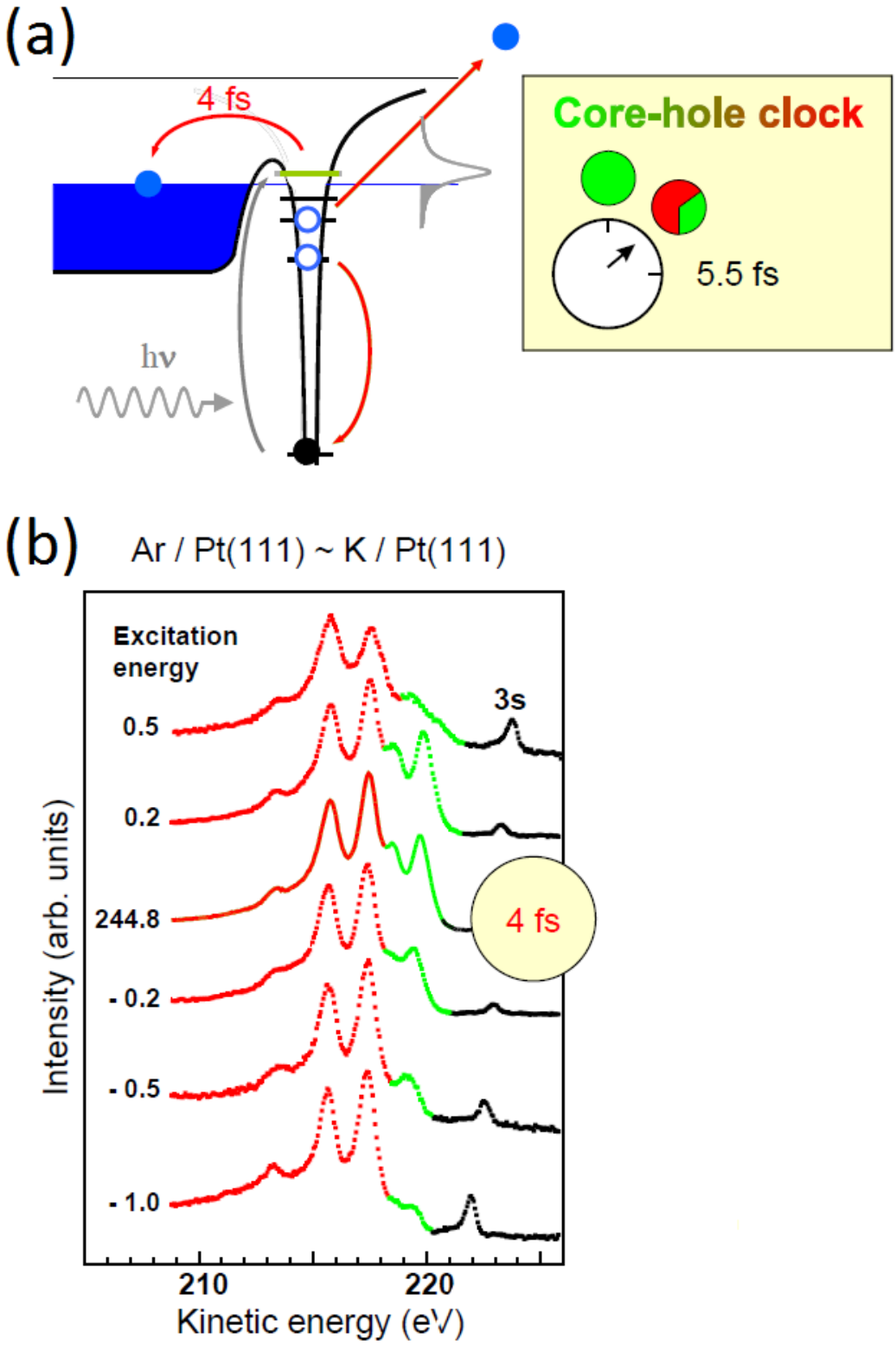

Fig. 1.13 (a) Diagrams for the core-hole clock lifetime calculation (b) Energy spectra used to calculate the time scale of electron transport [40, 42].

1.1.5 Evolution of molecular switches

To solve the problem of the electron taking 4 fs to transition from the molecule to the substrate [40], a surface that is completely inert is used. Unfortunately such surfaces are challenging to create.

In Fig: 1.14 the switch is directly bound to the surface [43]. This device will not be practical because the electron transitions would occur too quickly [44]. It will not be possible to measure the transition using the microwire field effect transistor. Alternatively the receptor molecule can be modified not to be directly bound to the surface (Fig: 1.14 b, c) [45]. One way is to place lift substituents which act as electronic couples (Fig: 1.14 b). These lift the switch off the substrate. Alternatively an anchor and linker (Fig: 1.14 c) can be used. The linker acts as an insulator between the switch and the surface. The anchoring group secures the switch to the substrate.

One prominant example of lift substituents switch is TBI on Au (111) (Fig: 1.14 b). In this experiment the substituents were four inert saturated hydrocarbons [46–49]. The coverage of the molecule was 5 percent because of the bulkiness of the hydrocarbons. Attempts were made to switch this molecule using light but they were unsuccessful.

To solve the low coverage predicament and allow for optical switching the “linker and insulator” system was adopted (Fig: 1.14 c). This involved the use of a self-assembled monolayer on an Au/mica substrate [31]. This system was relatively easier to create and the molecules are more stable compared to TBI on Au (111). They are capable photo-isomerization but require a femtosecond laser to operate. This is not efficient due to the a large number of photons are needed for the device to perform. A femtosecond laser is used because of the fast charge transfer rates [44] and tunnelling of electrons onto the substrate. What is needed is a molecular switch that has a high coverage, is easy to assemble, stable and can undergo

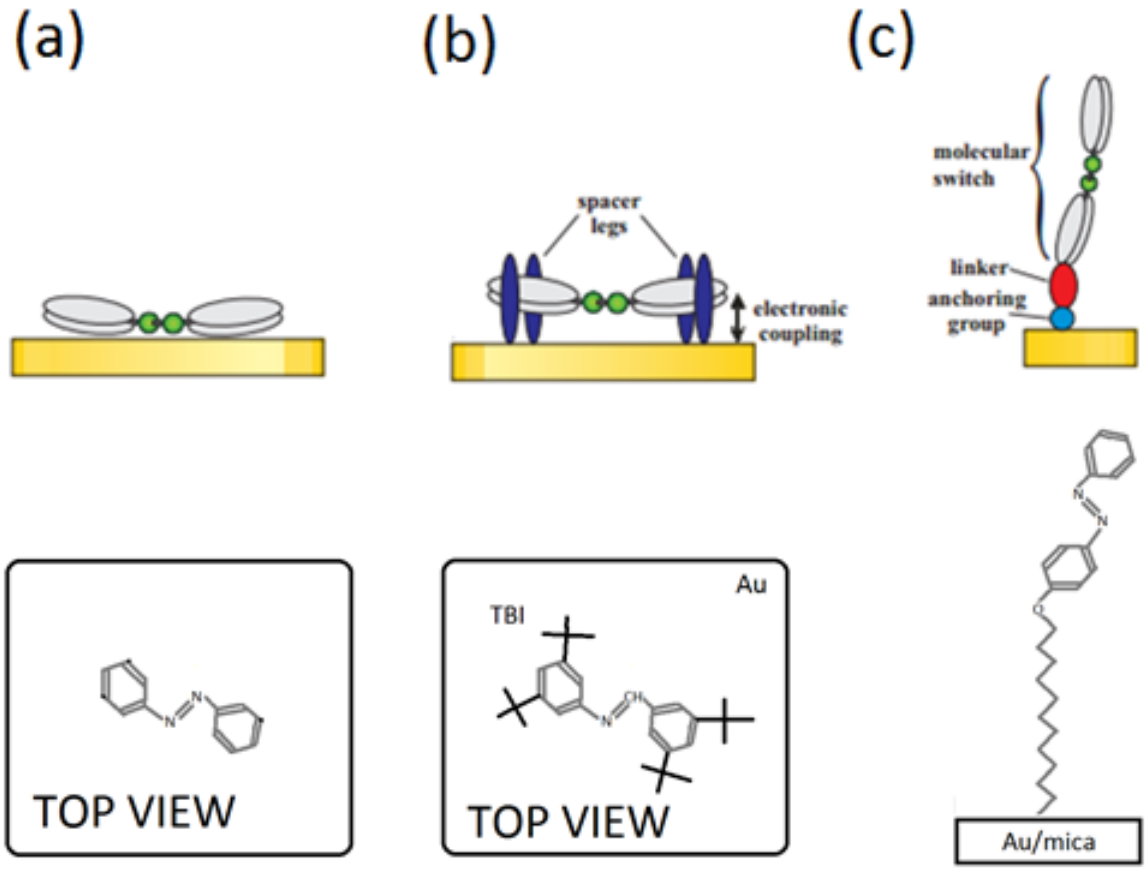

Fig. 1.14 Various ways molecular switches are bound to substrates with examples (a) Azobenzene chromophore directly bound to substrate [45]. (b) TBI attached to a gold substrate [46]. (c) Az11 attached to a Gold/ Mica substrate [31].

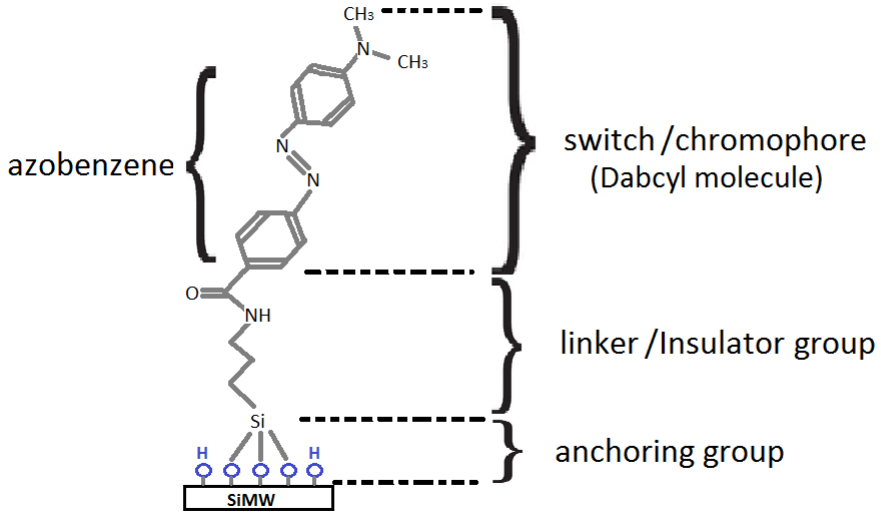

Fig. 1.15 Molecular switch with its parts [50].

photoisomerization with low intensity light.

In a collaborative effort between the University of KwaZulu-Natal and Academia Sinica, a self assembled molecular switch which can undergo photoisomerization with low intensity light was created (Fig: 1.15). The molecule used has a higher coverage than TBI on Au (111) and was found to undergo photoisomerization using Vis and UV LEDs. This molecule is an improvement on the Az11/C12 self assembled monolayer of Au/Mica substrate because it does not need a laser to function. This makes it a more energy efficient and practical device.

The anchoring group attaches the linker and switch to the substrate. A large anchor group also allows the space between neighbouring molecules to be sufficient for the chromophores to enter the *cis* state without being sterically hindered [51]. The linker acts as an insulator by electronically decoupling the switch from the substrate. In the absence of an insulator group the switch would be too close to the Fermi level of the substrate and quenching would occur.

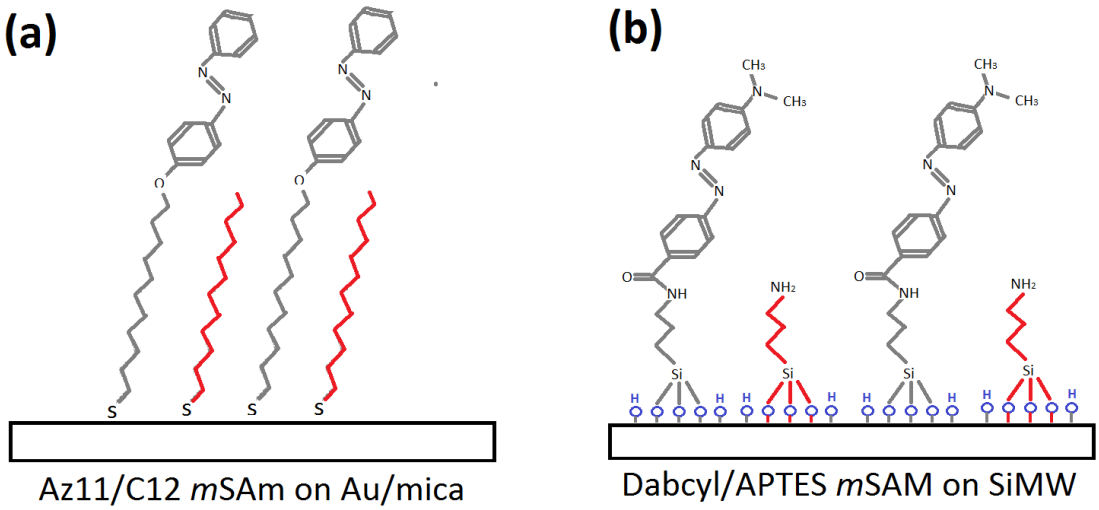

Fig. 1.16 Different types of spacer intergated onto *m*SAMs: (a) Az11 (chromophore functionalized thiol) with C12 spacers (red) and one legged anchoring groups [31] (b) Dabcyl (chromophore functionalized thiol) with APTES spacer (red) used in this research (note the 3 legged anchoring groups which also contribute to lateral spacing).

1.2 Increasing Photoisomerization efficiency

If an azobenzene functionalised Self Assembled monolayer Azo-SAM is too densely packed, the molecular switched can become sterically hindered by their neighbours [9]. This problem can be addressed by mixing the molecular switches with spacer molecules, creating free volume between molecular swiches [10]. One way to make free volume for photoisomerization is to create mixed (bicomponent) self assembled monolayers (*m*SAM). These consist of the chromophore functionalised thiol and a shorter spacer molecule (Fig: 1.16). Typically *m*SAMs are created using a solution which is a mixture of the chromophore functionalized thiol and the unfuctionalized thiol. Due to the difference in intermolecular interactions between the lingand molecules in solution the ratio of thiols in solution does not necessarily correspond to the ratio on the *m*SAM.

To counteract this problem a two step SAM creation method. Another solution to create free volume is to make each chromophore functionalized thiol molecule have more than one surface anchor. This technique was used and taken one step further by increasing the anchor of not just the chromophore functionalized thiol but also the unfunctionalized thiol.

These improvements greatly increase the efficiency of photoisomerization. In the following chapter the isomerization kinetics of the *m*SAM will be derived, microwire field effect transistor theory and emerging applications of molecular switches will be briefly discussed.

1.3 Molecular switch operation

Diagrams illustrate the reversible photoisomerization process of dabcyl/APTES *m*SAM are shown in Fig: 1.17 and Fig: 1.18. For simplicity the APTES spacers are not included (Fig: 1.17).

The I versus t plot of the microwire was obtained in the absence of optical excitation for 50 seconds to allow the current to stabilize (Fig: 1.17 a). To trigger the isomerization cycles, the SiMWFET was exposed to UV light (365 nm) for 1 second (Fig: 1.17 b). This causes the majority of the molecular switches to enter the *cis* state along with the excitation of electron-hole pairs in the substrate. The drop in the microwire's conductance is detected during the 0.4 second rest period in the dark (Fig: 1.17 c). The transition from the thermodynamically stable *trans* to the metastable *cis* form is induced via irradiation with visible light (Fig: 1.18 a). The migration of electrons to the surface of the substrate is detected during the 0.4 second rest in the dark (Fig: 1.18 b).

A simplified diagram describing the molecular switching process is represented in Fig: 1.19. The APTES spacers act as insulators preventing quenching from occurring. The negative gate voltage is causes electrons to migrate onto the surface of the channel. The electron transitions cause a change in conductance which is measurable from source to drain. In the following chapter the isomerization kinetics of *m*SAMs will be derived.

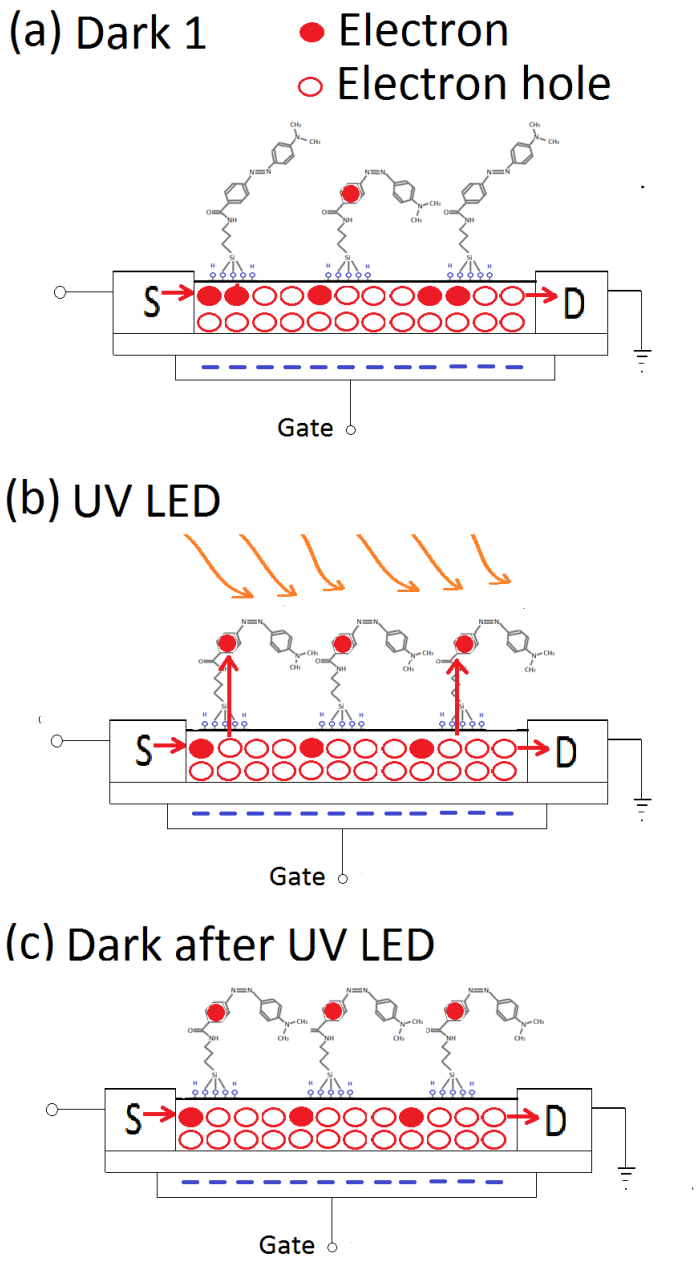

Fig. 1.17 (a) Natural state of the dabcyl/APTES *m*SAM. (b) UV illumination phase. (c) Electron hole pair excitation and electron tunnelling [52].

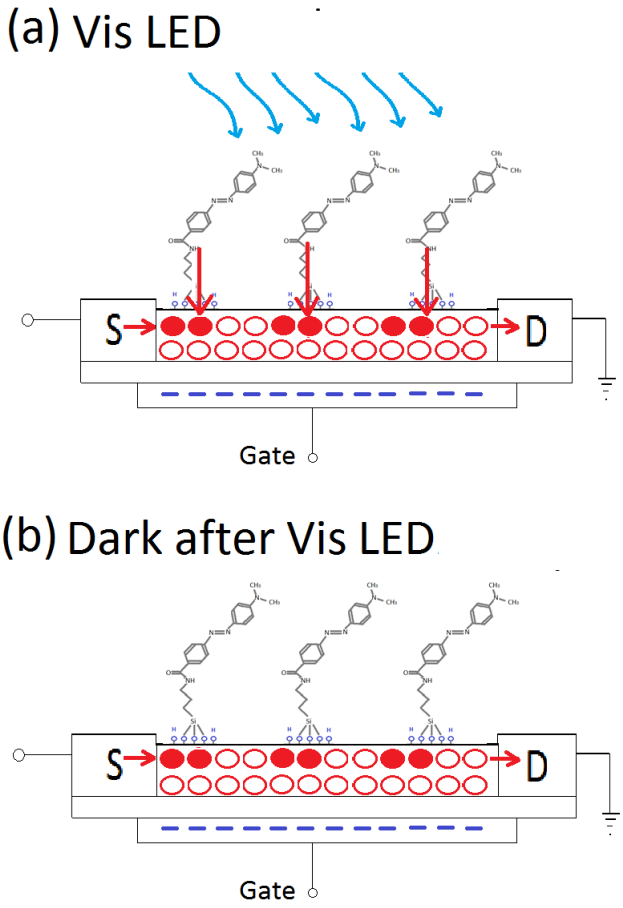

Fig. 1.18 (a) Visible light illumination on dabcyl/APTES *m*SAM. (b) Charge injection into the microwire FET [52].

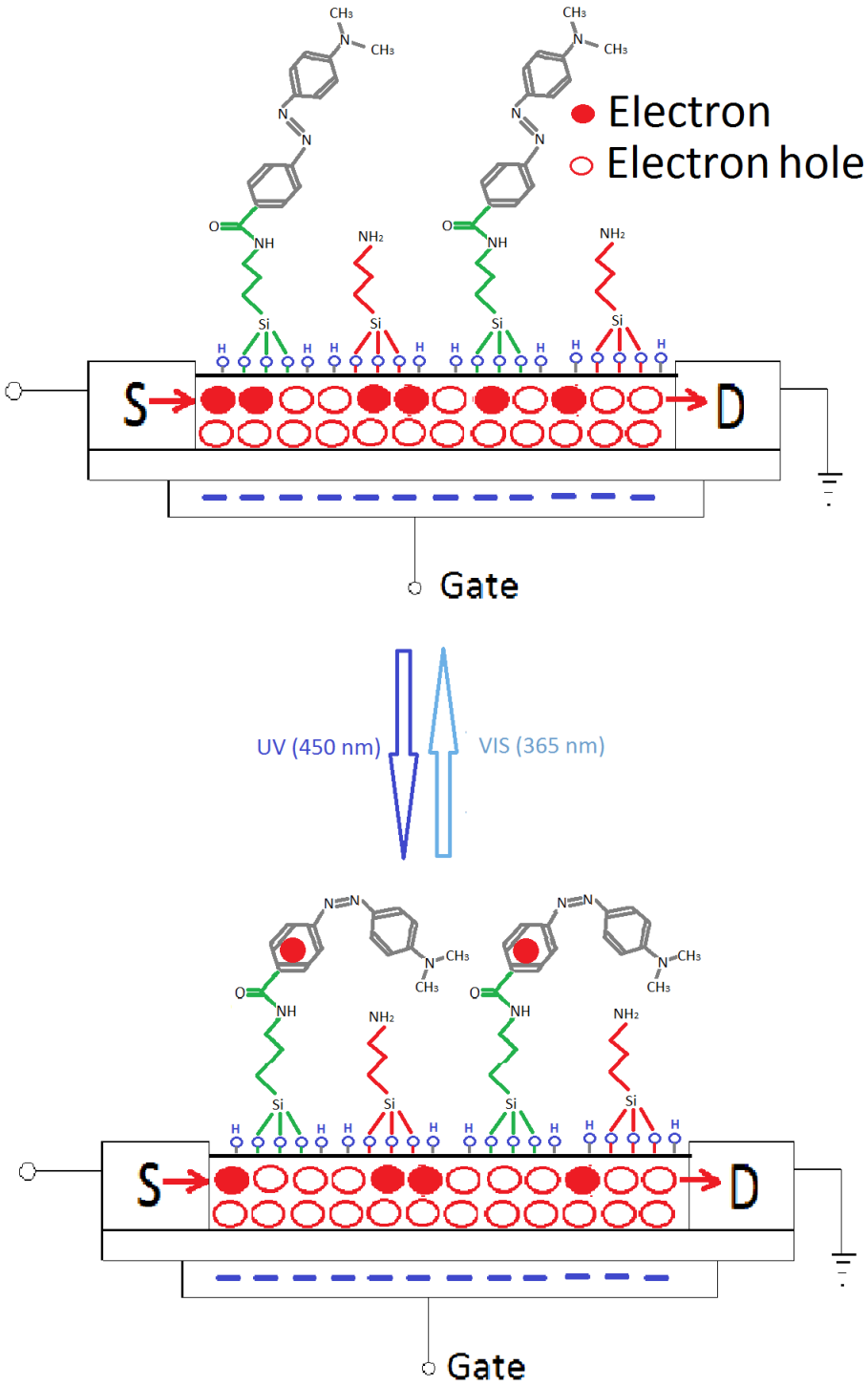

Fig. 1.19 Photo-isomerism of dabcyl/APTES *m*SAM [52].

Chapter 2

Isomerization Kinetics and SiMW-FET Theory

2.1 Derivation of Isomerization Kinetics

2.1.1 Differential Equation

In this section a theoretical model is used to propose a method to calculate the photoswitching efficiency of dabcyl/APTES *m*SAM. Pioneering work by Thomas Moldt et al. [53] resulted in the derivation of isomerization kinetics of the bicomponent Az11/C12 *m*SAM. Since the Az11/C12 *m*SAM and dabcyl/APTES *m*SAM operate under similar governing dynamics we adapt their findings in our research. These equations appear as (2.1.1) to (2.35) in [53].

Consider an equilibrium reaction between the *trans* and *cis* isomer of azobenzene:

$$trans \underset{k_c}{\overset{k_t}{\rightleftharpoons}} cis.$$

The *trans* isomer is thermodynamically stable. Both *trans* and *cis* isomerization reactions can be driven by light. Isomerization rate constant of *trans* molecules is totally dependent on the photon-induced k_t^{ph}, whereas the rate constant of the *cis* molecules consists of a photon-induced rate constant k_c^{ph} as well as the thermal relaxation rate constant which can be expressed as k_t^{th}. These can be expressed as:

$$k_t = k_t^{ph} \qquad \text{and} \qquad k_c = k_c^{ph} + k_c^{th}. \tag{2.1}$$

The equilibrium constant K is the ratio of the reaction rate constants of the *trans* and *cis* molecules, respectively. It can be expressed as:

$$K = \frac{k_t}{k_c} = \frac{k_t^{ph}}{k_c^{ph} + k_c^{th}}. \tag{2.2}$$

Assuming the total number of molecules is N remains the same, given that

$$N = N_c + N_t. \tag{2.3}$$

Where N_c and N_t are the numbers of *cis* and *trans* molecules respectively. The mole functions of *cis* and *trans* are defined as

$$\chi_c(t) = \frac{N_c(t)}{N} \qquad \text{and} \qquad \chi_t(t) = \frac{N_t(t)}{N}. \tag{2.4}$$

Assuming first order kinetics the differential equation for χ_c is:

$$\frac{d\chi_c}{dt} = -(k_c^{ph} + k_c^{th})\chi_c(t) + k_t^{ph}\chi_t(t) \tag{2.5}$$

$$= -(k_c^{ph} + k_c^{th})\chi_c(t) + k_t^{ph}\left[1 - \chi_c(t)\right] \tag{2.6}$$

$$= -(k_c^{ph} + k_c^{th} + k_t^{ph})\chi_c(t) + k_t^{ph}. \tag{2.7}$$

With the initial condition $\chi_c(0) = \chi_{c,0}$, the solution of the differential equation is:

$$\chi_c(t) = \frac{1}{k_t^{ph} + k_c^{ph} + k_c^{th}} \cdot \Big[k_t^{ph} + \big[-k_t^{ph} + \chi_{c,0}(k_t^{ph} + k_c^{ph} + k_c^{th}) \big] exp[-(k_c^{ph} + k_c^{th} + k_t^{ph})t] \Big]. \tag{2.8}$$

2.1.2 Transient Auger Yield

The photoisomerization kinetics are examined by Thomas Moldt et al using Auger yield Near Edge X-Ray Absorption Fine Structure (NEXAFS) [53]. Due to radiation damage the total number of molecules N is not constant but decreases over time. We assume an exponential decay with N_0 being the total number of molecules at $t = 0$ and k_{rad} being the decay rate constant:

$$N(t) = N_0 exp(-k_{rad} t) \tag{2.9}$$

Using this relation and the definition of the mole fraction of *cis* molecules in equation (2.4), the number of molecules in the *cis* state can be written as

$$N_c(t) = N_0 exp(-k_{rad} t) \chi_c(t). \tag{2.10}$$

The Auger electron yield $A_{Auger}(t)$ at the trailing edge of the π^* resonance was recorded (Fig: 2.1). The Auger yield $A_{Auger}(t)$ is a linear combination of N_c and N_t, with a_c and at being the respective coefficients. A background C of secondary electrons was also observed [53].

$$A_{Auger}(t) = a_c N_c(t) + a_t N_t(t) + C \tag{2.11}$$

$$= a_c N_c(t) + a_t [N(t) - N_c(t) + C \tag{2.12}$$

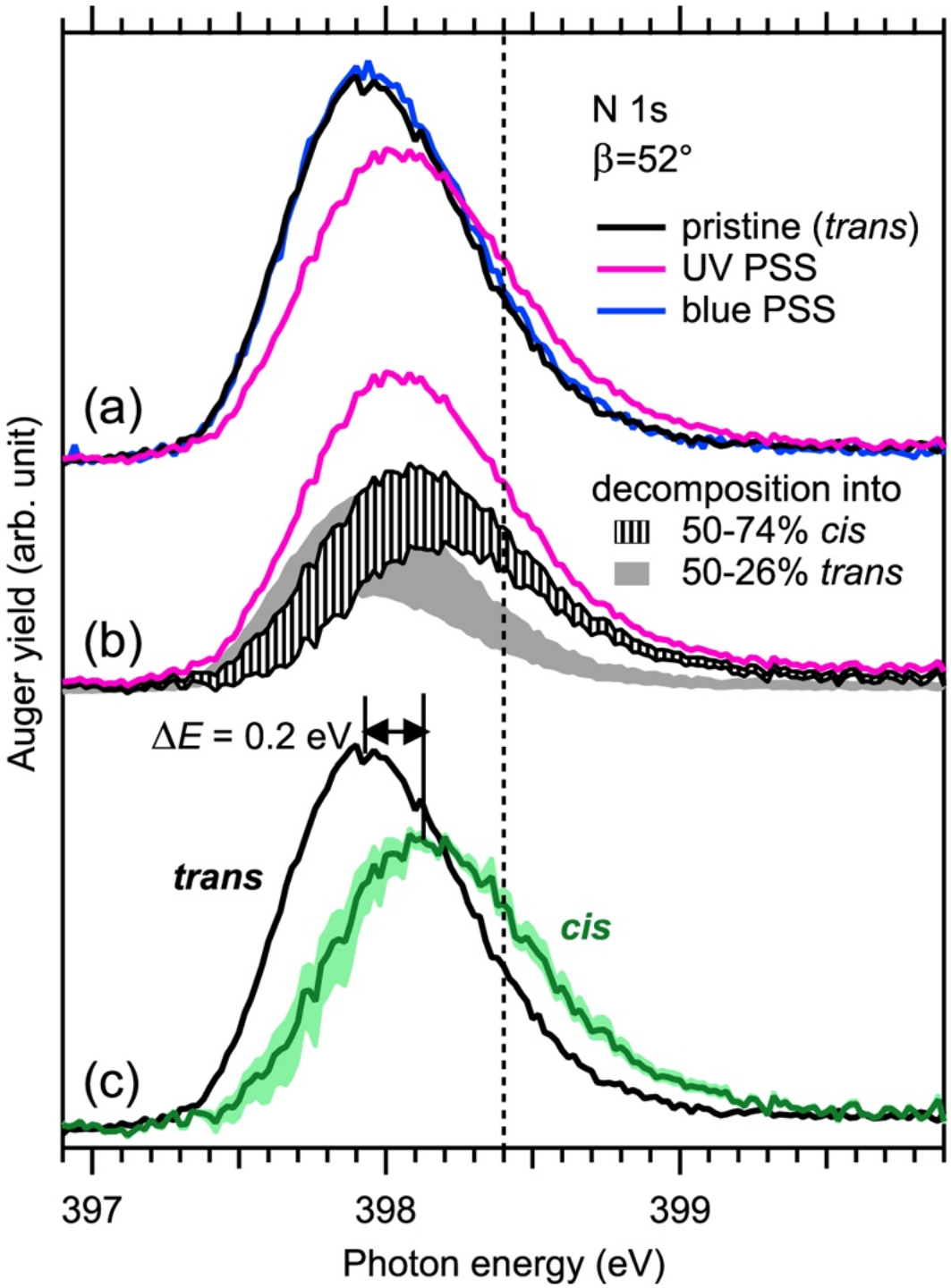

Fig. 2.1 High-resolution N 1s NEXAFS spectra of the LUMO resonance. (a) Pristine state (i.e., pure *trans*) and the PSSs under UV and blue light exposures. The dashed line at 398.4 eV represents the photon energy at which the isomerization kinetics were monitored (Fig: 2.2). (b) Spectrum of the UV PSS decomposed into its *trans* and *cis* components. (c) Spectrum of the pure *cis* isomer. The range of uncertainty corresponds to the upper and lower limits of the amount of *cis* molecules [53]

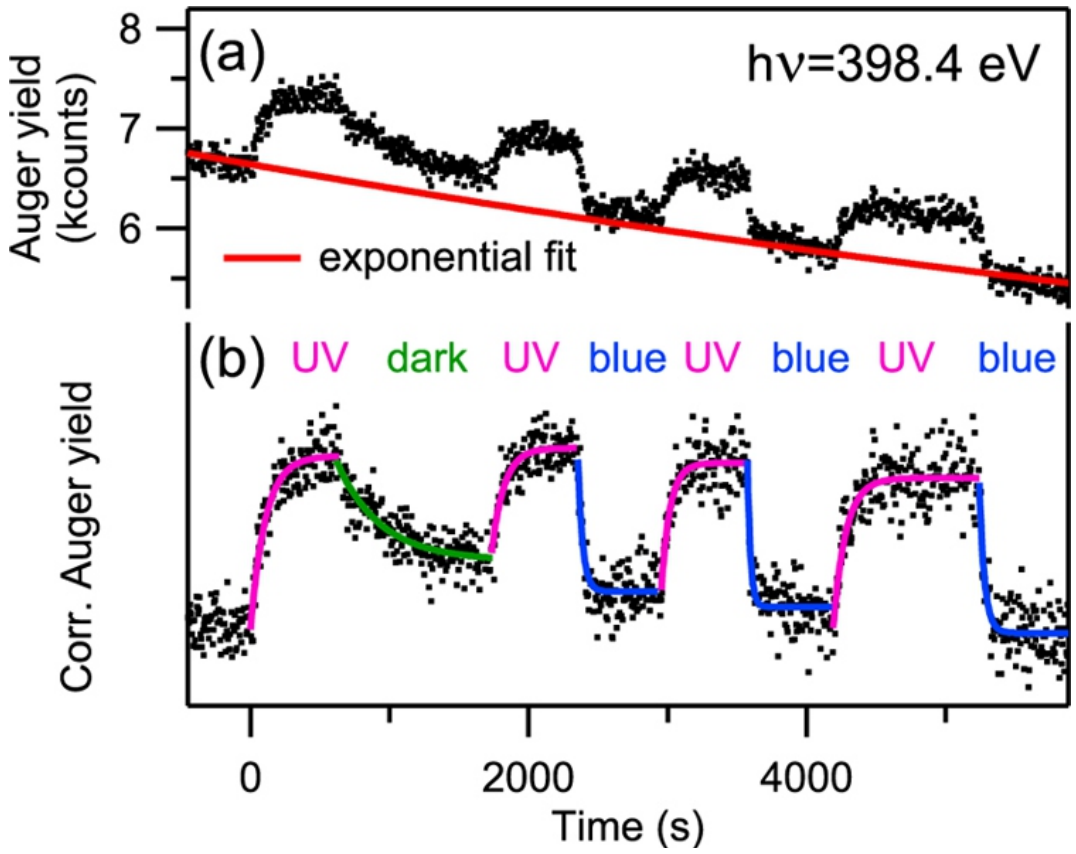

Fig. 2.2 NEXAFS measurements on Az11/C12 *m*SAM [53]. (a) The overall decrease in the signal caused by X-ray beam damage and is corrected for by an exponential fit (red line). (b) Corrected data.

Using (2.9) and (2.10), we obtain:

$$A_{Auger}(t) = N_0 exp(-k_{rad}t)a_c\chi_c(t) + a_t[1-\chi_c(t)] + C \tag{2.13}$$

$$= N_0 exp(-k_{rad}t)[(a_c - a_t)\chi_c(t) + a_t] + C \tag{2.14}$$

We apply the solution (2.8) of the differential equation (2.7) into the expression of the Auger electron yield (2.14). We define the effective rate constant k_{eff} and the number of *cis* molecules $N_{c,0}$ at $t = 0$:

$$k_{eff} = k_c^{ph} + k_c^{th} + k_t^{ph} \tag{2.15}$$

$$N_{c,0} = N_0\chi_{c,0} \tag{2.16}$$

Thus, we obtain the expression:

$$A_{Auger}(t) = \frac{1}{k_{eff}} exp(-k_{rad}t)\Big(N_0[a_c k_t^{ph} + a_t(k_c^{ph} + k_c^{th})] + (a_c - a_t).$$

$$[k_t^{ph}(N_{c,0} - N_0) + (k_c^{ph} + k_c^{th})N_{c,0}]exp(-k_{eff}t)\Big) + C \tag{2.17}$$

We correct the Auger yield (2.17) for the beam damage in order to be able to fit the transient Auger signal with a single exponential function [53]. We subtract the constant C and then divide by $exp(k_{rad}t)$ and obtain the corrected Auger yield $A_{Auger}^{corr}(t)$:

$$A_{Auger}^{corr}(t) = \frac{1}{k_{eff}}\Big(N_0[a_c k_t^{ph} + a_t(k_c^{ph} + k_c^{th})] + (a_c - a_t).$$

$$[k_t^{ph}(N_{c,0}-N_0)+(k_c^{ph}+k_c^{th})N_{c,0}]exp(-k_{eff}t)\Big) \tag{2.18}$$

The offset C was read from the uncorrected spectra below the N 1s edge,the rate constant k_{rad} was determined by fitting an exponential function to the sections of data assigned to the *trans* species [53].

2.1.3 Isomerization Rate Constants

In the dark (2.18) reduces to

$$A_{Auger}^{corr}(t) = a_t N_0 + (a_c - a_t)N_{c,0}exp(-k_c^{th}t). \tag{2.19}$$

Thus, the transient signal of the corrected Auger yield showed only one rate constant k_c^{th} for thermal isomerization of the *cis* molecules [53]. Upon illumination with light of arbitrary wavelength an effective rate constant was observed (2.15). We first want to extract an expression for the light-induced *trans–cis* isomerization rate constant k_t^{ph} [53]. We factor out k_T^{ph} in (2.15) and then apply the definition for the equilibrium constant (2.2):

$$k_{eff}^{ph} = k_t^{ph}\left(\frac{k_c^{ph}+k_c^{th}}{k_t^{ph}}+1\right) \tag{2.20}$$

$$= k_t^{ph}\left(\frac{1}{K}+1\right). \tag{2.21}$$

Rearranging the equation for k_t^{ph} we obtain:

$$k_t^{ph} = k_{eff}^{ph}\left(\frac{1}{K}+1\right)^{-1}. \tag{2.22}$$

Instead of the equilibrium constant K, we want to express k_t^{ph} as a function of the mole fraction of *cis* molecules χ_c^{ph} in the PSS, i.e. the *trans–cis* isomerization yield [53]. We define

the symbols N_c^{ph} and N_t^{ph} for the number of *cis* and *trans* molecules in the PSS, respectively, use the definition of the mole fraction (2.4) and the expression (2.3) for the total number of molecules and obtain the equation for χ_c^{ph} to be

$$\chi_c^{ph} = \frac{N_c^{ph}}{N} = \frac{N_c^{ph}}{N_c^{ph} + N_t^{ph}}. \tag{2.23}$$

To obtain χ_c^{ph} as a function of the equilibrium constant K, we invert χ_c^{ph} to get

$$\frac{1}{\chi_c^{ph}} = \frac{N_c^{ph} + N_t^{ph}}{N_c^{ph}} = \frac{N_t^{ph}}{N_c^{ph}} + 1 = \frac{1}{K} + 1. \tag{2.24}$$

In the last step we used the law of mass action from which it follows that in the Photo stationary state (PSS), the equilibrium constant K for the *trans-cis* photoisomerization is equal to the number of molecules in the *cis* state divided by the number of molecules in the *trans* state [53]. The right side of (2.24) is inserted into (2.22), obtain

$$k_t^{ph} = k_{eff}^{ph} \chi_c^{ph}. \tag{2.25}$$

In (2.23) we assume that all molecules in the system are part of the equilibrium reaction, i.e., all molecules are photoswitchable [53]. This assumption is justified for the mixed SAMs with $\approx 20\%$ Az11. In the following we rearrange (2.15) in order to obtain an expression for k_c^{ph} which is expressed as

$$k_c^{ph} = k_{eff}^{ph} - k_c^{th} - k_t^{ph} = k_{eff}^{ph}(1 - \chi_c^{ph}) - k_c^{th} = k_{eff}^{ph} \chi_t^{ph} - k_c^{th}. \tag{2.26}$$

In this case $\chi_t^{ph} = 1 - \chi_t^{ph}$ is the photoisomerization yield [53]. This yield and the rate of constants are dependent on the wavelength of light used in the experiment [53]. The equations that follow are applicable for the irradiation of visible (ph = Vis) and UV light (ph = UV).

2.1.4 Determination of Cross Sections

The isomerization cross section is given by [53]:

$$\sigma = \frac{k}{J} = k\frac{E_{ph}}{I_{ph}}, \tag{2.27}$$

with the rate constant k, the photon flux J, the photon energy E_{ph} and the light intensity I_{ph}. Therefore, effective cross sections σ_{eff}^{ph} for UV and blue illumination were calculated according to

$$\sigma_{eff}^{UV} = k_{eff}^{UV}\frac{E_{ph}}{I_{ph}}; \qquad \sigma_{eff}^{Vis} = k_{eff}^{Vis}\frac{E_{ph}}{I_{ph}}. \tag{2.28}$$

These effective cross sections neglect the fact that isomerization is an equilibrium reaction [53]. The *trans–cis* photoisomerization cross section σ_t^{ph} can be calculated according to

$$\sigma_t^{ph} = k_t^{ph}\frac{E_{ph}}{I_{ph}} = k_{eff}^{ph}\chi_c^{ph}\frac{E_{ph}}{I_{ph}}. \tag{2.29}$$

Similarly, using (2.26), the *cis – trans* photoisomerization cross section σ_c^{th} is given by

$$\sigma_c^{ph} = \left(k_{eff}^{ph}\chi_t^{ph} - k_c^{th}\right)\frac{E_{ph}}{I_{ph}}. \tag{2.30}$$

2.1.5 Determination of Photoisomerization Yields

The calculation of cross sections according to (2.29) and (2.30) requires the determination of the respective isomerization yields [53]. For the case of illumination with UV light (ph = UV), a *trans-cis* photoisomerization yield χ_c^{UV} of at least 50% was determined by NEXAFS spectroscopy [53], as illustrated in Fig: 2.1. In order to obtain an upper limit for χ_c^{UV} we rearrange (2.24) to give

$$\chi_c^{UV} = \left(1+\frac{1}{K}\right)^{-1} = \left[1+\frac{k_c^{UV}+k_c^{th}}{k_t^{UV}}\right]^{-1} = \frac{k_t^{UV}}{k_c^{UV}+k_c^{th}+k_t^{UV}}. \tag{2.31}$$

By using (2.15) we obtain the expression [53]:

$$\chi_c^{UV} = \frac{k_{eff}^{UV} - k_c^{th} - k_c^{UV}}{k_{eff}^{UV}}. \tag{2.32}$$

For $k_c^{UV} \to 0$ the upper limit of 74 % for the experiment at ca. 110 K [53], the value for χ_c^{UV} lies between 50 and 74 %. The rate of thermal isomerization should be considered because it limits the yield [53]. It is possible to increase the yield by having a higher UV photon dosage or by changing the medium of operation to air where the thermal isomerization constant is negligible [53]. Applying these limits, the yield can be estimated using the equations (2.29) and (2.30) for σ_t^{UV} and σ_c^{UV}, respectively:

$$\frac{\sigma_t^{UV}}{\sigma_t^{UV} + \sigma_c^{UV}} = \frac{k_{eff}^{UV}\chi_c^{UV}}{k_{eff}^{UV}\chi_c^{UV} + k_{eff}^{UV}(1 - \chi_c^{UV}) - k_c^{th}} = \frac{k_{eff}^{UV}\chi_c}{k_{eff}^{UV} - k_c^{th}}. \tag{2.33}$$

The equation is rearranged for χ_c^{UV} to obtain:

$$\chi_c^{UV} = \frac{\sigma_t^{UV}}{\sigma_t^{UV} + \sigma_c^{UV}} \left(1 - \frac{k_c^{th}}{k_{eff}^{UV}}\right). \tag{2.34}$$

In the case where $k_c^{th} \ll k_{eff}^{UV}$ it is possible to obtain:

$$\chi_c^{UV} \approx \frac{\sigma_t^{UV}}{\sigma_t^{UV} + \sigma_c^{UV}}. \tag{2.35}$$

When evaluating equation 2.35 using the values given in Tables 2.1 and 2.2 [53], it was found that the yield expected would lie between 67% and 100% [53]. In the case of blue illumination the spectrum of the blue photo stationary state (PSS) is almost identical to the

Table 2.1 Cross sections of two samples with σ_t^{UV} and σ_c^{UV} are the *trans-cis* and *cis-trans* photoisomerization cross sections under irradiation of UV light. [c]Az11/C12 *m*SAM with 20 % chromophore coverage and [d]Measured at room temperature. Table sourced from [53].

sample	method	σ_t^{UV}($\times 10^{-18}$, cm ^{2})	σ_c^{UV}($\times 10^{-18}$, cm ^{2})
Az11/C12 in vacuum [c]	NEXAFS	0.9 ± 0.2	0.2 ± 0.2
Az11 in methanol [d]	UV/vis	27 ± 2	0.82 ± 0.06

Table 2.2 Cross sections of two samples with σ_t^{blue} and σ_c^{blue} are the *trans-cis* and *cis-trans* photoisomerization cross sections under irradiation blue light. [c]Az11/C12 *m*SAM with 20 % chromophore coverage and [d]Measured at room temperature. Table sourced from [53].

sample	method	σ_t^{blue}($\times 10^{-18}$, cm ^{2})	σ_c^{blue}($\times 10^{-18}$, cm ^{2})
Az11/C12 in vacuum [c]	NEXAFS	0.05 ± 0.01	1.0 ± 0.3
Az11 in methanol [d]	UV/vis	1.8 ± 0.1	5.2 ± 0.3

pristine spectrum in Fig: 2.1, therefore we assume a *cis–trans* isomerization yield χ_t^{Vis} of 95% for Az11/C12 *m*SAMs [53].

By performing NEXAFS measurements on the dabcyl/APTES *m*SAM system as well as UV/vis spectroscopy on a dabcyl in methanol it would be possible to accurately calculate the isomerization yield of the dabcyl/APTES *m*SAM. It is important to note that these experiments were are not performed on pure *trans* or *cis* isomers but on a photo-stationary mixtures enriched in one of the two isomers.

Attention is will now be drawn to the substrate which the molecules are attached to, in this case the SiMWFET. We will briefly explain its suitability as a substrate due to its variable conductance.

2.2 Isomerization and environmental conditions

Isomerization in dabcyl functionalised SAMs is strongly dependent upon the environmental conditions [53]. Thermal relaxation times were observed of the order of seconds in vacuum whereas in air it was hindered, occurring on a time scale of more than a minute. This observation

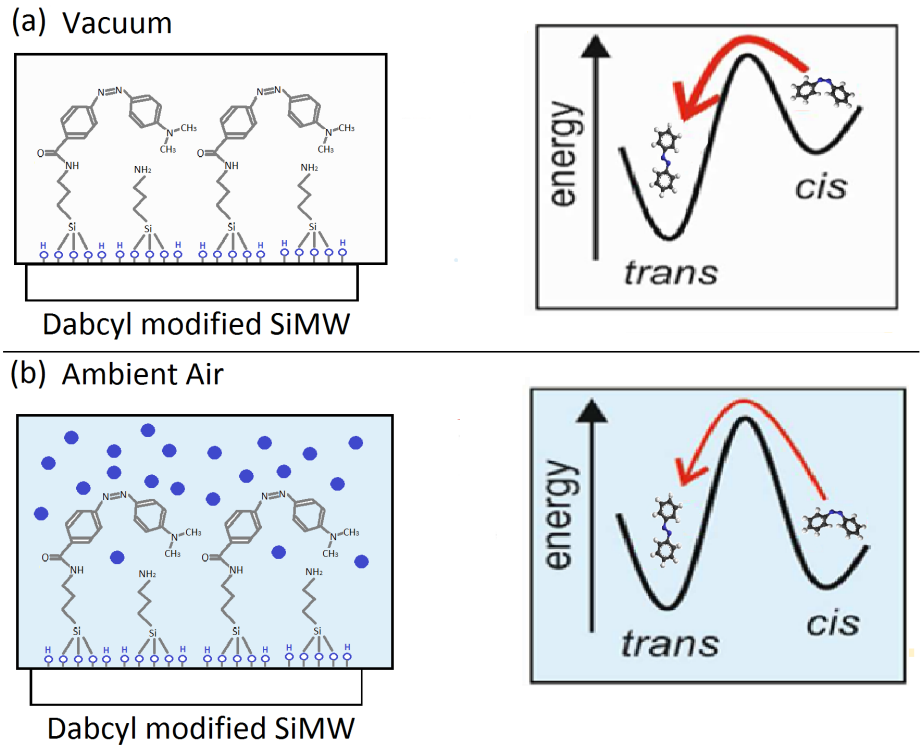

Fig. 2.3 Operation of the device in and out of a vacuum. The energy barrier is much lower from *cis* to *trans* out of a vacuum than in ambient conditions [53]. (a) In air thermal relaxation occurs more easily because there is a lower energy barrier (right). (b) In ambient conditions (left) adventitious water (blue dots) on the *m*SAM forms a higher energy barrier, delaying thermal relaxation (right).

is attributed to the presence of adventitious water on the SAM under ambient conditions [53], which stabilizes the more polar *cis* state of the azobenzene chromophores in the SAM (Fig: 2.3). The photoisomerization of the *m*SAM is very efficient. This yield is limited by the rapid thermal relaxation [53].

2.3 Microwire FET Operation

This section discusses the theory behind the selection of ground and source to drain voltage that allowed the FET to detect the photoisomerization of the molecular switch.

Silicon has four outer electrons in its valence shell. This allows it to form bonds with its four nearest neighbours. Since all electrons are stuck in bonds few of them ever get enough energy to travel through the lattice. Silicon is a semiconductor because it has a small number of mobile charges. Semiconductors were not really useful until the advent of doping. There are two kinds of doping, n-type and p-type. To make n type silicon a small amount of phosphorous is doped into it. Phosphorous has an extra electron so the new silicon material has more mobile charge carriers so it conducts current better then pure silicon.

P-type doping is performed with boron, added in small quantities into the pure silicon lattice. Boron has three electrons in its valence shell so when it is in the silicon lattice there will be a missing electron or hole. This increases the conductivity of the silicon allowing electrons to freely move into it. Both n and p-type semi-conductors are electrically neutral.

The microwire field effect transistor used in this dissertation was p-doped. By applying a negative voltage at the gate, the conductance of the channel can be varied. The negative ground voltage creates an electric field that pushes electrons away from it. The electrons move towards the surface of the channel. This causes the channel to be more conductive. The lower the ground voltage the more conductive the channel becomes. Therefore more electrons can move from the source to the drain. If the substrate is a metal then it is highly probable for the electrons to inject from the molecule to the substrate. Semi-conductive substrates are ideal because their conductance can be easily altered allowing control of the probability of charge transfer. Since the substrate is a semi-conductor its conductance can be varied by changing the gate voltage. If the gate voltage is too negative there will be an absence of electron holes on the surface of the channel. In order for an electron-hole pairs to become excited or for an electron to tunnel from a molecule to a silicon, substrate there has to be the presence of electron holes. If there are

no electron-hole pairs the changes in current due to the photoisomerization can not be measured.

If the gate voltage is too large, the channel become less conductive. The channel behaves like an insulator and electrons struggle to move from one contact to the other. Therefore the probability of charge injection from the molecule to the substrate is highly dependent on the gate voltage. By varying the gate voltage it is possible to slow down the rate of charge transfer and increase the chances of successful photoisomerization detection.

We now dedicate our attention to how the conductance of the SiMWFET changes as the gate voltage is varied.

Imagine a thin piece of p-doped silicon, with two metal contacts on each end (source and drain), and a third contact underneath. We connect a source contact as a source of electrons and a drain contact to drain electrons (Fig: 2.4). What is effectively created is a variable resistor where the amount of current entering the drain and leaving the source is controlled by the voltage V_g (see Fig: 2.5 (b)).

As the voltage V_g is increases the depletion zone becomes larger. So there will be a reduction in the size of the actual effective cross sectional area for the current to pass would be less. Therefore the resistance of the device between the drain and the source would be higher as more V_g is applied [55]. The more negative the gate is with respect to the source, the lower the resistance and the larger the current I_d will be for a given value of voltage (V_d) [54].

In summary, increasing V_g causes a larger depletion zone which in turn creates more resistance between the source and the drain (Fig: 2.5 c). After a certain point of increasing V_g the channel will be blocked, in other words the channel is said to be pinched off. The specific

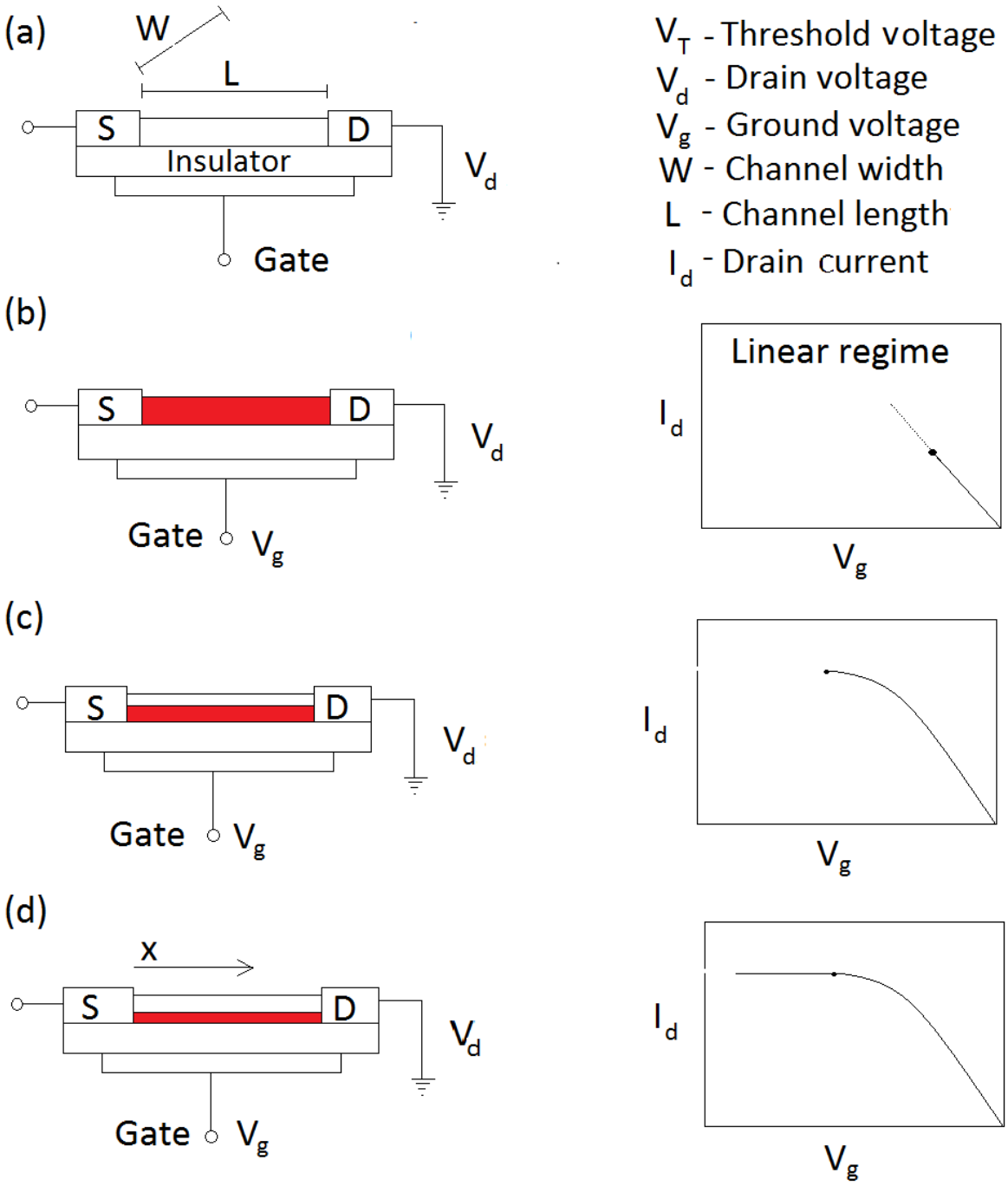

Fig. 2.4 Operation of a microwire field effect transistor with I versus V_g [54] (shaded region has a high concentration of electron holes).

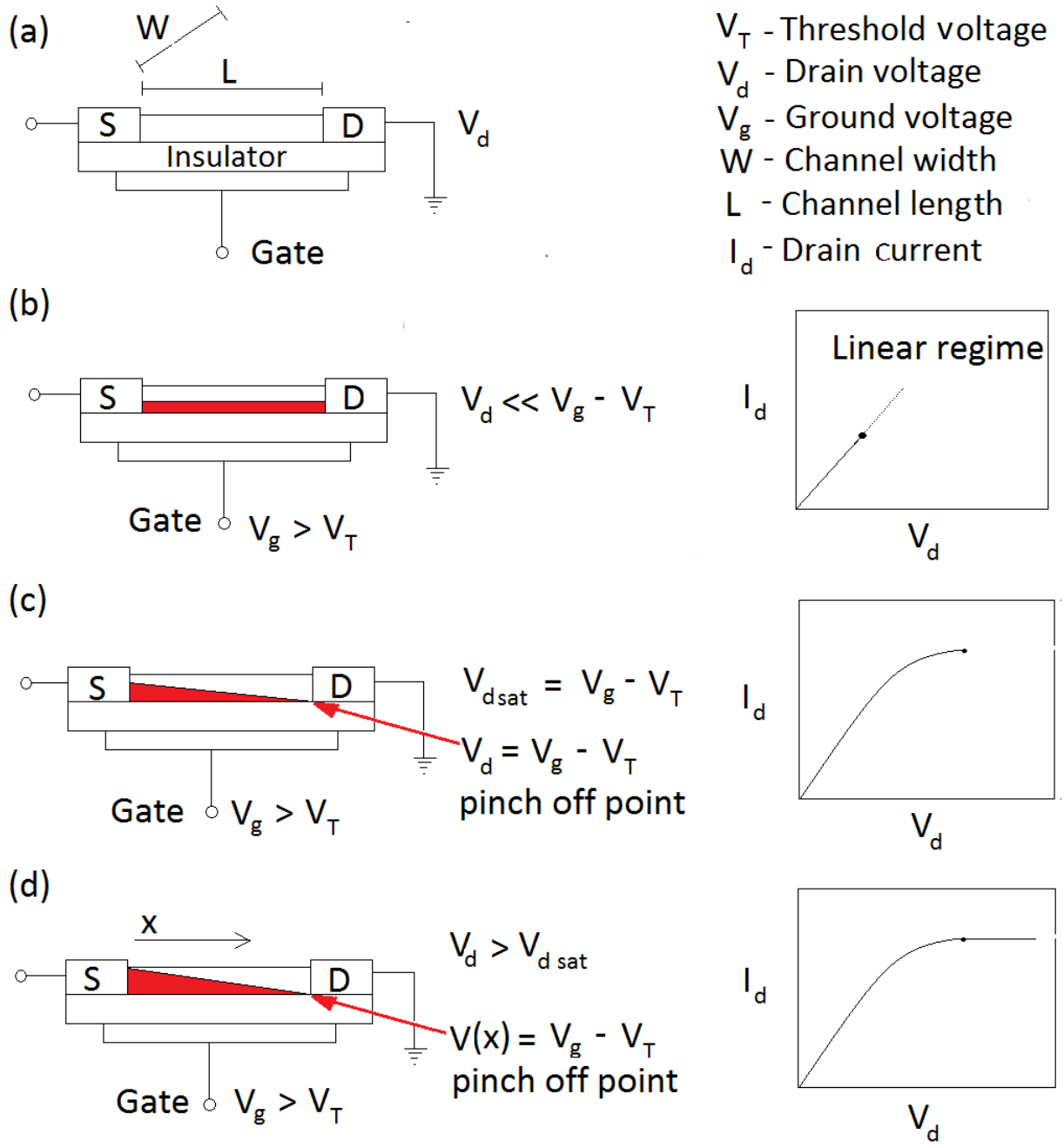

Fig. 2.5 Operation of a microwire field effect transistor (shaded region has a high concentration of electron-hole pairs). (b) Charge carrier concentration profile in the linear regime. (c) Carrier concentration profile when the pinch off occurs near the drain electrode $V_g - V_T = V_d$ [54]. (d) Carrier concentration profile in the saturation regime.

value of V_g is known as the pinch off voltage (see Fig: 2.5 d). How much voltage is needed between the gate and the source to cut the current in the channel is represented by a value of V_g which lies on the x axis of V_{ds}. When the transistor is not on cut-off mode, it operates as a variable resistor between the drain and the source. The drain to source resistance is controlled by the voltage between the gate and the source [54].

Cut off mode is attained when $V_g \leqslant V_{g(off)}$ and $I_d = 0$ A. When V_g is greater then $V_{g(off)}$ the channel will not be completely closed off so current will flow from the drain to the source. There will be voltage drop across the channel. In other words the depletion zone will be wider at the end close to the drain [54].

The resistance of the channel also depends on the magnitude of V_d. As the drain to source voltage is increased there is an uneven change in the shape of the channel due to the gradient of the voltage potential from the source to the drain (Fig 2.5).

So the greater V_d is, the greater the value of I_d becomes, which in turn leads to a more noticeable reduction in the channel width until the shape of the inversion region becomes pinched off close to the drain end of the channel. When increasing the value of V_d further the "pinch off" point migrates towards the source [55]. The FET is now in the saturation mode [54]. These equations appear as (2.36) to (2.37) in [55].

The margin of safety is given by:

$$V_d = V_g - V_{g(off)} \tag{2.36}$$

When the above condition is satisfied the cut off point is attained .

$$V_{gd} = V_g - V_d = V_{g(off)} \tag{2.37}$$

(In this case the channel will be closed and there will be no current flowing between the drain and source)

In the next section the applications of molecular switches on surfaces will be discussed.

2.4 Applications of molecular switches

Molecular switches have many potential applications, here we briefly discuss a few of them.

Molecular switching has been used to control the wetting of surfaces. This process has been proven using contact angle measurement which provides the simplest way to monitor switching of surface-immobilized molecular switches [56]. It is usually the case that UV irradiation of *trans*-AB-covered surface with a water droplet resting on it leads to the spreading out of the liquid (Fig: 2.6). The increased wettability is usually attributed to the higher dipole moment of the *cis* isomer [57].

Larger differences would be beneficial for the development of new photoswitchable surfaces. But by increasing the roughness of the hydrophilic and hydrophobic surfaces they can be turned into superhydrophilic and superhydrophobic ones respectively [56].

It is possible to create surfaces which have switchable interactions with underlying Azobenzene coated surfaces [58]. This property can lead to 'smart' surfaces capable of capturing and releasing entities on demand [57]. The recognition units can be hidden when the molecular switch is in the *cis* state and exposed when the molecular switch is in the *trans* state (Fig: 2.7).

If molecular switches are attached to catalytic metals they can be used to control the catalytic activity by allowing or blocking access to substrates. This allows chemical reactions to

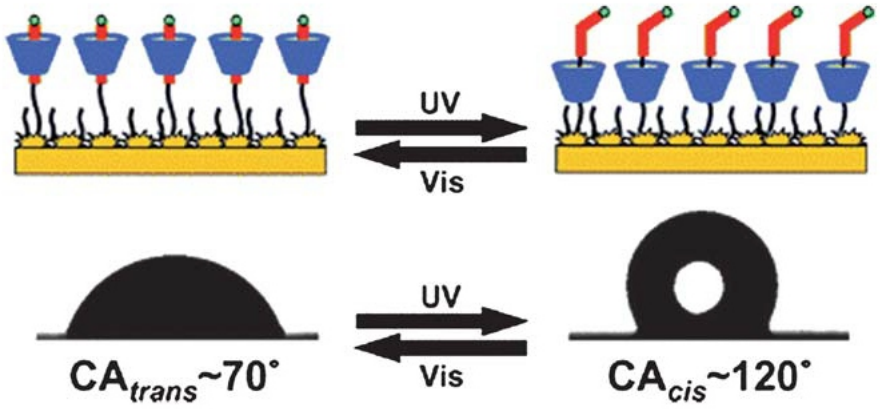

Fig. 2.6 Azobenzene switching controlling wetting of surfaces [57].

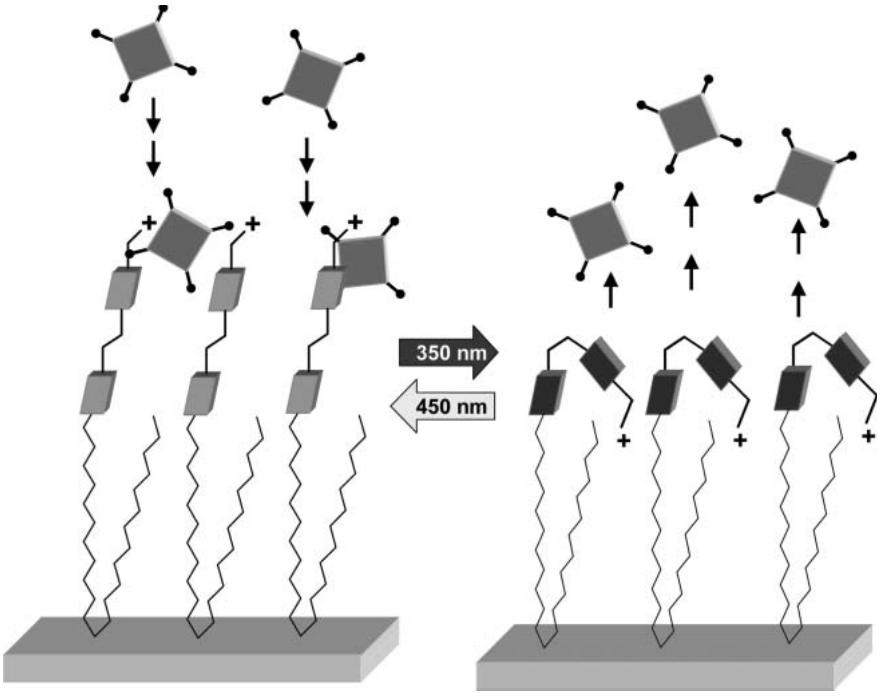

Fig. 2.7 "Catch and release" of porphyrins by photoswitchable self-assembled monolayers [57].

be carefully controlled.

One of the most promising uses of molecular switches is to convert light into movement [59, 60] using a bistable photosensitive polymer [61]. This was confirmed using single molecule force microscopy that the polymer produced an external force along a polymer backbone thus performing mechanical work (Fig: 2.8 b).

On Fig: 2.8a the synthesis of polyazobenzene peptides is displayed. Force extension traces of a single polyazopeptide. A polymer in a nondefined initial configurationally mixed state (black trace). After five 420 nm pulses, the polymer was switched to the saturated trans state and lengthened (red trace). After pulses at 365 nm, the same molecule shortened [59].

In the *trans* configuration, the tip apex with a functional group (R) will interact with specific functional groups (R¢) on the substrate surface to provide chemical information (Fig: 2.9). In the *cis* configuration, the tip apex does not present the functional group for specific chemical interactions with the substrate surface and provides only topographical information [62, 63].

In the next chapter the fabrication and electrical characteristics of the SiMWFET will be briefly discussed.

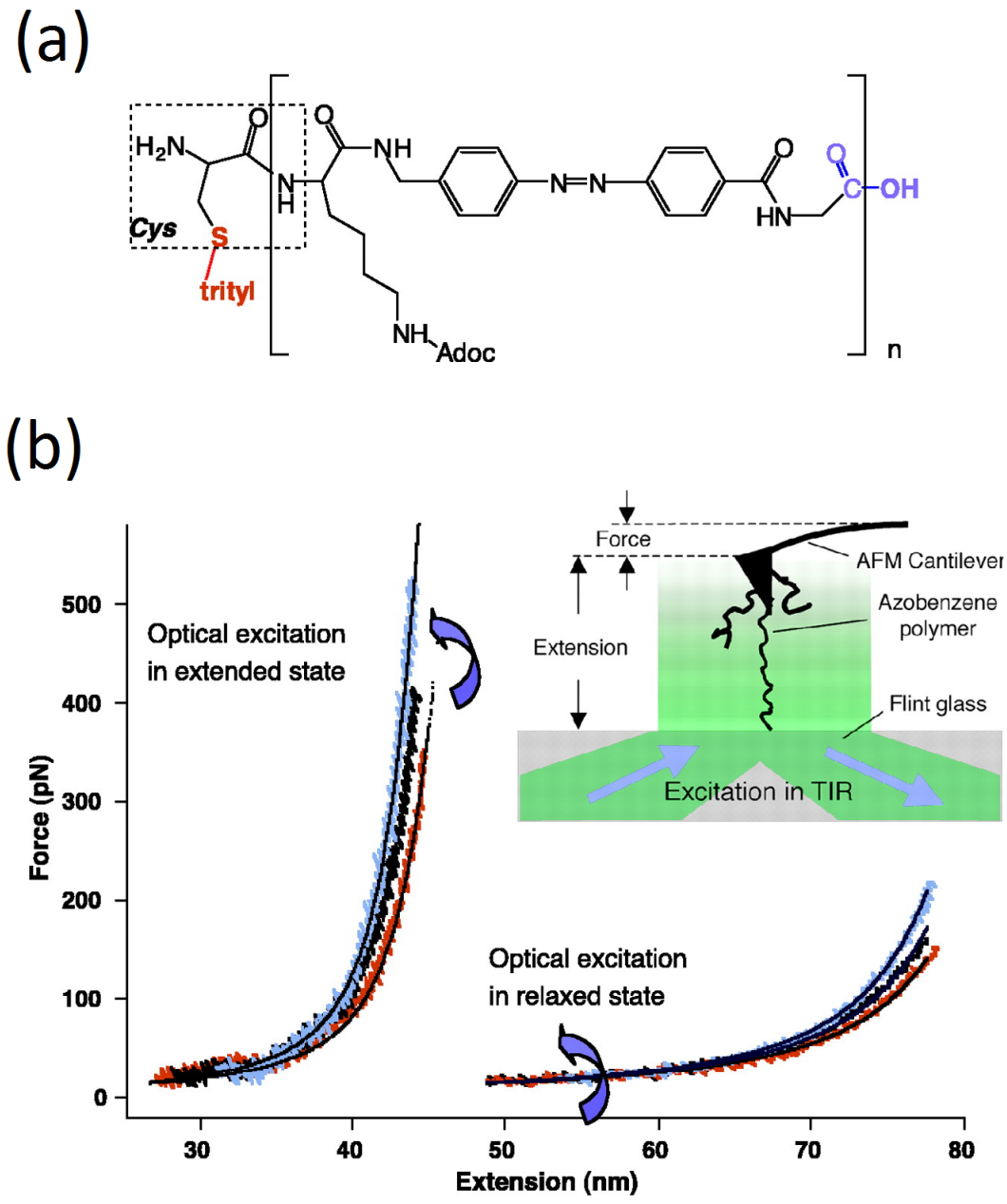

Fig. 2.8 (a) Synthesis of polyazobenzene peptides. (b) Force extension traces of a single polyazopeptide [59].

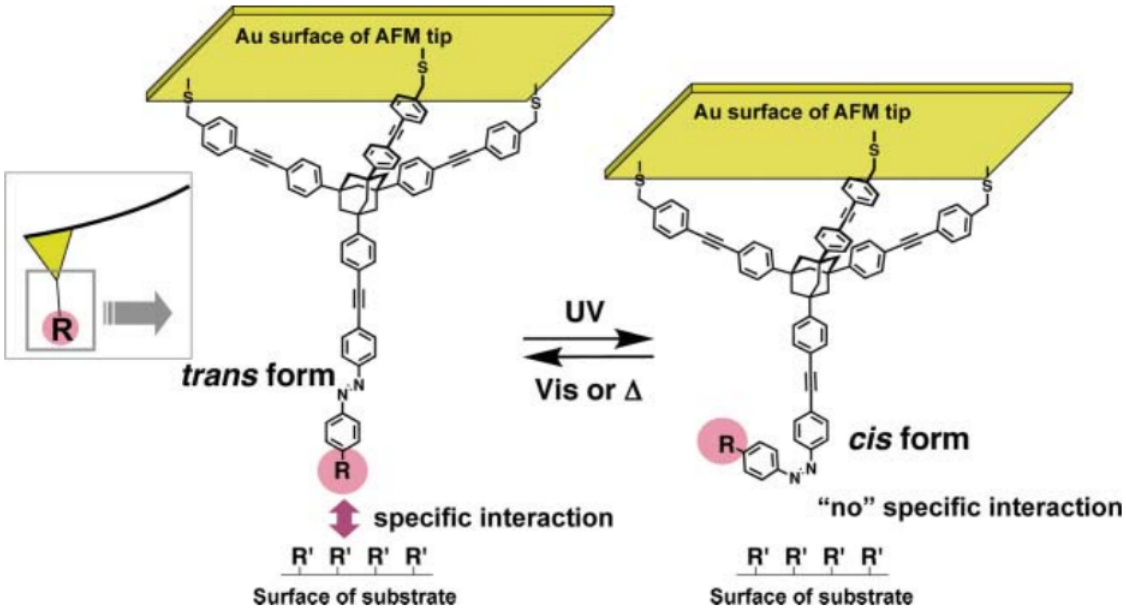

Fig. 2.9 Photoswitching molecular tip [62].

Chapter 3

Electrical characteristics and Fabrication of Si-MW FETs

3.1 Electrical characteristics of SiMWFET

In this section the methodology in the selection of the ground and drain to source voltages will be discussed along with the SiMWFET fabrication process.

The process begins with plotting the I versus V_d plots with varying ground voltages V_g (Fig: 3.1). To remain in the linear regime the drain to source voltage (V_d) should be above 0 volts but below 4 V. This is true for the voltage ranges between -8 and 0 V.

We plot I versus V_g of the microwire with drain to source voltages varying from 1 to 9 V (Fig: 3.2). The channel remains in the linear regime when the drain to source voltage is equal to or less then 4 V. This true for the ground voltage between 0 and -10 V. The lower the drain to source voltage is the less likely the channel will saturate.

For lower drain to source voltages between 0 to 1.3 V (Fig: 3.3). It is noticeable that the

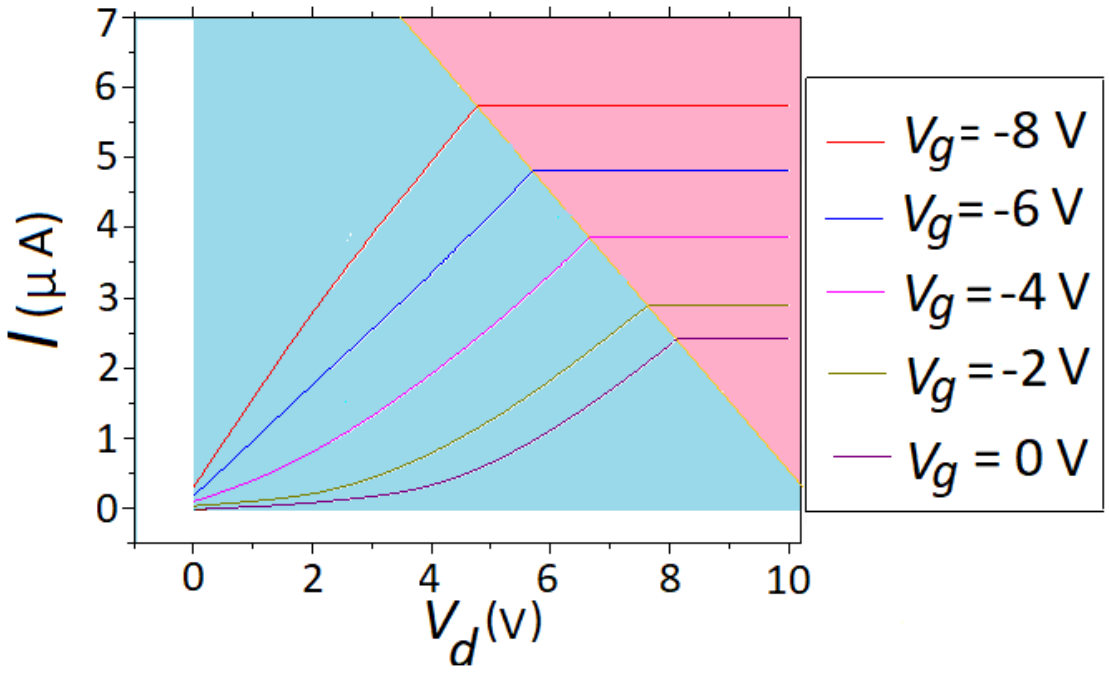

Fig. 3.1 I versus V_g plots of a single pristine microwire with drain to source voltage ranging from 0 to 1.3 V.

channels remain in the linear regime from 0 to -10 V. The lowest possible drain to source voltage the microwire could operate with was 0.2 V. To remain in the linear regime the gate voltage should be as large as possible to account for the right shift due to APTES and dabcyl modification. If the selected ground voltage is too small (lies at the left of the plot) then the channel will saturate prematurely and changes in current would not be detected. From the I versus V_g (Fig: 3.3) plot the best possible value for the ground voltage V_g is -3 V.

In order to remain in the linear regime the best possible combination of drain to source V_{ds} and gate V_g voltages was 0.2 V and -3 V respectively.

We have briefly discussed how the SiMWFETs are fabricated. In the next section we will describe the creation of the *m*SAM onto the SiMWFET and the experimental procedure to detect photoisomerisation of dabcyl modified SiMWFETs.

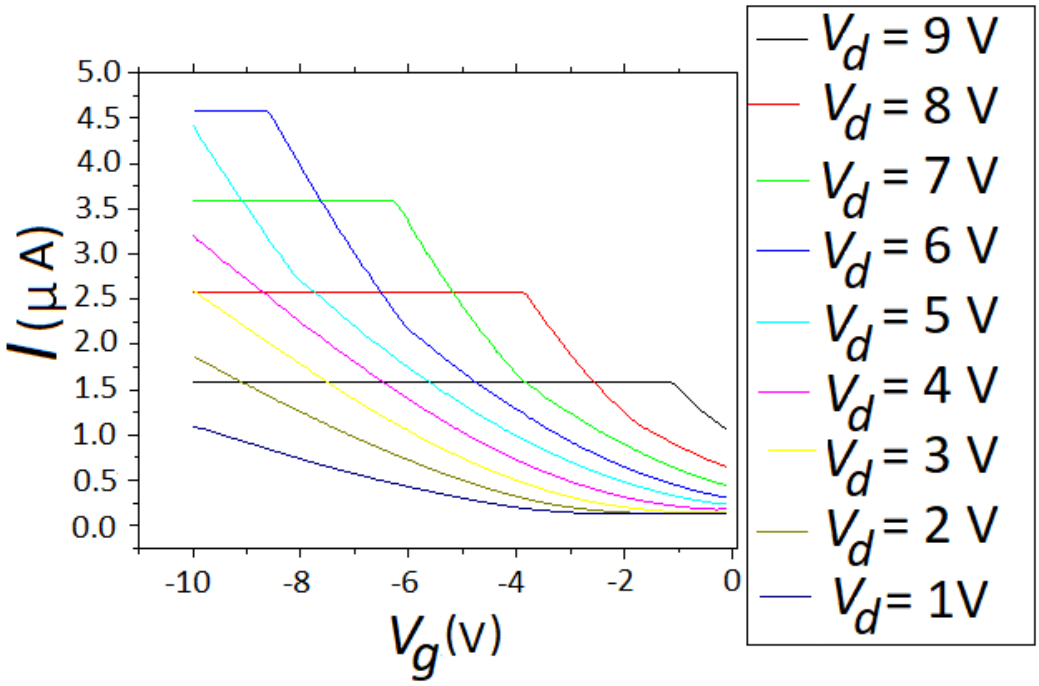

Fig. 3.2 I versus V_d plots of a single pristine microwire with ground voltage ranging from -9 to 4 V.

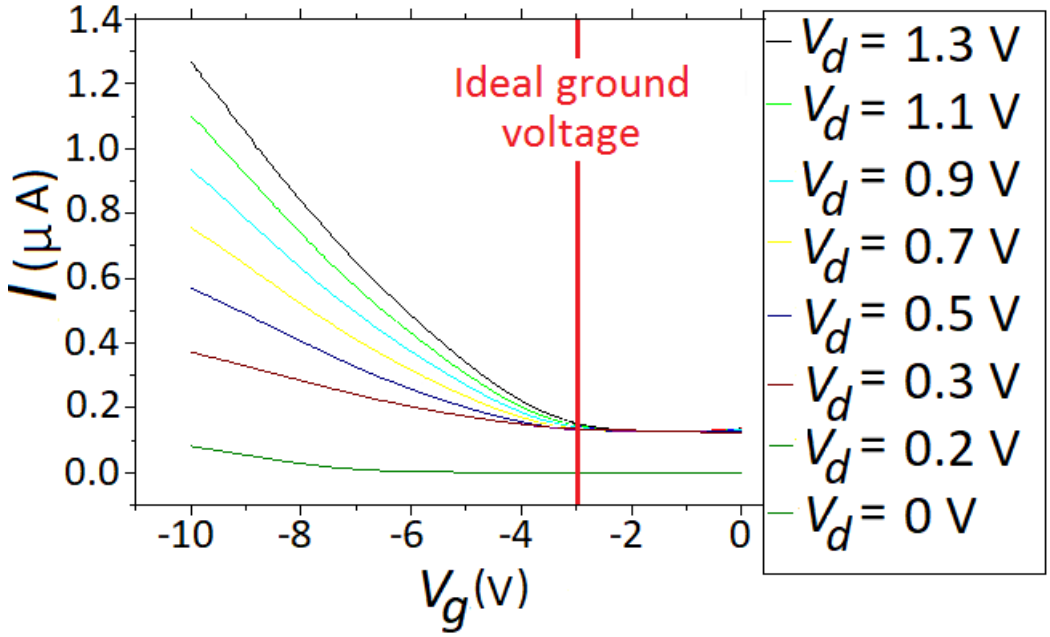

Fig. 3.3 I versus V_g plots of a single pristine microwire with drain to source voltage ranging from 1 to 9 V.

3.2 Fabrication of SiMWFET

The SiMWFET forms the substrate to which the spacers and molecular switches are attached. In order to gain a better understanding of the interactions between the molecules and the SiMW substrate the fabrication of the SiMWFET is of importance.

This chapter offers a more detailed fabrication process of the SiMWFET [64–66]. The scanning electron microscope image of a single microwire with its source and drain contacts is shown in Fig: 3.4. Microwire fabrication consist of multiple steps (Refer to Fig: 3.5): The silicon wafer is prefabricated with a metal backgate and thin layer of silicon dioxide on its surface (Fig: 3.5 (1)).

The wafer is first spin coated with a thin layer of photo-resistant polymer coating of a few nano-meters deposited on the silicon dioxide surface (Fig: 3.5 (2)). The photoresist polymer is hardened by baking it at 200 °C (Fig: 3.5 (2)). The wafer is inserted into the electron microscope and an electron beam is used to draw a circuit (Fig: 3.5 (3)). The electron beam precisely follows the design of the circuit and only irradiates the defined parts of the wafer. The wafer is placed in a solvent which only dissolves those parts of the polymer which were irradiated with the electron beam while leaving the rest of the polymer intact (Fig: 3.5 (4)). The newly exposed layer of silicon dioxide is dry etched. This process removes unwanted areas of the film by reacting them with gases in a plasma forming volatile products (Fig: 3.5 (5)). The remaining non-radiated photoresist is dissolved in a solution (Fig: 3.5 (6)).

A new layer of photoresist is applied to the wafer (Fig: 3.5 (7)) and an electron beam with a pattern for the pad is used (Fig: 3.5 (8)). The irradiated pattern is dissolved (Fig: 3.5 (9)) and the wafer is implanted with boron ions (Refer to Fig: 3.6 (10)). Ion implantation is the process where dopant atoms are introduced to pure silicon. This process is governed by dose and energy of the dopants. An intense electric field accelerates boron ions which penetrate the surface of

the wafer. This process changes the electrical characteristics of the silicon forming the p-doped silicon channel. When ions collide into silicon they disrupt the crystal structure thus creating an amorphous layer. The ions are not yet integrated into the silicon structure. After the wafer undergoes annealing, atoms in the amorphous layer to move in more stable states. The atoms re-establish the crystal structure along with the dopant atoms, in a process known as substitution.

After the remaining photoresist has been removed (Fig 3.6 (11)), the wafer is oxidised with a 10 nm layer of silicon dioxide (Fig 3.6 (12)). The thermal oxidation process is an oxide growth, in which oxygen is supplied to the surface of the wafer and oxidises it at high temperatures to form SiO_2 layer. A layer of photoresist is spin coated on top of the silicon dioxide layer and baked (Fig: 3.6 (13)). The wafer subjected to e-beam lithography (Fig: 3.6 (14)) and the irradiated photoresist is removed exposing the silicon dioxide surface (Fig: 3.6 (15)).

The wafer is then cleaned using oxygen plasma resist cleaning which involves the removal of surface contaminants through the use of energetic plasma. The plasma is created using high frequency voltages that cause gas atoms to be excited. The exposed silicon dioxide is wet etched using a chemical solution (Fig: 3.6 (16)). The wafer is placed into an apparatus which sputters nickel or gold over its whole surface (Fig: 3.6 (17)) forming the source and drain contacts. On the parts where the polymer was dissolved, the metal sticks directly onto the silicon. The rest of the wafer there is still a polymer between the metal and the silicon dioxide layer. The wafer is placed in a different solvent which dissolves the polymer (Fig: 3.6 (18)). The metal attached to the polymer floats off while the metal that is directly on the silicon remains (Fig: 3.6 (19)) [67].

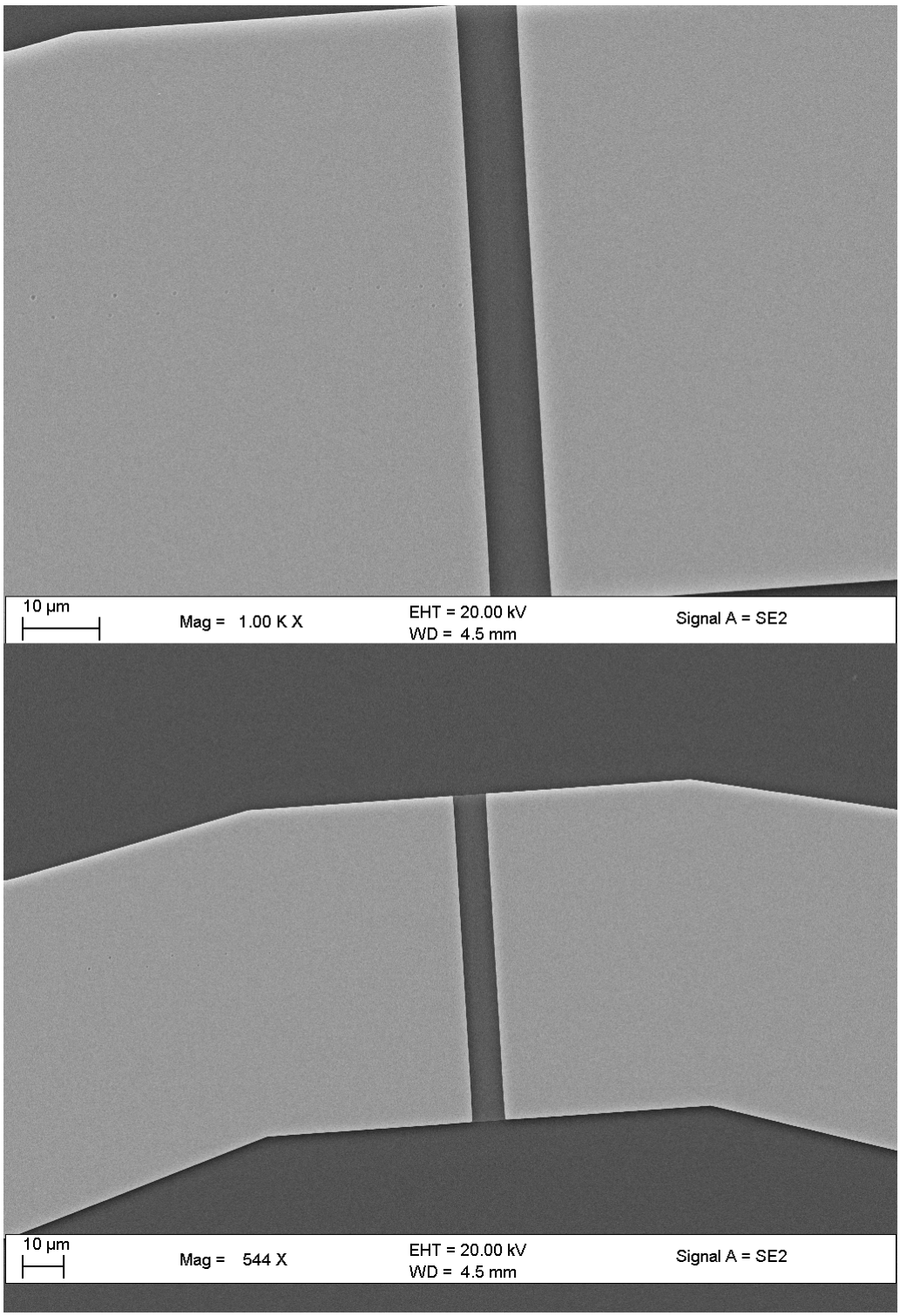

Fig. 3.4 Scanning electron microscope image of a single microwire channel (Image courtesy of the University of KwaZulu-Natal Microscopy and Microanalysis Unit).

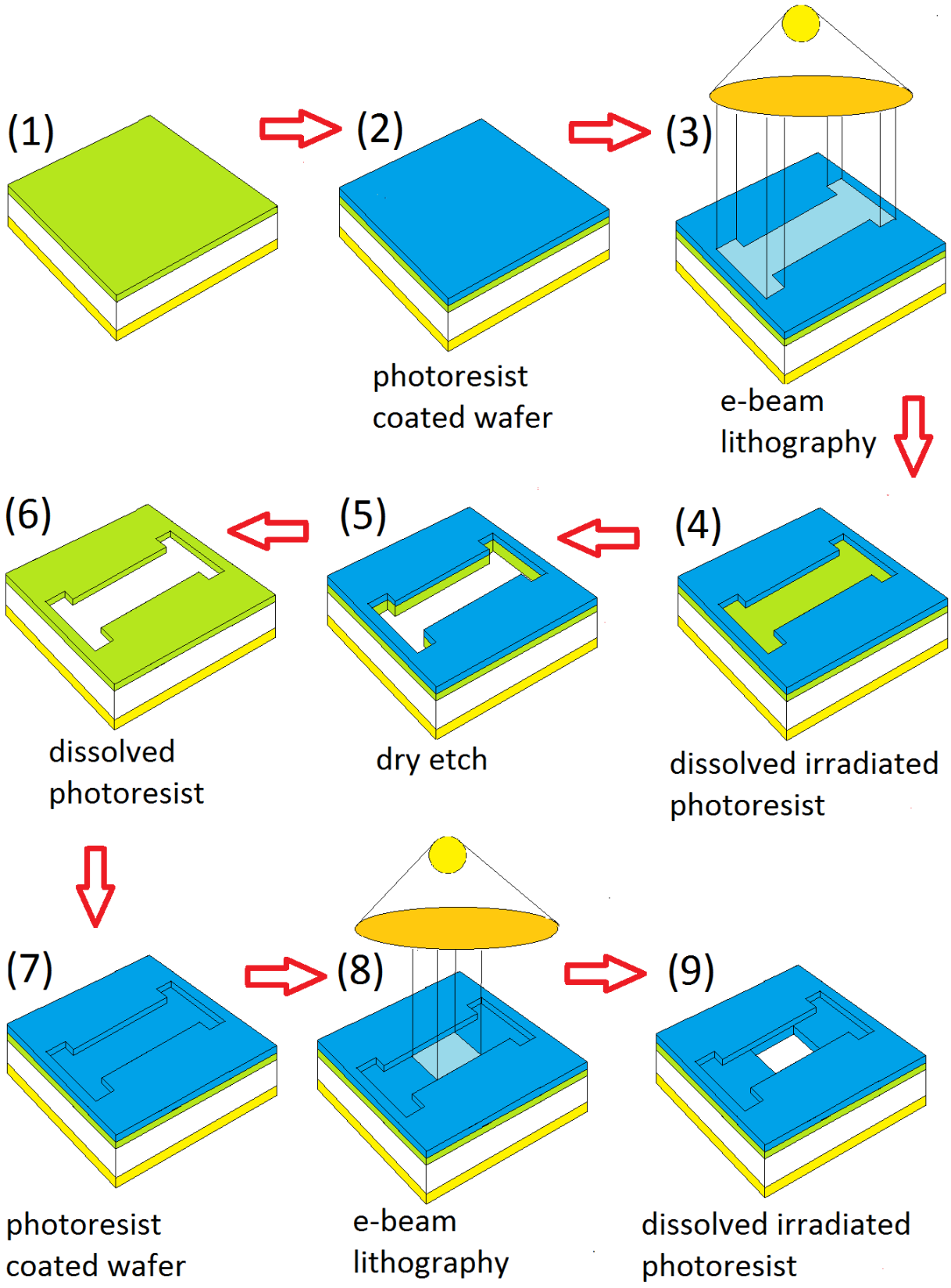

Fig. 3.5 Steps 1 - 9 of the fabrication of the SiMW FET (information courtesy of Academia Sinica).

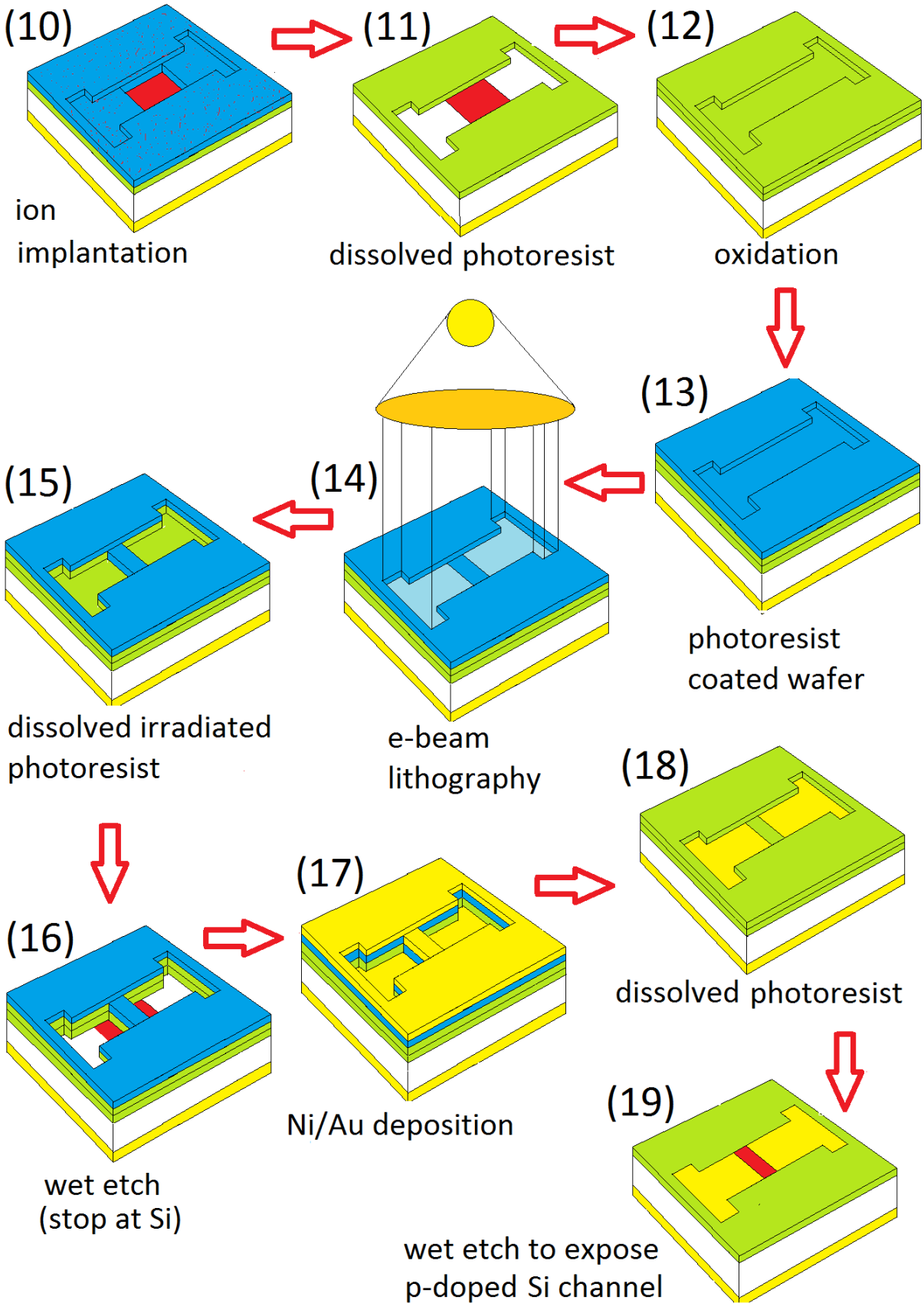

Fig. 3.6 Steps 10 - 19 of the SiMWFET fabrication (information courtesy of Academia Sinica).

We have briefly discussed how the SiMWFETs are fabricated. In the next chapter we will describe the creation of the *m*SAM onto the SiMWFET and the experimental procedure to detect photoisomerisation of dabcyl modified SiMWFETs.

Chapter 4

Experimental methods

4.1 Chemical modification procedure of SiMWFET

4.1.1 Preparation of *m*SAM on SiMWFET

Pre-preparation Protocol

The chemical functionalization of the Silicon microwire Field Effect Transistor (SiMWFET) and the real-time detection of isomerization with the use of I versus V_g, I versus V_d and I versus t plots will be discussed.

All sonication is done at lowest setting, the stirrer is always set at 50 rpm and hotplate is pre-set to 110 °C. Prior to experimentation, all beakers and tweezers were rinsed with acetone (once). Beakers are placed on the sonicator at the lowest setting, rinsed with dH_2O (3 times) and hang dried. Chemical modification is always performed in a fume cardboard.

Chip Cleaning

Chip cleaning is performed if the chip was chemically modified and if there is a need to remove the modification or if an unmodified chip has to simply be cleaned. This process increases the

probability of successful chemical modification.

The chip is rinsed with (isopropanol). This is followed by rinsing it with dH_2O. It is then blow dried with nitrogen. Placed in a Acetone and ethyl alcohol (1:1) solution for 10 min on lab rotator. Followed by rinsing it with acetone, then dH_2O and blow dried with nitrogen. It is submerged in dH_2O at 80 °C for 10 minutes. The chip is rinsed with dH_2O and blow-dried with nitrogen. The SiMWFET is lastly baked at 110 °C for 10 min.

Self-assembly has emerged as the method of choice for constructing micrometer-sized objects from nanoscopic components [68]. The methods employed to modify the SiMWFET will now be discussed in more detail as per (Fig:4.1).

APTES functionalization procedure

The APTES modification protocol followed is identical to that outlined in the paper titled "Control and Detection of Organosilane Polarization on Nanowire Field-Effect Transistors" [68]. This process generates and APTES monolayer on the Silicone microwire Field Effect Transistor.

The chip is immersed in a 2 % solution of cholic acid ($C_{24}H_{10}O_5$, Fluka, Biochemika purity 99.0 %) in ethyl alcohol for 12 hours. This process generates -OH groups on the microwire surface (Fig: 4.1 b).

The chip is transferred into a solution containing 200 micro litres of APTES (3-amino proplyl) trimethylsaline (Sigma-Aldrich, purity 99 %) and 10 ml of acetone for 1 hour (Fig: 4.1 c). This generates a single layer of APTES on the microwire surface. The chip is rinsed with acetone, blow-dried with nitrogen and baked at 110 °C for 1 hour.

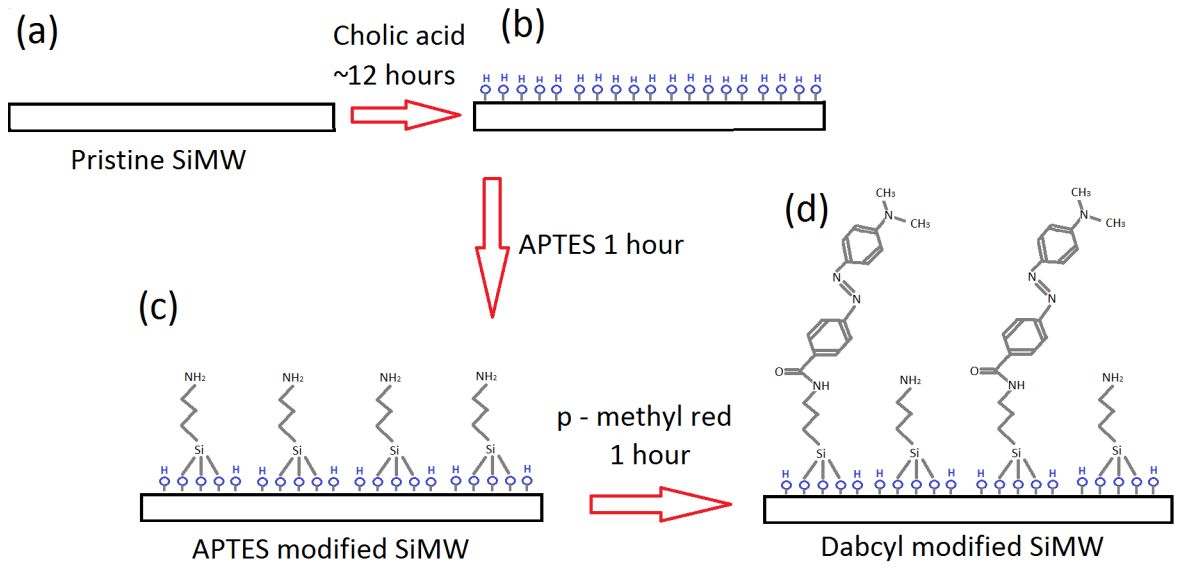

Fig. 4.1 Schematic drawings illustrating (a) Pristine microwire. (b) The silicon oxide layer formation. (c) APTES surface modification. (d) Dabcyl surface modification [69].

Dabcyl functionalization procedure

This process functionalizes the APTES monolayer with dabcyl which acts as the chromophore.

The APTES modified chip (Fig: 4.1 (c-d)) is heated at 70 °C for 1 hour in a 10 ml N,N-Dimethylformamide (DMF) solution containing 0.0115 g of (dabcyl) 4-Dimethylaminoazobenzene-4'-carboxylic Acid ($C_{15}H_{15}N_3O_2$) and 0.0115 g N, N- dicyclohexylcarbodi-imide. It is then rinsed with DMF and blow dried with nitrogen. Lastly it is baked for 1 hour at 110 °C [69] .

Utilising the above modification procedures the SiMWFET was successfully modified with the dabcyl/APTES *m*SAM. We briefly discuss the electrical properties of this *m*SAM.

4.2 Electrical properties of dabcyl/APTES *m*SAMs

This section discusses in detail how to use the capabilities of the SiMWFET. All experiments and measurements were carried out on a single micro wire, making it possible to obtain accurate electrical comparative measurements between a single pristine and dabcyl/APTES *m*SAM modified microwire. For the overall layout of the experiment refer to Fig: 4.10. Descriptions of previous conduction experiments will be discussed in the following subsection.

4.2.1 Prior electrical conduction experiments

As mentioned before in chapter 1 (Fig: 1.6) there has been I versus V_g measurements of photo-switching using Organic Field Effect Transistors (OFETs). It was concluded that the *cis* state has a higher conductance than the *trans* state. This dissertation aims to detect isomerization using I versus V_g and I versus V_d measurements to verify these findings.
There has also been research into the changes in conductance of the azobenzene functionalised surfaces due to irradiation cycles of UV and Vis light [31, 70, 71]. Az11/C12 *m*SAMs displayed efficient and stable photoisomerisation (Fig: 4.2). DR1P/graphene using a FET to detect changes in current (Fig: 4.3) [70], with the gate bias fixed at 0 V the conductance of the channel was constant. This made it possible to detect the changes in conductance from photoisomerization. The current increased with visible light illumination and decreased with UV illumination. These two experiments (Figs: 4.2 and 4.3) were able to detect isomerization but they also detected illumination.

In order to negate the illumination, non-irradiated sections were added as per Fig: 4.4 (b). In this dissertation the same approach was used along with a FET to detect the changes in current.

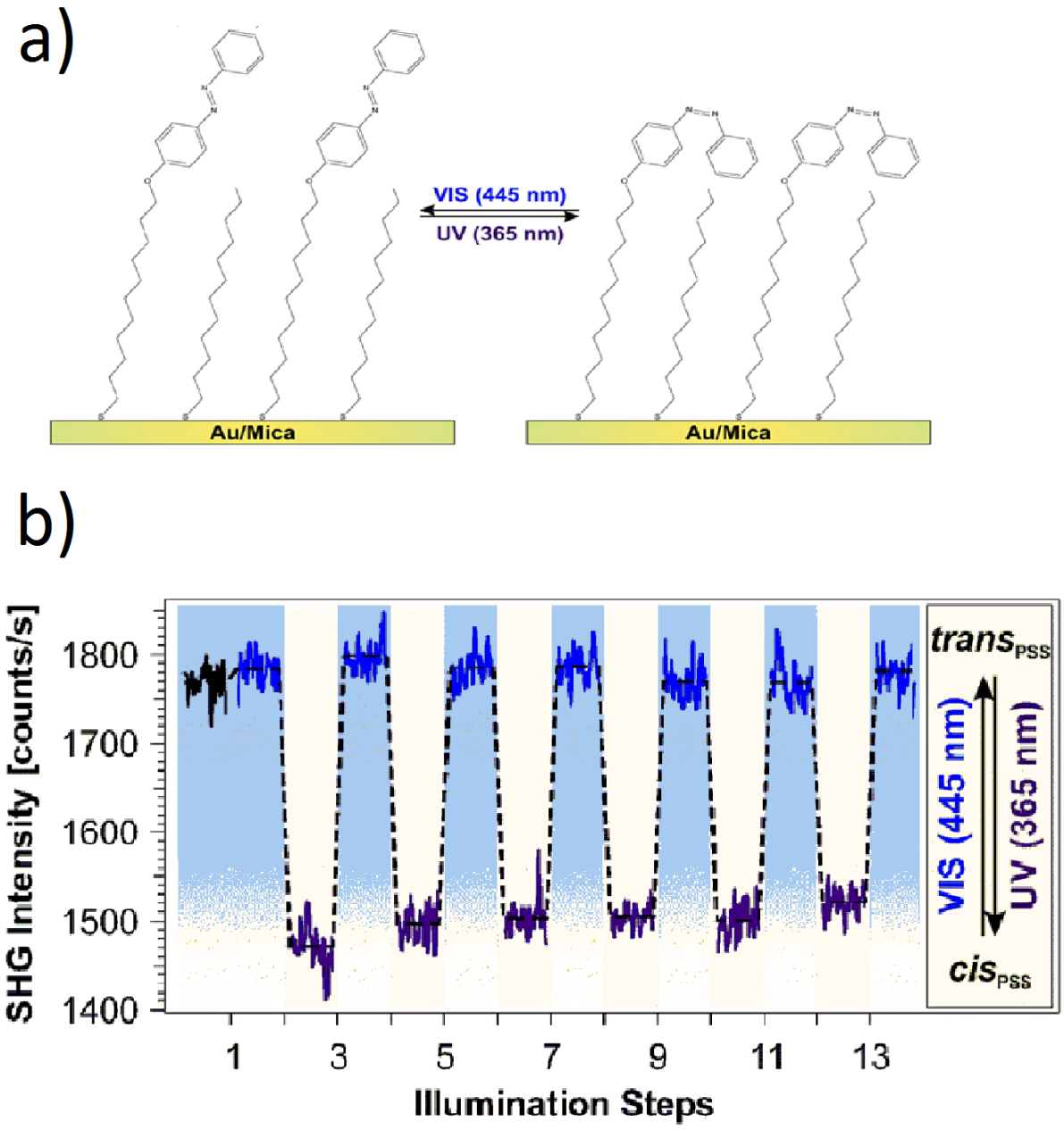

Fig. 4.2 (a) Az11 with C12 spacers, (b) Second Harmonic Generation (SHG) measurements showing photoisomerism [31].

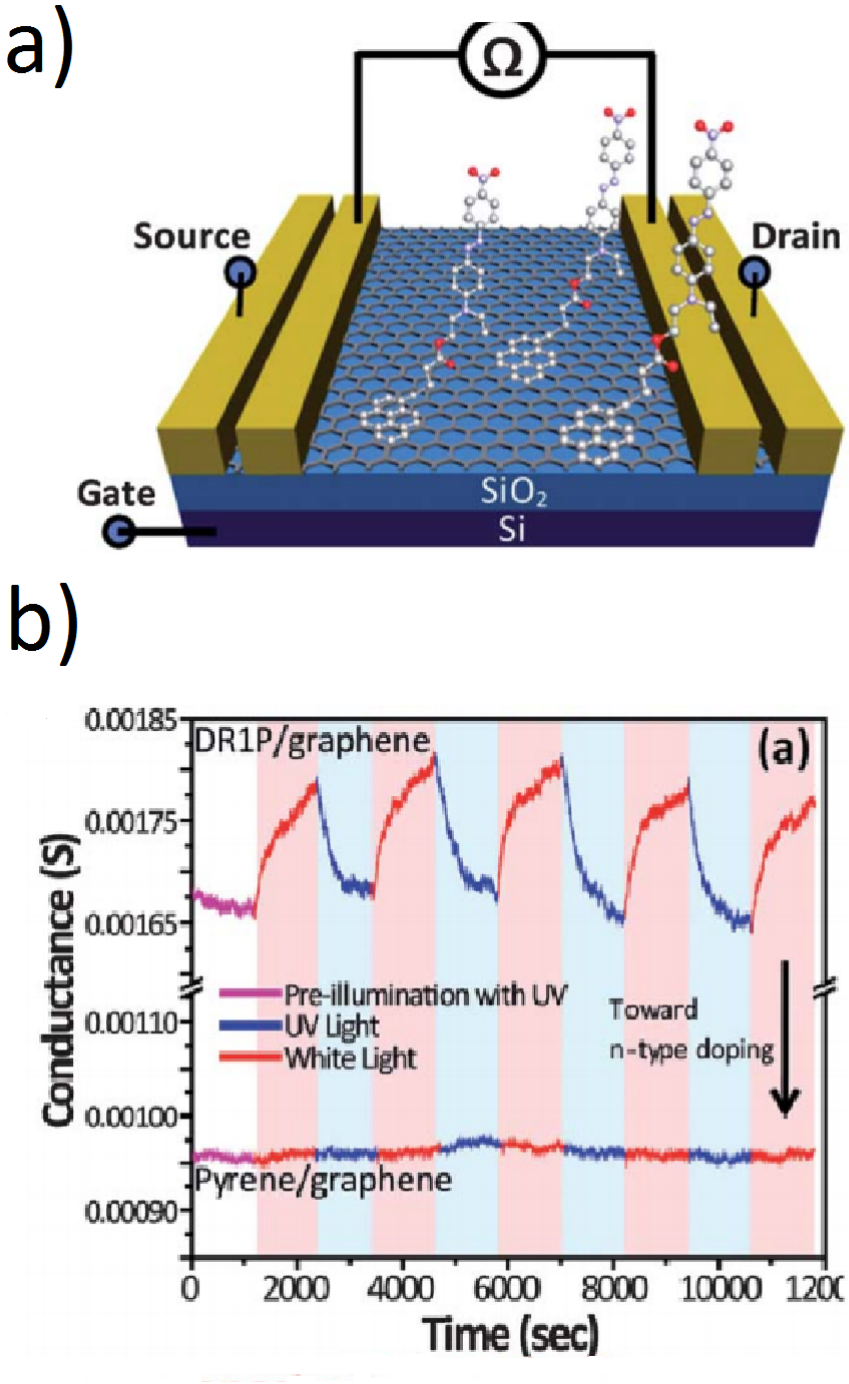

Fig. 4.3 (a) Azobenzene functionalized thiols molecular switches have been bonded onto graphene [70]. (b) Real-time conductance measurement of DR1P/graphene transistor at 0 V gate bias.

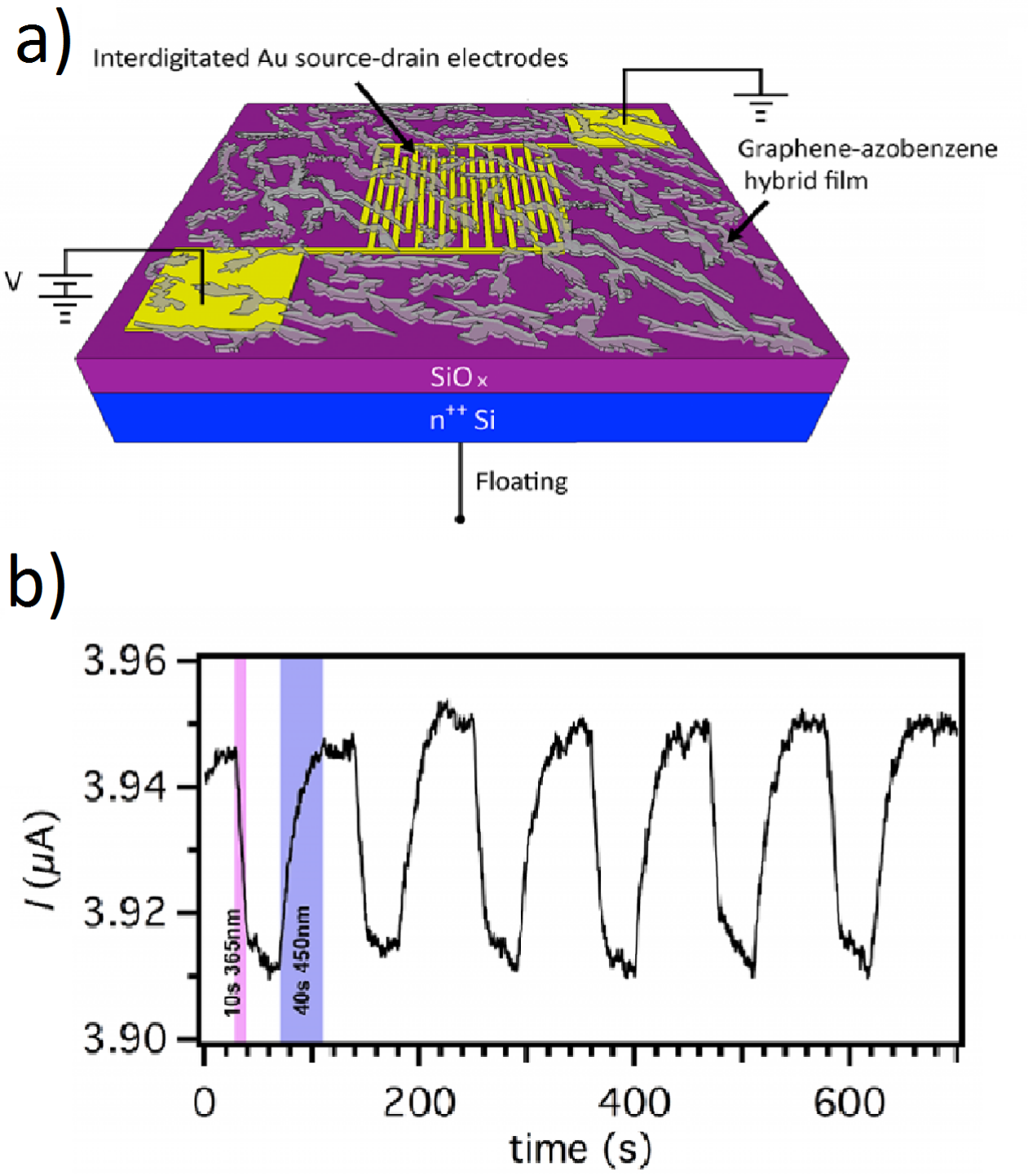

Fig. 4.4 (a) Graphene-azobenzene hybrid film bridging Au source drain electrodes. (b) *Cis-trans* isomerism detection using changes in current(right) [71]. Notice the spacing between the irradiation cycles.

4.2.2 Measurement of I versus V_g with V_d = 0.2 V

After I versus V_g plot of the SiMWFET had been recorded (Fig: 4.5 a), the sample was illuminated with UV light for 2 minutes in normal incidence (Fig: 4.5 b). This was followed by a I versus V_g plot of a non-irradiated SiMWFET to obtain the plot of the *cis* state of the *m*SAM (Fig: 4.5 c). The reversible thermal back reaction was achieved by utilizing visible light (450 nm) for 2 minutes (Fig: 4.5 d). Lastly a third I versus V_g plot of the SiMWFET is obtained (Fig: 4.5 e).

4.2.3 Measurement of I versus V_d with V_g = -3 V

Firstly the microwire current versus drain to source voltage is obtained. This is done in order to establish a control. Observing the wires behaviour under non-illuminated conditions with V_g fixed at -3 volts (Fig: 4.6 a). The UV LED was turned on illuminating the microwire for 2 minutes (Fig: 4.6 b). The UV LED was turned off, and the experiment is redone under dark conditions (Fig: 4.6 c). The *cis-to-trans* isomerization is triggered by irradiation with visible light which facilitates the de-excitation of the molecular switches (Fig: 4.6 d). A third non-illuminated reading is performed on the microwire channel (Fig: 4.6 e).

4.2.4 Measurement of I versus t with V_g = -3 V and V_d = 0.2 V

The experiment is carried out as follows (Please refer to Fig: 4.7): The current versus time graph is plotted for a 50 second non-illumination period in order for the current to stabilize (Fig: 4.7 a). One cycle consists of 1 second UV light at 365 nm (Fig: 4.7 b), 0.4 seconds rest in dark (Fig: 4.7 c) followed by 1 second visible light (450 nm) irradiation (Fig: 4.7 d).

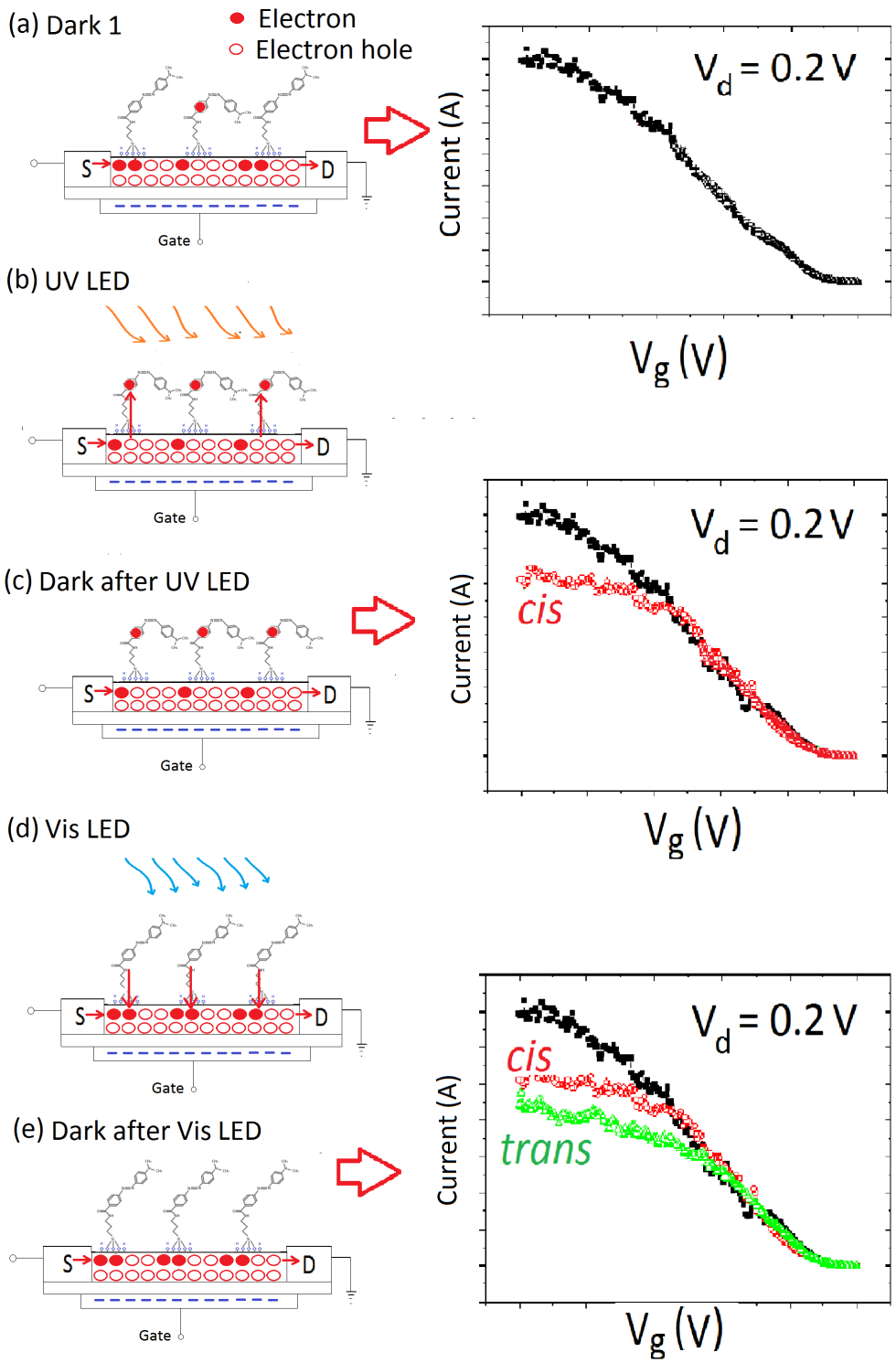

Fig. 4.5 A diagram explaining molecular switching process with the I versus V_g with V_d= 0.2 V. For simplicity the APTES spacers are not shown.

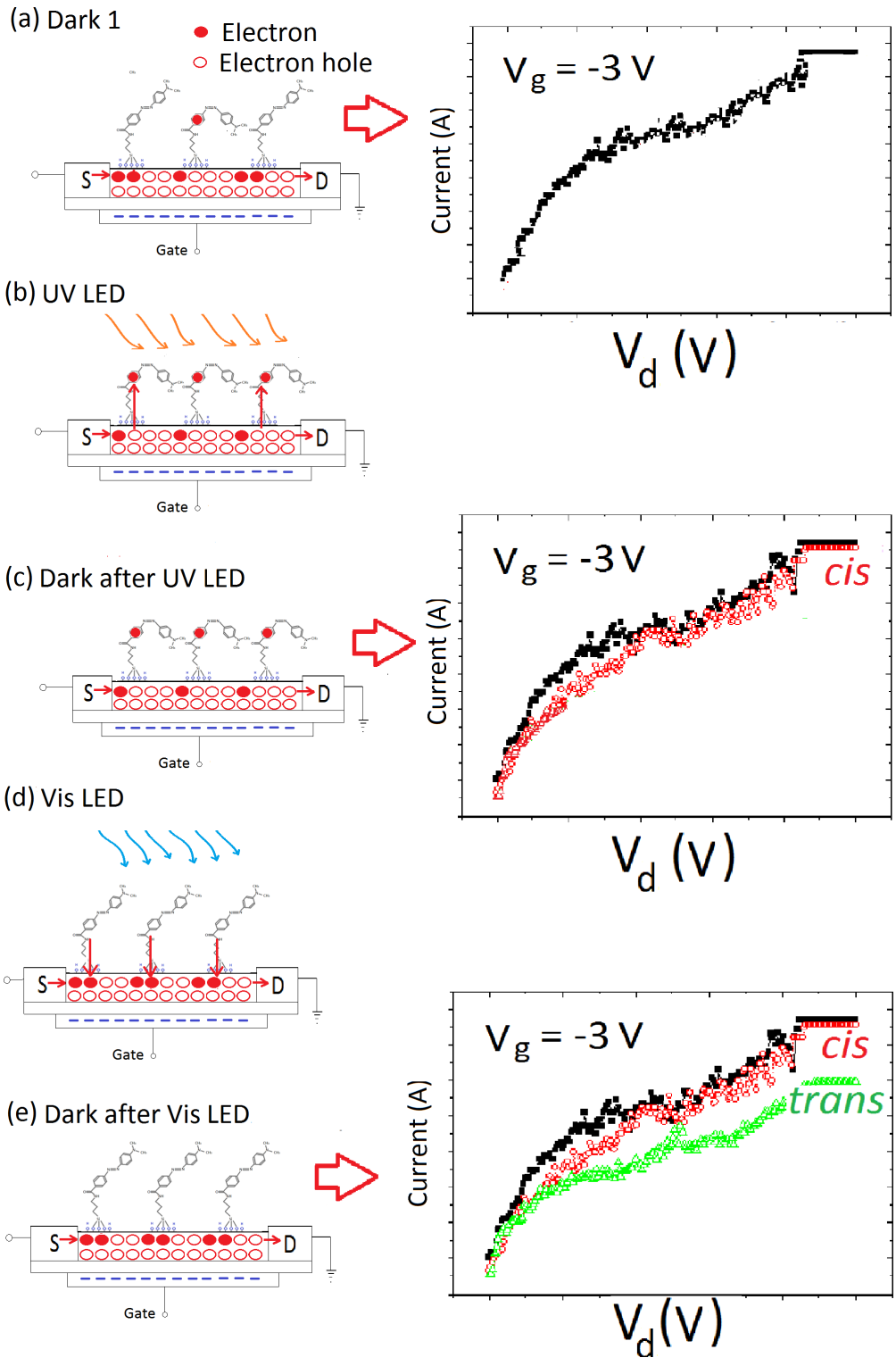

Fig. 4.6 A diagram explaining molecular switching process with the I versus V_d and V_g= -3 V. For simplicity the APTES spacers are not shown.

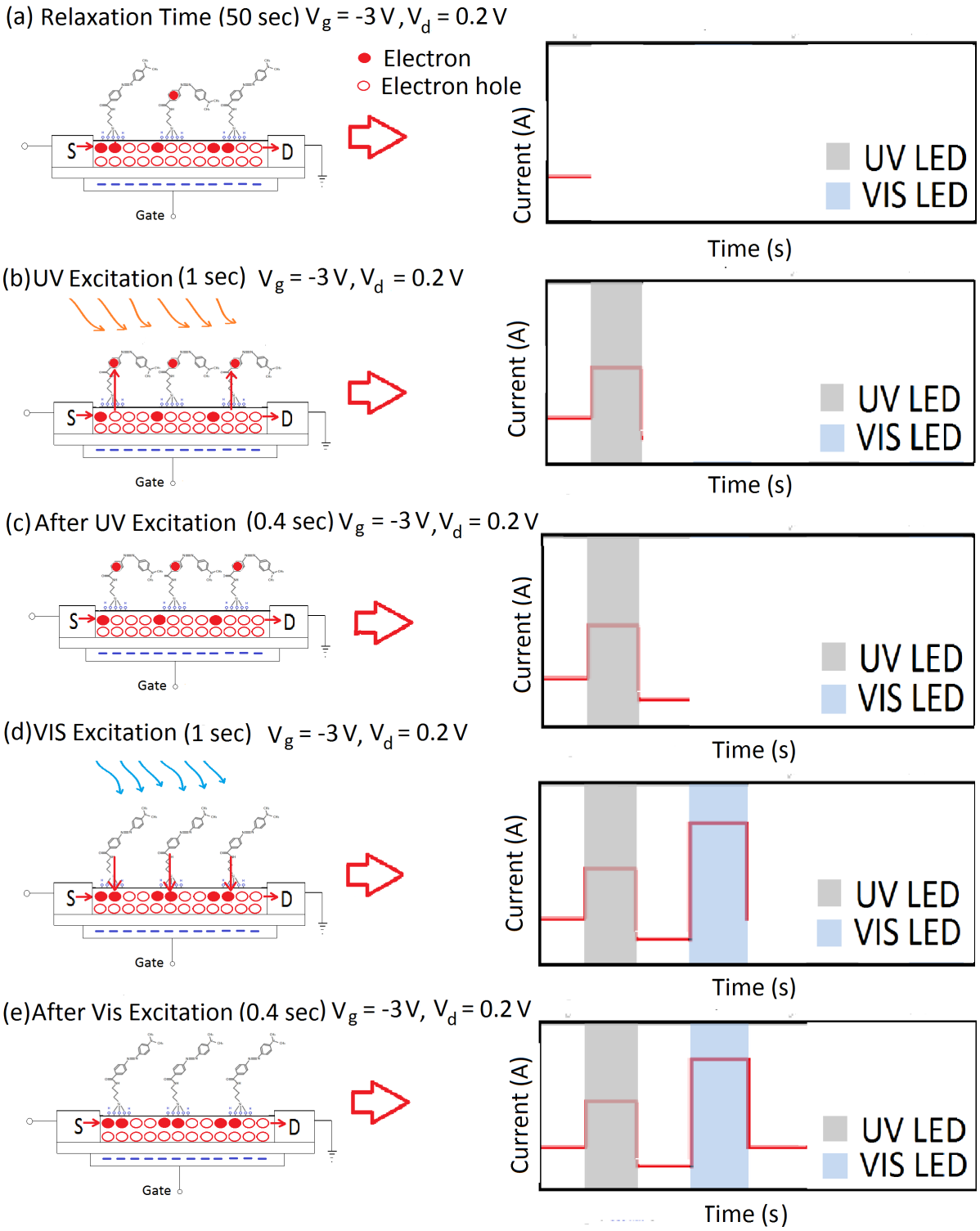

Fig. 4.7 A diagram explaining molecular switching process with the I versus t with V_g= -3 V and V_d= 0.2 V. For simplicity the APTES spacers are not shown.

4.3 Characterizations of modified SiMWFET

In order to verify whether the chip modification is successful, the I versus V_g plots of a pristine, APTES and dabcyl modified micro wire are compared to each other [72, 73]. By observing how the plots shift it is possible to determine whether the modification is successful (Fig: 4.8 and Fig: 4.9). APTES modification causes the graph to shift to the right and dabcyl modification causes a left shift. The Dabcyl modification is successful if it lies between the Pristine (control) and APTES modification as per Fig: 4.8 and Fig: 4.9.

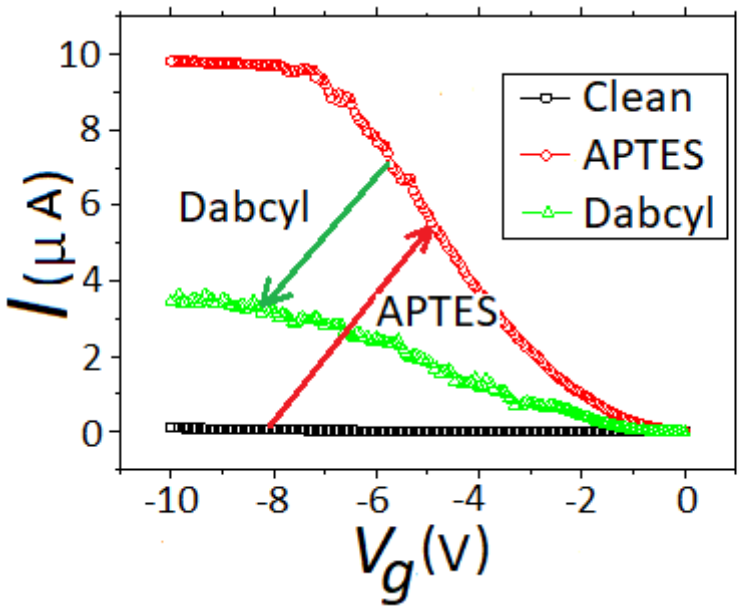

Fig. 4.8 Current versus ground voltage of a single microwire from pristine through to APTES then to dabcyl modification out of vacuum. Note the changes in the plots (shift from left to right upon APTES modification and shift from right to left with dabcyl modification.

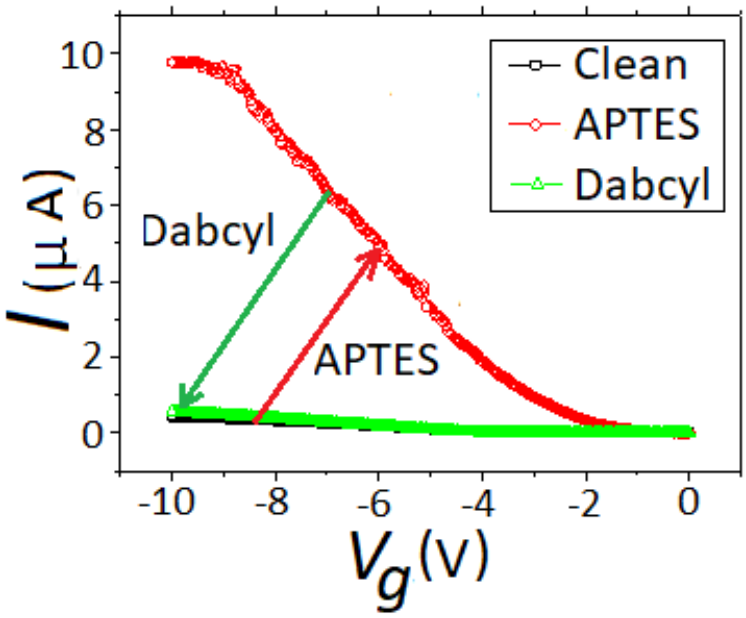

Fig. 4.9 Comparison of a single microwire as it undergoes the process from pristine to APTES then to dabcyl in a vacuum. By noting the shifts in the curves: from pristine to APTES modified creates a right shift. From APTES to dabcyl creates a left shift. This finding proves that a successful chip modification has taken place.

4.4 Experimental Layout

In the previous sections the chemical modification and electrical measurements of the silicon microwire were discussed. By integrating them, a general layout of the experiment is formulated.

A pristine microwire as presented in Fig: 4.10 a undergoes electrical conduction experiments as per Fig: 4.10 b (I versus V_g, I versus V_d and I versus t). APTES modification is used to generate a monolayer on the microwire surface (Fig: 4.10 c). Electrical conduction experiments under the same conditions are repeated on the newly modified microwire (Fig: 4.10 d). Dabcyl characterization was performed on the APTES monolayer (Fig: 4.10 e) and electrical measurements are redone for the third time. This method allows for an accurate comparison of a single microwire through its surface modification processes.

We will now use the information form chapter 1 on the interactions between the molecules and the microwire substrate as well as the electrical measurements to assist in the interpretation of the experimental results.

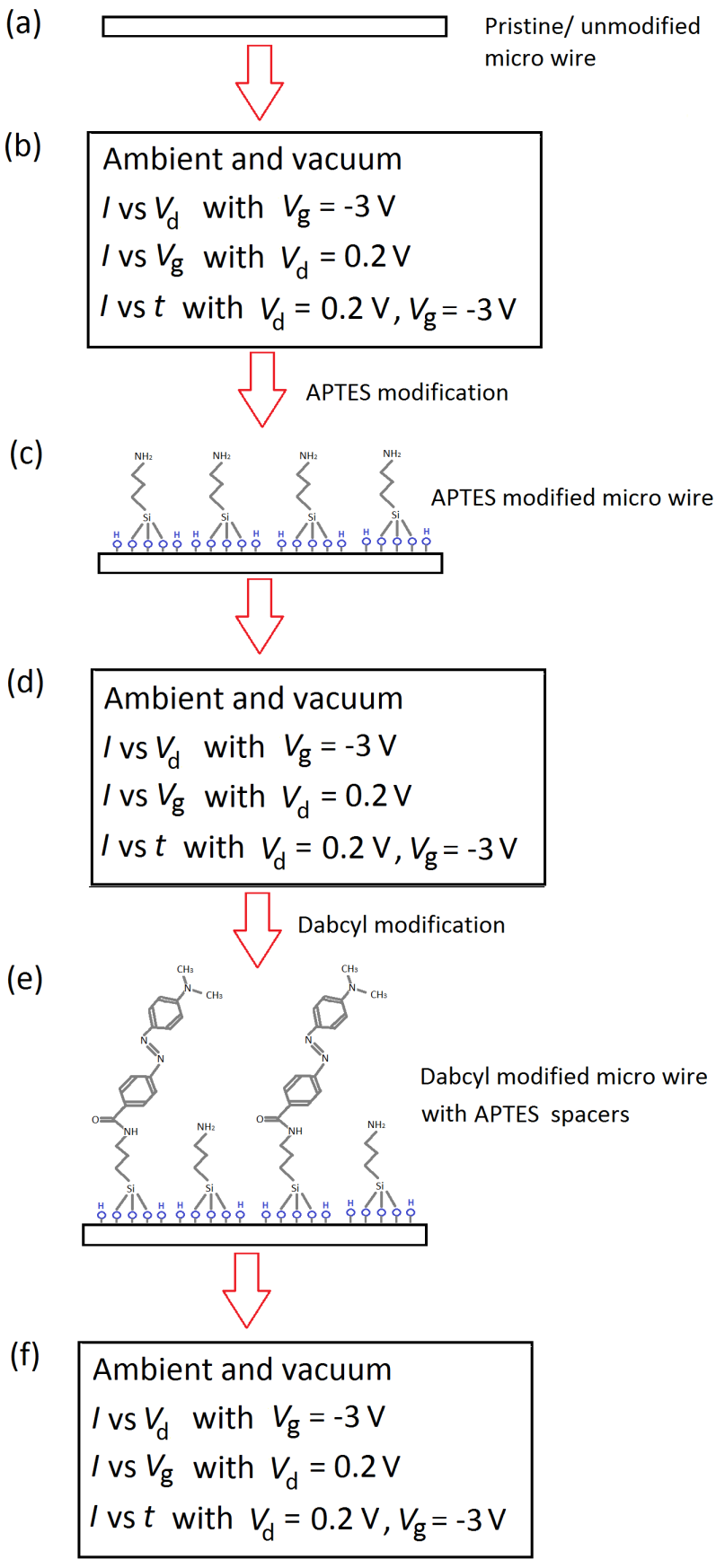

Fig. 4.10 General layout of the experiment.

4.5 Molecular switch operation

In chapter 1 charge and electron transfers between the substrate (SiMWFET) and molecular switches were discussed. Fig: 4.7 describes this reversible interaction between the molecular switches and substrate (SiMWFET) in more detail.

The group of atoms responsible for the colour of a compound are known as chromophores, in our case dabcyl molecules form the chromophores. During the relaxation time the chomophores have a mixed state. Due to UV excitation the majority of the molecular switches enter the *cis* state. UV light also excites electron-hole pairs in the substrate causing electrons to migrate from the substrate to the chromophore. After UV excitation the time when the decrease in current is detected (Fig: 4.7 c), vis excitation causes the majority of the molecular switches to enter into the *trans* state (Fig: 4.7 d). Photons excite the electron-hole pairs in the substrate and some electrons tunnel into the SiMWFET. After Vis excitation the increase in current is detected (Fig: 4.7 e) by the SiMWFET.

As a result of the chemical modification processes explained along with the electrical experiments covered, experimental findings and conclusions are drawn in the following chapter.

Chapter 5

Experimental results

5.1 Introduction

In this chapter the results of the reversible photoisomerization operation in vacuum and ambient conditions using low power Light Emitting Diodes (LEDs) is addressed. I versus V_g and I versus V_d and I versus t plots of a single micro wire from pristine to dabcyl modification under ambient and vacuum conditions will be analysed.

5.2 Measurements in ambient conditions

5.2.1 Results and Discussion

Prior to dabcyl modification there was barely a distinguishable change in current as per Fig: 5.1 and 5.2. Unsurprisingly there was no change in current due to photoisomerization. APTES modified microwires did display an increase is current post UV illumination due to the light strengthening the APTES molecules internal dipoles (Fig: 5.3 and 5.4) [74].

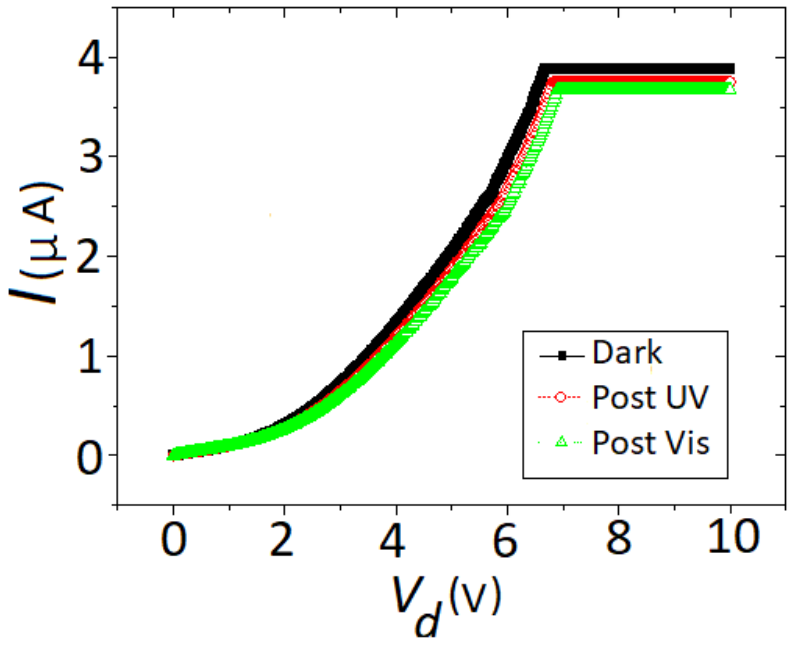

Fig. 5.1 Current against drain to source voltage of a single pristine microwire out of vacuum.

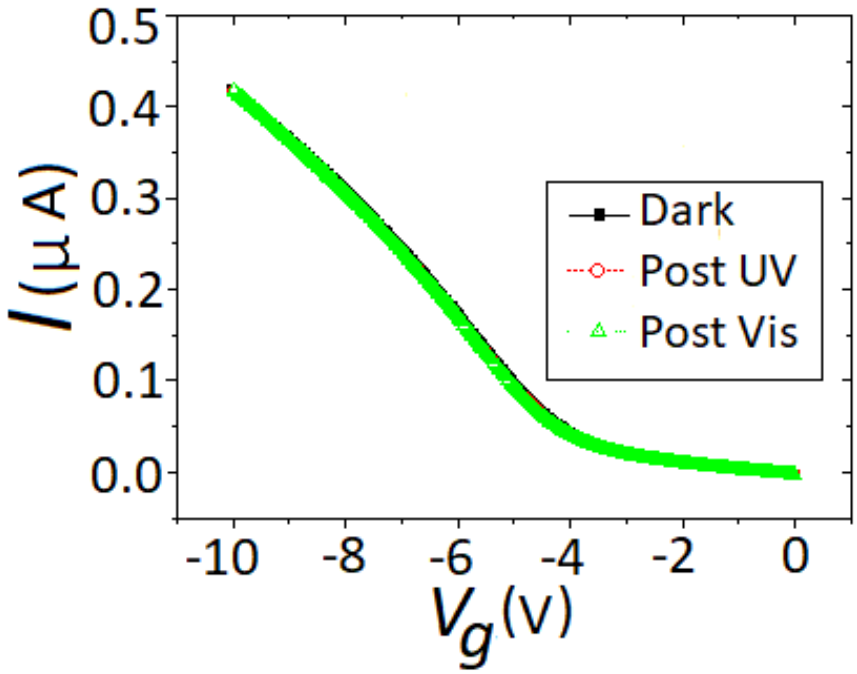

Fig. 5.2 Current versus ground voltage graph of a single pristine microwire out of vacuum.

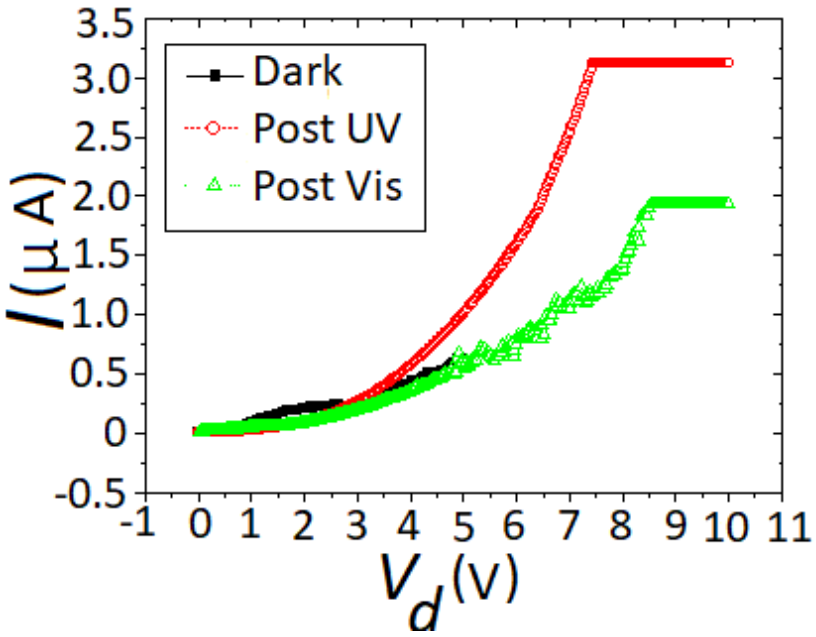

Fig. 5.3 Current versus drain voltage graph of a single APTES modified microwire out of vacuum.

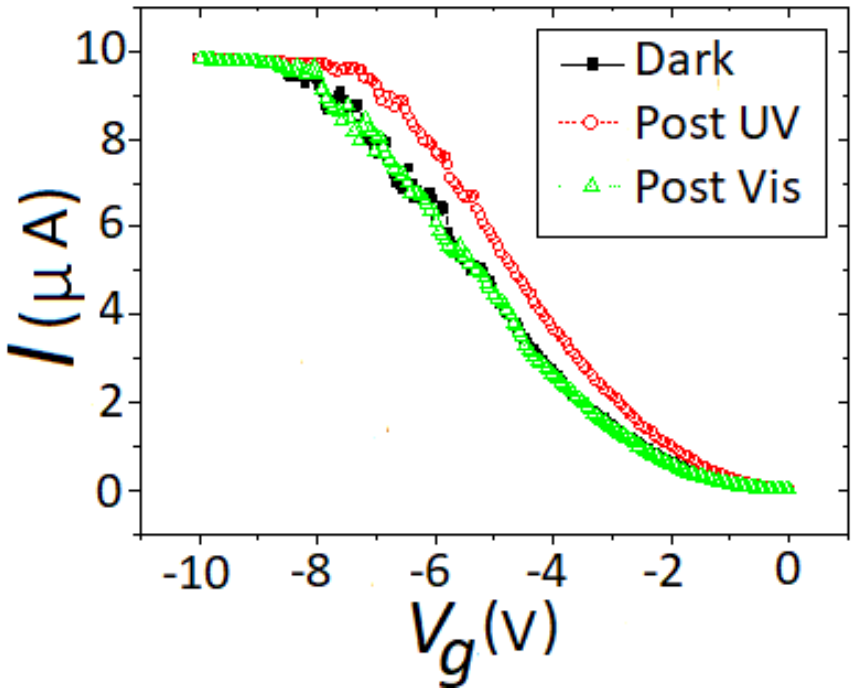

Fig. 5.4 Current versus ground voltage graph of a single APTES modified microwire out of vacuum.

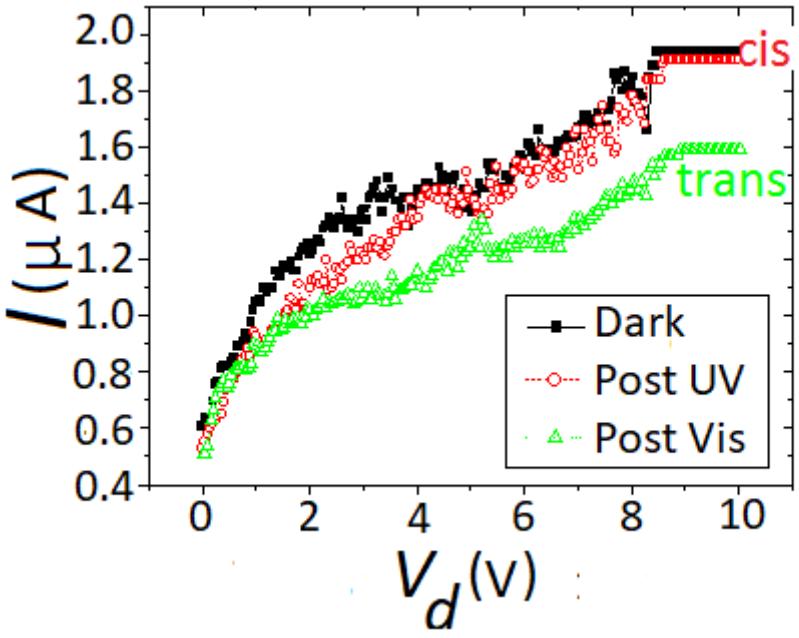

Fig. 5.5 Current versus drain to source voltage of a single dabcyl modified microwire out of vacuum.

Successful photoisomerization was detected in the I versus V_g and I versus V_d plots of Fig: 5.5 and Fig: 5.6. Fig 5.7 displays a comparison of clean, APTES and dabcyl modified microwires in response to illumination cycles. It is evident that APTES modified microwires are most photo-responsive compared to dabcyl modified microwires. Comparing a pristine microwire to dabcyl modified microwire (Fig: 5.8) it is noticeable that the clean micro wire barely has any responsiveness to light. Closely examining a single dabcyl modified microwire (Fig: 5.9) it is evident that during the relaxation time the molecular switches have a mixed state. When they are irradiated with UV light not all the molecules undergo *cis* isomerization. The current decreases post UV excitation but not substantially.

The *cis* state of the molecules decreases the conductance of the micro wire channel. Once the switches become reset to the *trans* state with the Vis LED, the current across the channel increases. Upon UV excitation the conductance decrease but with a higher efficiency. This marks the largest difference in conductance between the post UV and post Vis irradiation. The

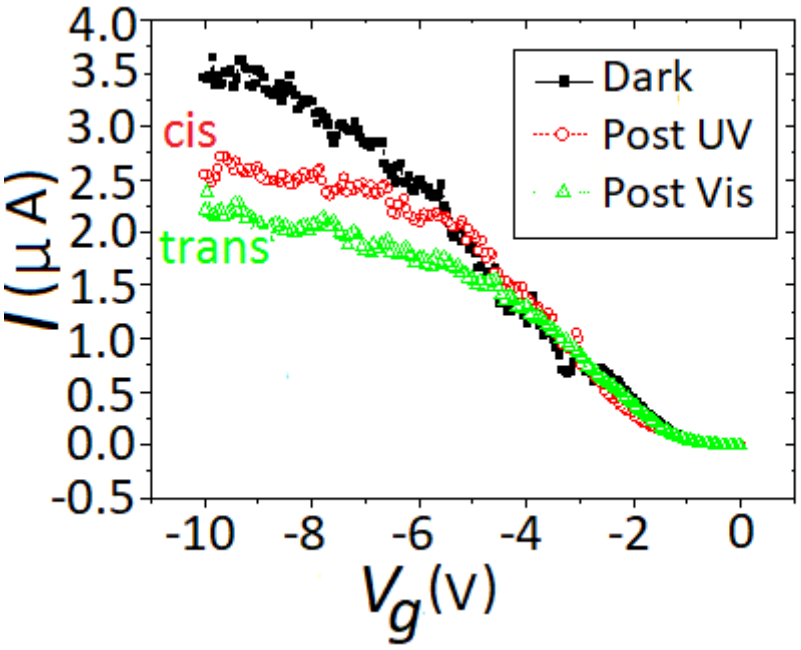

Fig. 5.6 Current versus ground voltage of a single dabcyl modified microwire out of vacuum.

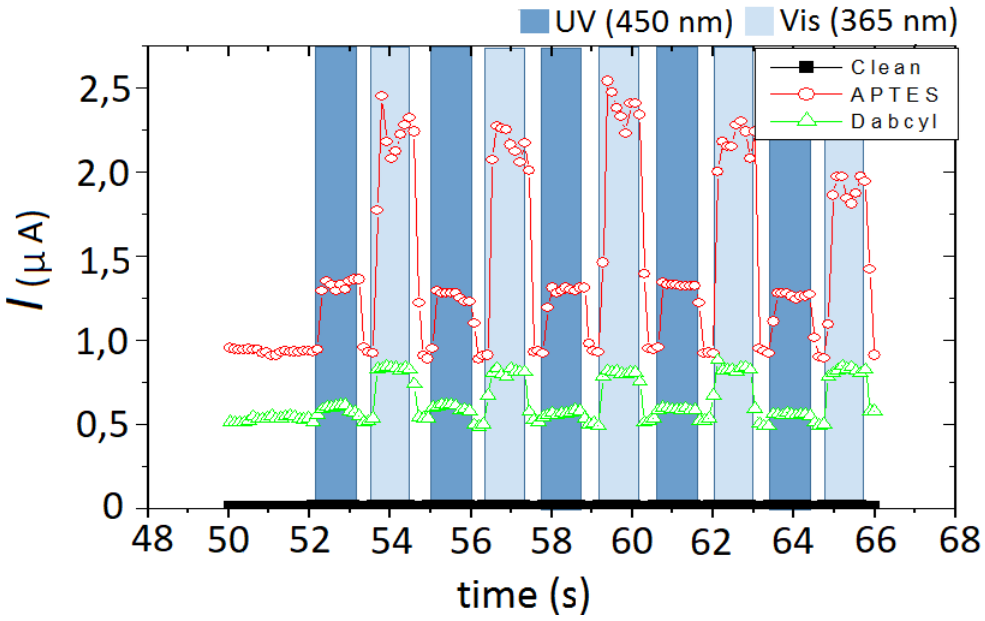

Fig. 5.7 Current versus ground voltage comparing a single pristine, APTES and dabcyl modified microwire out of vacuum.

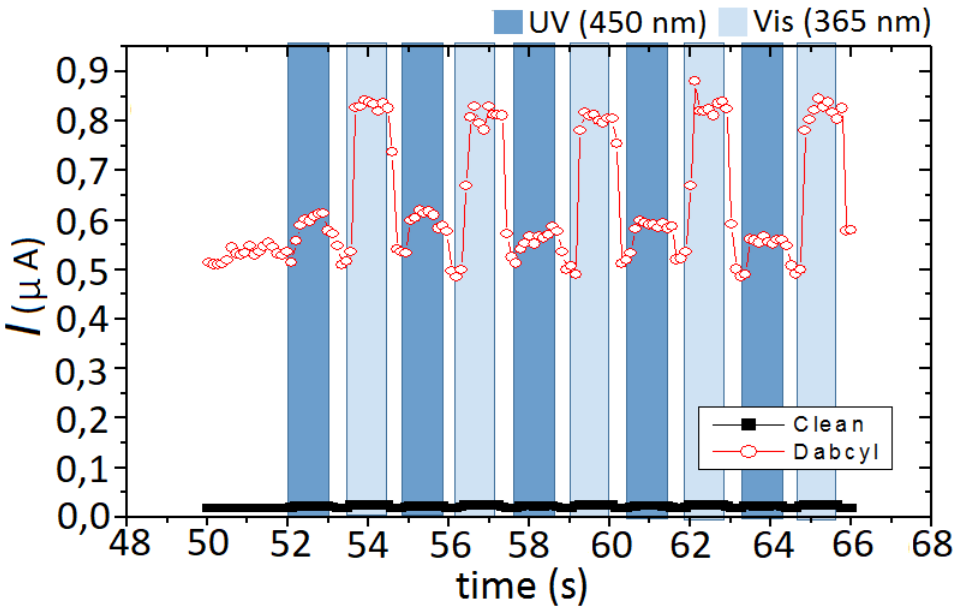

Fig. 5.8 Comparison between a clean and dabcyl modified microwire.

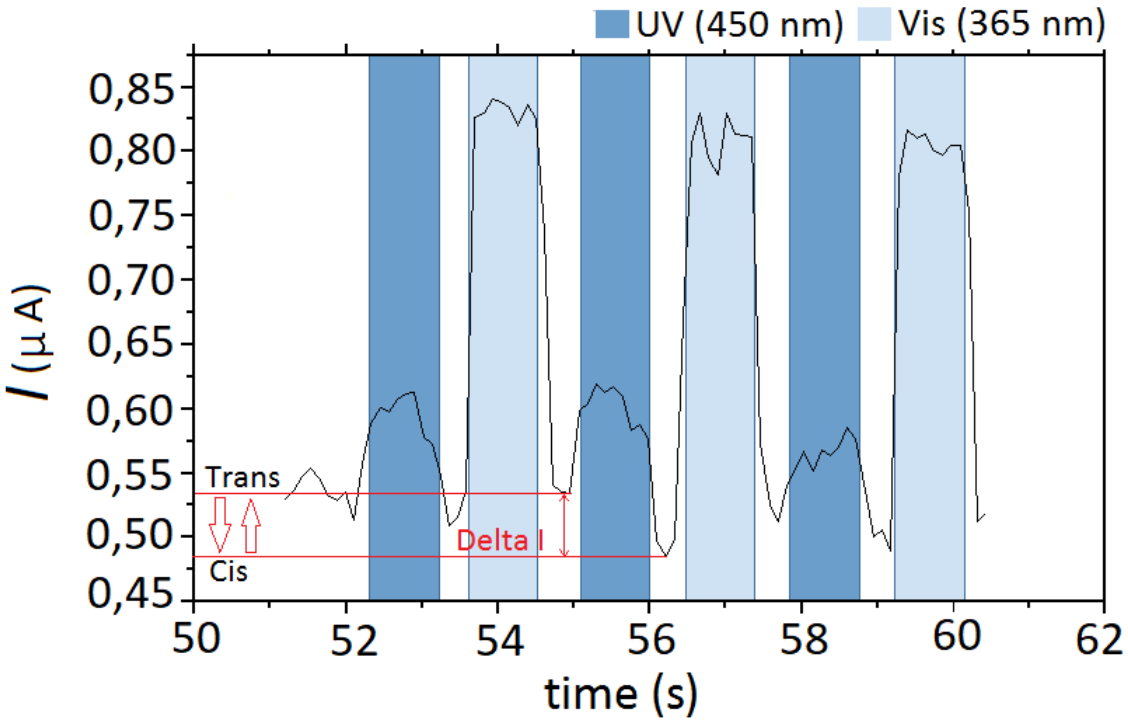

Fig. 5.9 Measured microwire conductance in response to the charge injection of dabcyl molecules. Real time current against time measurement of a single dabcyl modified micro wire under ambient conditions with Delta I equal to 0.05 μA.

change was 0.05 μA. In the second cycle the change diminished to half of the previous amount. The ambient air in the environment stabilizes the more polar *cis* state of the dabcyl molecules.

The electrical measurements are redone in vacuum conditions to reveal the environmental contributions to isomerization stabilization.

5.3 Measurements in vacuum

5.3.1 Results and Discussion

The photo-conductivity of a single microwire from pristine to APTES to dabcyl modification in a vacuum is discussed. For pristine microwires the current remains the same after UV and after Vis excitation Fig: 5.10 and Fig: 5.11.

APTES modified microwires did display an increase is current post UV illumination in vacuum conditions due to the light strengthening the APTES molecules internal dipoles (Fig: 5.12 and 5.13) [74]. Due to the absence of molecules on the microwire surface there is no isomerization. Photoisomerization of dabcyl modified microwire was detected for I versus V_g and I versus V_d plots of Fig: 5.14 and 5.15. A comparison of clean, APTES and dabcyl modified microwires in response to illumination cycles under vaccuum conditions is displayed in Fig: 5.16. It is evident that APTES modified microwires are most photo-responsive followed by dabcyl then clean microwires. In Fig: 5.17 the changes in the dabcyl microwire are clearly evident. The microwire has a greater increase in current when irradiated with light. Closely examining a single dabcyl modified microwire (Fig: 5.18) it is evident that during the relaxation time the molecular switches have a mixed state.

When molecules are irradiated with UV light they partially undergo *cis* isomerization (Fig:

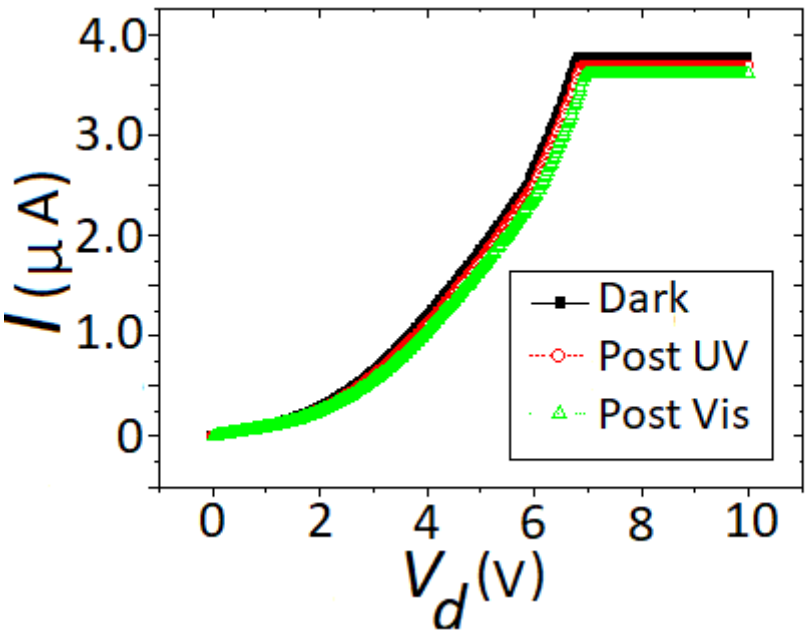

Fig. 5.10 Current versus drain to source voltage of a single pristine microwire in a vacuum.

5.18). The current decreases post UV excitation but not substantially. The *cis* state of the molecules decreases the conductance of the microwire channel. Once the switches are reset to the *trans* state with the Vis LED the current across the channel increases. Upon UV excitation the conductance decrease but with a higher efficiency. This is when the greatest difference in conductance between the post UV and post Vis irradiation is observed. The largest change detected was 0.05 μA. On the second cycle the change diminished to less than a third of the previous amount.

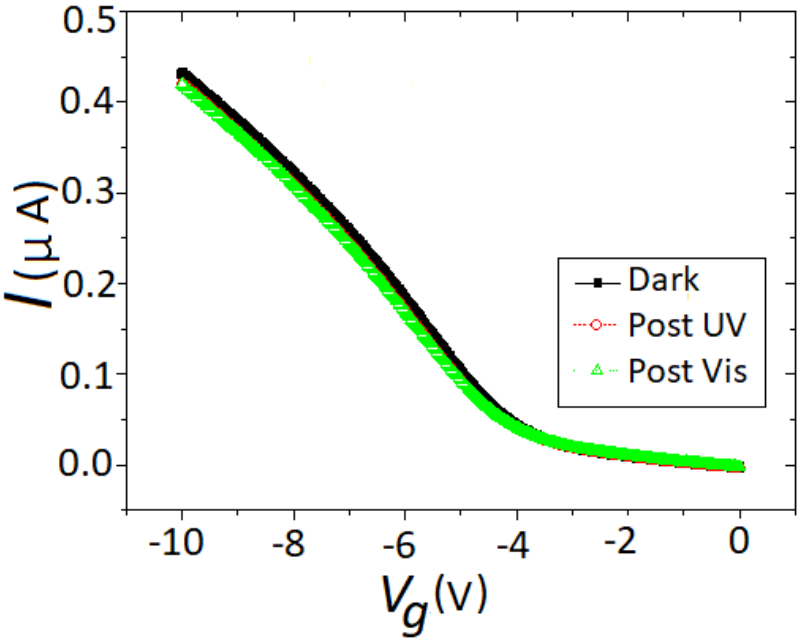

Fig. 5.11 Current against ground voltage of a single pristine microwire in a vacuum.

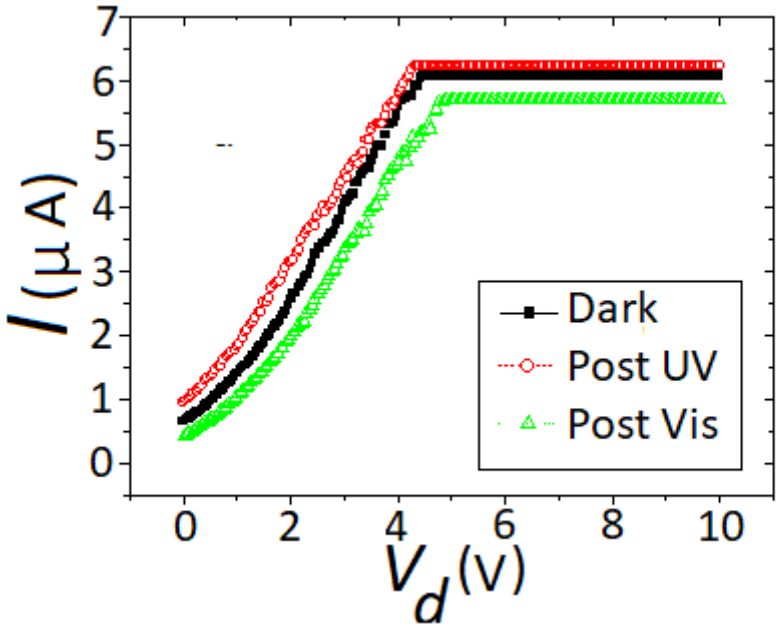

Fig. 5.12 Current against drain voltage of a single APTES modified microwire in a vacuum.

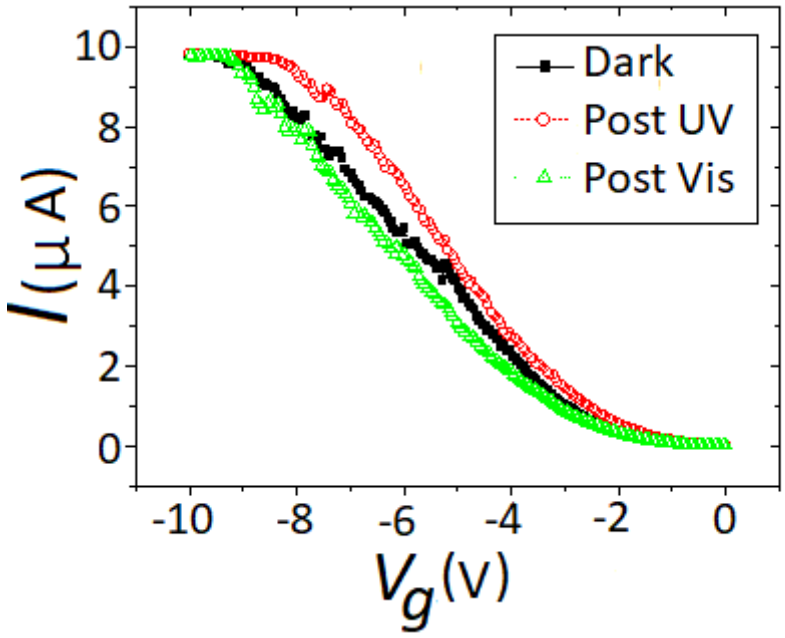

Fig. 5.13 Current versus ground voltage of a single APTES modified microwire in a vacuum.

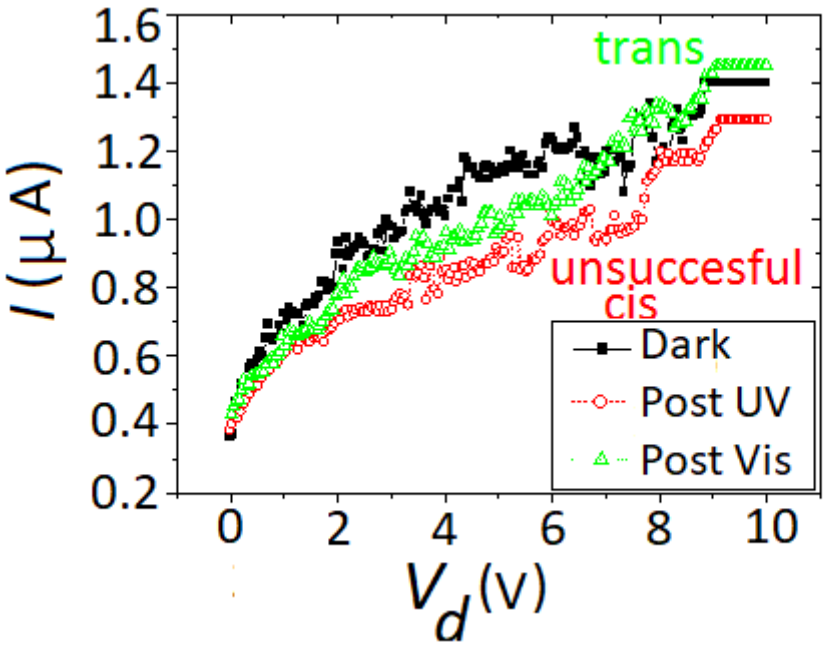

Fig. 5.14 Current versus drain to source voltage of a single dabcyl modified microwire in a vacuum.

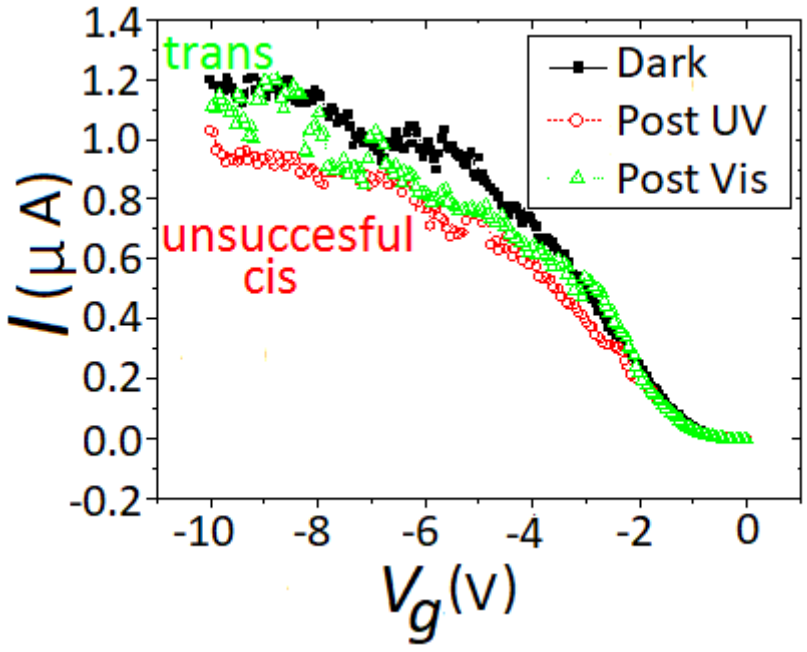

Fig. 5.15 Current versus ground voltage of a single dabcyl modified microwire in a vacuum.

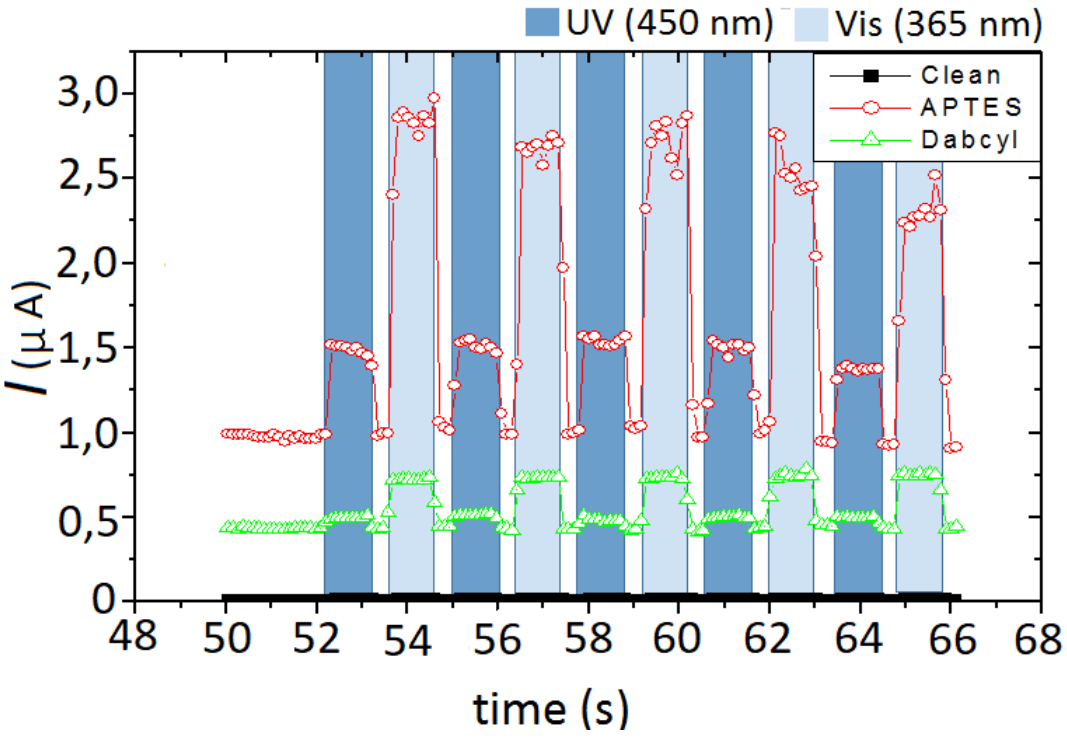

Fig. 5.16 Current versus ground voltage comparing a single pristine, APTES and dabcyl modified microwire in a vacuum.

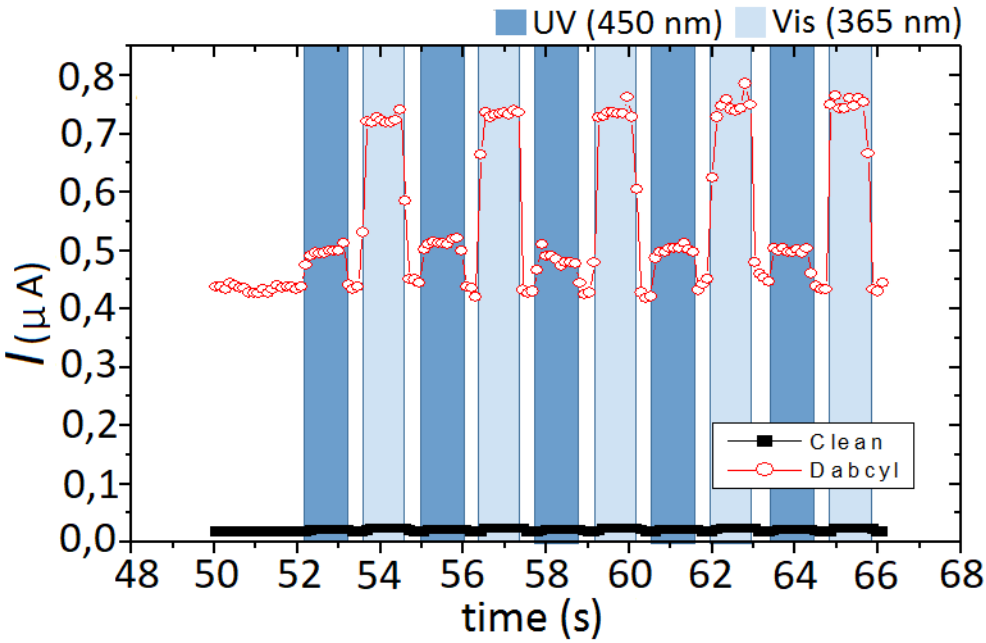

Fig. 5.17 *I* versus *t* comparison between a clean and dabcyl modified microwire.

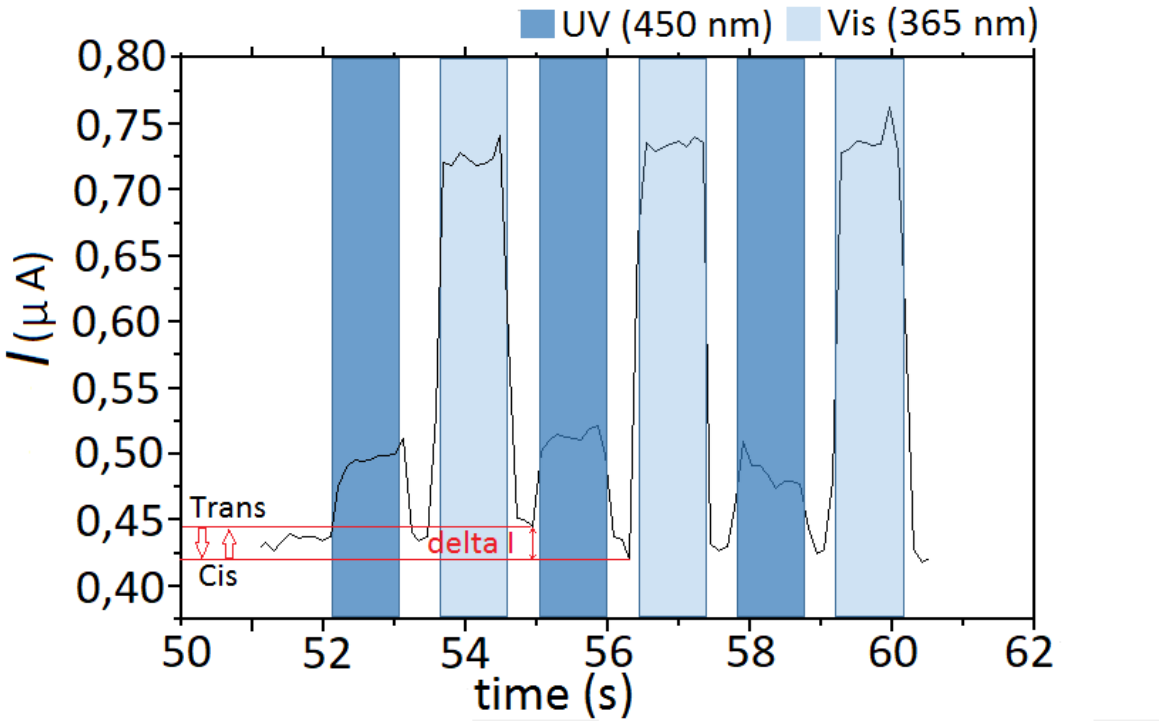

Fig. 5.18 Real-time conductance measurement of a single chromophore functionalized micro wire transistor at -3 V gate bias and source to drain voltage of 0.2 V in vacuum. Delta *I* from *cis* to *trans* equal to 0.025 μA.

Chapter 6

Conclusions

6.1 Introduction

The experimental results demonstrated that dabcyl/APTES *m*SAMs form mixed layers that promote efficient photoswitching. Coverage dependence and reversibility of the *trans-to-cis* photoisomerization all indicate cooperativity in a step-by-step switching process.

The use of changes in the substrates conductance, spacer molecules and large anchor groups were utilized successfully to insure efficient photoisomerization. The linker groups successfully slowed the charge transfer rates and electronically de-coupled the molecular switches from the SiMWFET. The APTES spacers and three legged anchor groups provided the molecular switches with free - volume which reduced steric hindrance and excitonic coupling.

In dabcyl functionalized *m*SAMs steric hindrance has been minimized by reducing the chromophore density [9]. Mixed SAMs were prepared on planar substrates by the dilution of p-methyl red in DMF. The dilution of dabcyl with APTES is a prerequisite for efficient and reversible photoswitching of the SAM. Isomerization from *trans* to *cis* of a given dabcyl chromophore leads to decoupling of the neighbouring dabcyl molecules and reduces steric

hindrance, which promotes further switching [53]. The derivation of isomeization kinetics used to calculate the photoisomerzation yield of Az11/C12 *m*SAMs was adapted to predict the photoswitching efficiency of dabcyl/APTES *m*SAM.

After visible light excitation APTES modified microwires out of vacuum do not show a noticeable increase in current when compared to pristine microwires out of vacuum. In a vacuum APTES modified microwires after visible light excitation show a decrease in current compared to pristine microwires. It was experimentally proven that the *cis* state is more conductive then the *trans* state. This was in agreement with experiments conducted on OFETS [33]. It was also proven experimentally that UV excitation resulted in a decrease of dabcyl modified SiMWFET channel conductance. Visible light illumination resulted in a increace in the dabcyl modified SiMWFET channel conductance [71]. The difference in conductance between the two photoisomerization states was 0.5 μA under ambient and 0.025 μA under vacuum conditions.

Photoisomerization can occur in a vacuum but this is true for short time scales (Fig 5.18). The lack of a relatively dense medium (air), causes the *cis* state to destabilise within a few seconds. Under ambient conditions the *cis* state of dabcyl is more stable due to the presence of adventitious water (Fig 5.9). We have shown that the thermal isomerization in dabcyl/APTES *m*SAMs is strongly dependent upon the environmental conditions. We observed thermal relaxation times on the order of seconds in vacuum. The thermal relaxation in ambient conditions is hindered, occurring on a time scale of more than a minute.

Some appreciable fatigue was observed after several switching cycles of I versus t under ambient and vacuum conditions. The results demonstrate that the environment has a major impact on the effectiveness of dabcyl functionalized *m*SAMs photoswitching.

6.2 Contribution to knowledge

This dissertation comprises the real time detection of photoisomerization of dabcyl functionalised *m*SAMs with the use of a Silicon microwire field effect transistor. We obtained a comparative study of I versus V_g, I versus V_d and I versus t of a single microwire from pristine, APTES to dabcyl modification in and out of a vacuum. The findings verified that the *cis* state of dabcyl/APTES *m*SAM is more conductive than the *trans* state. Our findings suggest that photoisomerization was strongly dependent on environmental conditions due to the prolonged thermal relaxation times of dabcyl under ambient conditions. This research paves the way toward tailoring surface and interface properties in a reversible fashion.

6.3 Future research

Further research is open to the investigation of the thermal relaxation rates of dabcyl/APTES *m*SAMs in other gases such as nitrogen and argon. Another promising avenue is to quantify the photoisomerzation yield of dabcyl/APTES *m*SAMs by means of NEXAFS and UV/vis spectroscopy. These remain as promising topics for further research.

References

[1] Sohyeon Seo, Misook Min, Sae Mi Lee, and Hyoyoung Lee. Photo-switchable molecular monolayer anchored between highly transparent and flexible graphene electrodes. *Nature Communications*, 4:1920, 5 2013.

[2] Melina Gilbert and Bo Albinsson. Photoinduced charge and energy transfer in molecular wires. *Chem. Soc. Rev.*, 44:845–862, 2015.

[3] Jia Lin Zhang, Jian Qiang Zhong, Jia Dan Lin, Wen Ping Hu, Kai Wu, Guo Qin Xu, Andrew T. S. Wee, and Wei Chen. Towards single molecule switches. *Chem. Soc. Rev.*, 44:2998–3022, 2015.

[4] Lanlan Sun, Yuri A. Diaz-Fernandez, Tina A. Gschneidtner, Fredrik Westerlund, Samuel Lara-Avila, and Kasper Moth-Poulsen. Single-molecule electronics: from chemical design to functional devices. *Chem. Soc. Rev.*, 43:7378–7411, 2014.

[5] Noelia Fuentes, Ana Martin-Lasanta, Luis Alvarez de Cienfuegos, Maria Ribagorda, Andres Parra, and Juan M. Cuerva. Organic-based molecular switches for molecular electronics. *Nanoscale*, 3:4003–4014, 2011.

[6] Nan Song and Ying-Wei Yang. Molecular and supramolecular switches on mesoporous silica nanoparticles. *Chem. Soc. Rev.*, 44:3474–3504, 2015.

[7] Christina R. Crecca and Adrian E. Roitberg. Theoretical study of the isomerization mechanism of azobenzene and disubstituted azobenzene derivatives. *The Journal of Physical Chemistry A*, 110(26):8188–8203, 2006. PMID: 16805507.

[8] Alessandro Cembran, Fernando Bernardi, Marco Garavelli, Laura Gagliardi, and Giorgio Orlandi. On the mechanism of the cistrans isomerization in the lowest electronic states of azobenzene: s0, s1, and t1. *Journal of the American Chemical Society*, 126(10):3234–3243, 2004. PMID: 15012153.

[9] Rafal Klajn, J. Fraser Stoddart, and Bartosz A. Grzybowski. Nanoparticles functionalised with reversible molecular and supramolecular switches. *Chem. Soc. Rev.*, 39:2203–2237, 2010.

[10] Thomas Moldt, Daniel Brete, Daniel Przyrembel, Sanjib Das, Joel R. Goldman, Pintu K. Kundu, Cornelius Gahl, Rafal Klajn, and Martin Weinelt. Tailoring the properties of surface-immobilized azobenzenes by monolayer dilution and surface curvature. *Langmuir*, 31(3):1048–1057, 2015. PMID: 25544061.

[11] Cornelius Gahl, Roland Schmidt, Daniel Brete, Erik R. McNellis, Wolfgang Freyer, Robert Carley, Karsten Reuter, and Martin Weinelt. Structure and excitonic coupling in self-assembled monolayers of azobenzene-functionalized alkanethiols. *Journal of the American Chemical Society*, 132(6):1831–1838, 2010. PMID: 20099853.

[12] Jun Hee Yoon and Sangwoon Yoon. Photoisomerization of azobenzene derivatives confined in gold nanoparticle aggregates. *Phys. Chem. Chem. Phys.*, 13:12900–12905, 2011.

[13] Valentina Cantatore, Giovanni Granucci, Guillaume Rousseau, Giancarlo Padula, and Maurizio Persico. Photoisomerization of self-assembled monolayers of azobiphenyls: Simulations highlight the role of packing and defects. *The Journal of Physical Chemistry Letters*, 7(19):4027–4031, 2016. PMID: 27669082.

[14] Jaume García-Amorós and Dolores Velasco. Recent advances towards azobenzene-based light-driven real-time information-transmitting materials. *Beilstein Journal of Organic Chemistry*, 8:1003–1017, 2012.

[15] Hai Li, Juan Zhang, Xiaozhu Zhou, Gang Lu, Zongyou Yin, Gongping Li, Tom Wu, Freddy Boey, Subbu S. Venkatraman, and Hua Zhang. Aminosilane micropatterns on hydroxyl-terminated substrates: Fabrication and applications. *Langmuir*, 26(8):5603–5609, 2010. PMID: 19947614.

[16] Joonyeong Kim, Paul Seidler, Lai Sze Wan, and Catherine Fill. Formation, structure, and reactivity of amino-terminated organic films on silicon substrates. *Journal of Colloid and Interface Science*, 329(1):114 – 119, 2009.

[17] Joonyeong Kim, Paul Seidler, Catherine Fill, and Lai Sze Wan. Investigations of the effect of curing conditions on the structure and stability of amino-functionalized organic films on silicon substrates by fourier transform infrared spectroscopy, ellipsometry, and fluorescence microscopy. *Surface Science*, 602(21):3323 – 3330, 2008.

[18] Joonyeong Kim, Joungmo Cho, Paul M. Seidler, Nicholas E. Kurland, and Vamsi K. Yadavalli. Investigations of chemical modifications of amino-terminated organic films on silicon substrates and controlled protein immobilization. *Langmuir*, 26(4):2599–2608, 2010. PMID: 20095550.

[19] Toshihiko Matsuo. In situ visualization of messenger {RNA} for basic fibroblast growth factor in living cells. *Biochimica et Biophysica Acta (BBA) - General Subjects*, 1379(2):178 – 184, 1998.

[20] Mina Han, Daisuke Ishikawa, Takumu Honda, Eisuke Ito, and Masahiko Hara. Light-driven molecular switches in azobenzene self-assembled monolayers: effect of molecular structure on reversible photoisomerization and stable cis state. *Chem. Commun.*, 46:3598–3600, 2010.

[21] Ajeet S. Kumar, Tao Ye, Tomohide Takami, Byung-Chan Yu, Austen K. Flatt, James M. Tour, and Paul S. Weiss. Reversible photo-switching of single azobenzene molecules in controlled nanoscale environments. *Nano Letters*, 8(6):1644–1648, 2008. PMID: 18444688.

[22] Mark Elbing, Alfred Błaszczyk, Carsten von Hänisch, Marcel Mayor, Violetta Ferri, Christian Grave, Maria Anita Rampi, Giuseppina Pace, Paolo Samorì, Andrei Shaporenko, and Michael Zharnikov. Single component self-assembled monolayers of aromatic azobiphenyl: Influence of the packing tightness on the sam structure and light-induced molecular movements. *Advanced Functional Materials*, 18(19):2972–2983, 2008.

[23] Stephanie L. Gould, David Tranchemontagne, Omar M. Yaghi, and Miguel A. Garcia-Garibay. Amphidynamic character of crystalline mof-5: rotational dynamics of terephthalate phenylenes in a free-volume, sterically unhindered environment. *Journal of the American Chemical Society*, 130(11):3246–3247, 2008. PMID: 18288839.

[24] Manuel Utecht, Tillmann Klamroth, and Peter Saalfrank. Optical absorption and excitonic coupling in azobenzenes forming self-assembled monolayers: a study based on density functional theory. *Phys. Chem. Chem. Phys.*, 13:21608–21614, 2011.

[25] Devens Gust, Thomas A. Moore, and Ana L. Moore. Molecular switches controlled by light. *Chem. Commun.*, pages 1169–1178, 2006.

[26] Yong Chen, Gun-Young Jung, Douglas A A Ohlberg, Xuema Li, Duncan R Stewart, Jan O Jeppesen, Kent A Nielsen, J Fraser Stoddart, and R Stanley Williams. Nanoscale molecular-switch crossbar circuits. *Nanotechnology*, 14(4):462, 2003.

[27] Ben L. Feringa. In control of motion: from molecular switches to molecular motors. *Accounts of Chemical Research*, 34(6):504–513, 2001. PMID: 11412087.

[28] Stephen G. Miller and Mary B. Kennedy. Regulation of brain type ii ca2+calmodulin-dependent protein kinase by autophosphorylation: A ca2+-triggered molecular switch. *Cell*, 44(6):861 – 870, 1986.

[29] Krzysztof Palczewski, Takashi Kumasaka, Tetsuya Hori, Craig A. Behnke, Hiroyuki Motoshima, Brian A. Fox, Isolde Le Trong, David C. Teller, Tetsuji Okada, Ronald E. Stenkamp, Masaki Yamamoto, and Masashi Miyano. Crystal structure of rhodopsin: A g protein-coupled receptor. *Science*, 289(5480):739–745, 2000.

[30] Hubbard and George Wald. Cis-trans isomers of vitamin a and retinene in the rhodopsin system. *J. Gen. Physiol*, page 269.

[31] Michael Schulze, Manuel Utecht, Thomas Moldt, Daniel Przyrembel, Cornelius Gahl, Martin Weinelt, Peter Saalfrank, and Petra Tegeder. Nonlinear optical response of photochromic azobenzene-functionalized self-assembled monolayers. *Phys. Chem. Chem. Phys.*, 17:18079–18086, 2015.

[32] Ben L Feringa and Wesley R Browne. *Molecular switches*, volume 42. Wiley Online Library, 2001.

[33] Núria Crivillers, Emanuele Orgiu, Federica Reinders, Marcel Mayor, and Paolo Samorì. Optical modulation of the charge injection in an organic field-effect transistor based on photochromic self-assembled-monolayer-functionalized electrodes. *Advanced Materials*, 23(12):1447–1452, 2011.

[34] Cornelius Gahl, Roland Schmidt, Daniel Brete, Stephanie Paarmann, and Martin Weinelt. Charge-transfer dynamics in azobenzene alkanethiolate self-assembled monolayers on gold. *Surface Science*, 643:183 – 189, 2016. Present challenges in surface science, a special issue in honour of Dietrich Menzel.

[35] Masayuki Suda, Naoto Kameyama, Aya Ikegami, Motohiro Suzuki, Naomi Kawamura, and Yasuaki Einaga. Size-reduction induced ferromagnetism and photo-magnetic effects in azobenzene-thiol-passivated gold nanoparticles. *Polyhedron*, 28(9-10):1868–1874, 6 2009.

[36] J. Griffiths. Ii. photochemistry of azobenzene and its derivatives. *Chem. Soc. Rev.*, 1:481–493, 1972.

[37] T. Nägele, R. Hoche, W. Zinth, and J. Wachtveitl. Femtosecond photoisomerization of cis-azobenzene. *Chemical Physics Letters*, 272(5):489 – 495, 1997.

[38] Enrico Benassi and Stefano Corni. Quenching of the photoisomerization of azobenzene self-assembled monolayers by the metal substrate. *The Journal of Physical Chemistry C*, 118(45):25906–25917, 2014.

[39] H. Petek and S. Ogawa. Femtosecond time-resolved two-photon photoemission studies of electron dynamics in metals. *Progress in Surface Science*, 56(4):239 – 310, 1997.

[40] Martin Weinelt. Pgqu - martin weinelt - azobenzene-derived molecular switches at surfaces. https://pgqu.iq.ufrj.br/seminarios/2014_2_martin_weinelt.html, December 2014.

[41] H Eckardt, L Fritsche, and J Noffke. Self-consistent relativistic band structure of the noble metals. *Journal of Physics F: Metal Physics*, 14(1):97, 1984.

[42] O. Karis, A. Nilsson, M. Weinelt, T. Wiell, C. Puglia, N. Wassdahl, N. Mårtensson, M. Samant, and J. Stöhr. One-step and two-step description of deexcitation processes in weakly interacting systems. *Phys. Rev. Lett.*, 76:1380–1383, Feb 1996.

[43] M. J. Comstock, Jongweon Cho, A. Kirakosian, and M. F. Crommie. Manipulation of azobenzene molecules on au(111) using scanning tunneling microscopy. *Phys. Rev. B*, 72:153414, Oct 2005.

[44] Naoto Tamai and Hiroshi Miyasaka. Ultrafast dynamics of photochromic systems. *Chemical Reviews*, 100(5):1875–1890, 2000. PMID: 11777424.

[45] Petra Tegeder. Optically and thermally induced molecular switching processes at metal surfaces. *Journal of Physics: Condensed Matter*, 24(39):394001, 2012.

[46] Sabri Alkis, Ping Jiang, Lin-Lin Wang, Adrian E. Roitberg, Hai-Ping Cheng, and Jeffrey L. Krause. Molecular dynamics simulations of alkanethiol monolayers with azobenzene molecules on the au(111) surface. *The Journal of Physical Chemistry C*, 111(40):14743–14752, 2007.

[47] Micol Alemani, Maike V. Peters, Stefan Hecht, Karl-Heinz Rieder, Francesca Moresco, and Leonhard Grill. Electric field-induced isomerization of azobenzene by stm. *Journal of the American Chemical Society*, 128(45):14446–14447, 2006. PMID: 17090013.

[48] Matthew J. Comstock, Niv Levy, Jongweon Cho, Luis Berbil-Bautista, Michael F. Crommie, Daniel A. Poulsen, and Jean M. J. Fréchet. Measuring reversible photomechanical switching rates for a molecule at a surface. *Applied Physics Letters*, 92(12), 2008.

[49] Felix Leyssner, Sebastian Hagen, Laszlo Ovari, Jadranka Dokic, Peter Saalfrank, Maike V. Peters, Stefan Hecht, Tillmann Klamroth, and Petra Tegeder. Photoisomerization ability of molecular switches adsorbed on au(111): Comparison between azobenzene and stilbene derivatives. *The Journal of Physical Chemistry C*, 0(proofing):null, 0.

[50] Hanne Jacob, Sandra Ulrich, Ulrich Jung, Sonja Lemke, Talina Rusch, Christian Schutt, Finn Petersen, Thomas Strunskus, Olaf Magnussen, Rainer Herges, and Felix Tuczek. Monitoring the reversible photoisomerization of an azobenzene-functionalized molecular triazatriangulene platform on au(111) by irras. *Phys. Chem. Chem. Phys.*, 16:22643–22650, 2014.

[51] J. M. Simmons, I. In, V. E. Campbell, T. J. Mark, F. Léonard, P. Gopalan, and M. A. Eriksson. Optically modulated conduction in chromophore-functionalized single-wall carbon nanotubes. *Phys. Rev. Lett.*, 98:086802, Feb 2007.

[52] Michael Schulze, Manuel Utecht, Andreas Hebert, Karola Rück-Braun, Peter Saalfrank, and Petra Tegeder. Reversible photoswitching of the interfacial nonlinear optical response. *The Journal of Physical Chemistry Letters*, 6(3):505–509, 2015. PMID: 26261971.

[53] Thomas Moldt, Daniel Przyrembel, Michael Schulze, Wibke Bronsch, Larissa Boie, Daniel Brete, Cornelius Gahl, Rafal Klajn, Petra Tegeder, and Martin Weinelt. Differing isomerization kinetics of azobenzene-functionalized self-assembled monolayers in ambient air and in vacuum. *Langmuir*, 32(42):10795–10801, 2016. PMID: 27681851.

[54] Richard Jaeger and Travis Blalock. *Microelectronic Circuit Design*. McGraw-Hill Education, 2010.

[55] C. K Alexander and M. Sadiku. *Fundamentals of Electric Circuits*, volume 4. McGraw-Hill, 2009.

[56] Xiaoyan Song, Jin Zhai, Yilin Wang, and Lei Jiang. Self-assembly of amino-functionalized monolayers on silicon surfaces and preparation of superhydrophobic surfaces based on alkanoic acid dual layers and surface roughening. *Journal of Colloid and Interface Science*, 298(1):267 – 273, 2006.

[57] Kesong Liu and Lei Jiang. Metallic surfaces with special wettability. *Nanoscale*, 3:825–838, 2011.

[58] Fiorella L. Callari and Salvatore Sortino. "catch-and-release" of porphyrins by photoswitchable self-assembled monolayers. *J. Mater. Chem.*, 17:4184–4188, 2007.

[59] Thorsten Hugel, Nolan B. Holland, Anna Cattani, Luis Moroder, Markus Seitz, and Hermann E. Gaub. Single-molecule optomechanical cycle. *Science*, 296(5570):1103–1106, 2002.

[60] Zhilin Yu and Stefan Hecht. Remote control over folding by light. *Chem. Commun.*, 52:6639–6653, 2016.

[61] Pintu K. Kundu and Rafal Klajn. Watching single molecules move in response to light. *ACS Nano*, 8(12):11913–11916, 2014. PMID: 25474733.

[62] Quan Li, Aleksey V. Rukavishnikov, Pavel A. Petukhov, Tatiana O. Zaikova, Changshu Jin, and John F. W. Keana. Nanoscale tripodal 1,3,5,7-tetrasubstituted adamantanes for afm applications. *The Journal of Organic Chemistry*, 68(12):4862–4869, 2003. PMID: 12790592.

[63] E. A. Shokova and V. V. Kovalev. Adamantane functionalization. synthesis of polyfunctional derivatives with various substituents in bridgehead positions. *Russian Journal of Organic Chemistry*, 48(8):1007–1040, 2012.

[64] Gun-Young Jung, Ezekiel Johnston-Halperin, Wei Wu, Zhaoning Yu, Shih-Yuan Wang, William M. Tong, Zhiyong Li, Jonathan E. Green, Bonnie A. Sheriff, Akram Boukai, Yuri Bunimovich, James R. Heath, and R. Stanley Williams. Circuit fabrication at 17 nm half-pitch by nanoimprint lithography. *Nano Letters*, 6(3):351–354, 2006. PMID: 16522021.

[65] Hong Chen, J. Michael Harrison, Avi Mandelbaum, Ann Van Ackere, and Lawrence M. Wein. Empirical evaluation of a queueing network model for semiconductor wafer fabrication. *Operations Research*, 36(2):202–215, 1988.

[66] Taho Yang, Chao-Ton Su, and Yuan-Ru Hsu. Systematic layout planning: a study on semiconductor wafer fabrication facilities. *International Journal of Operations & Production Management*, 20(11):1359–1371, 2000.

[67] Rainer Waser, editor. *Nanoelectronics and Information Technology: Advanced Electronic Materials and Novel Devices*. John Wiley & Sons, Inc., New York, NY, USA, 2003.

[68] Marek Grzelczak, Jan Vermant, Eric M. Furst, and Luis M. Liz-Marzán.

[69] Yanqing An, Miao Chen, Qunji Xue, and Weimin Liu. Preparation and self-assembly of carboxylic acid-functionalized silica. *Journal of Colloid and Interface Science*, 311(2):507 – 513, 2007.

[70] Wei Feng, Wen Luo, and Yiyu Feng. Photo-responsive carbon nanomaterials functionalized by azobenzene moieties: structures, properties and application. *Nanoscale*, 4:6118–6134, 2012.

[71] Markus Döbbelin, Artur Ciesielski, Sébastien Haar, Silvio Osella, Matteo Bruna, Andrea Minoia, Luca Grisanti, Thomas Mosciatti, Fanny Richard, Eko Adi Prasetyanto, Luisa De Cola, Vincenzo Palermo, Raffaello Mazzaro, Vittorio Morandi, Roberto Lazzaroni, Andrea C Ferrari, David Beljonne, and Paolo Samorì. Light-enhanced liquid-phase exfoliation and current photoswitching in graphene-azobenzene composites. *Nature communications*, 7:11090, 2016.

[72] Monia Demelas, Stefano Lai, Andrea Spanu, Sergio Martinoia, Piero Cosseddu, Massimo Barbaro, and Annalisa Bonfiglio. Charge sensing by organic charge-modulated field effect transistors: application to the detection of bio-related effects. *J. Mater. Chem. B*, 1:3811–3819, 2013.

[73] S. Lai, M. Demelas, G. Casula, P. Cosseddu, M. Barbaro, and A. Bonfiglio. Ultralow voltage, otft-based sensor for label-free dna detection. *Advanced Materials*, 25(1):103–107, 2013.

[74] M. C. Lin, C. J. Chu, L. C. Tsai, H. Y. Lin, C. S. Wu, Y. P. Wu, Y. N. Wu, D. B. Shieh, Y. W. Su, and C. D. Chen. Control and detection of organosilane polarization on nanowire field-effect transistors. *Nano Letters*, 7(12):3656–3661, 2007.